VOC determination with fast GC-MS – technical validation and indoor air measurements

JOHANNES GUTENBERG-UNIVERSITÄT MAINZ

Faculty of Chemistry, Pharmaceutical Sciences and Geoscience

MAX PLANCK INSTITUTE FOR CHEMISTRY

DISSERTATION

zur Erlangung des Grades
"Doktor der Naturwissenschaften"
im Promotionsfach Chemie

Lisa ERNLE
geb. in Herrenberg

Mainz, 2023

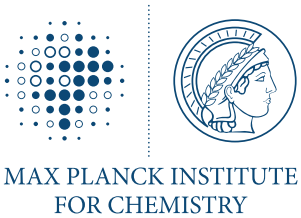

Dean: Prof. Dr. Eva Rentschler
1st examiner: Prof. Dr. Jonathan Williams
2nd examiner: Prof. Dr. Thorsten Hoffmann
Date of the oral exam:

Declaration of authorship

I hereby declare that I wrote the dissertation submitted without any unauthorized external assistance and used only sources acknowledged in the work. All textual passages that are appropriated verbatim or paraphrased from published and unpublished texts as well as all information obtained from oral sources are duly indicated and listed in accordance with bibliographical rules. In carrying out this research, I complied with the rules of standard scientific practice as formulated in the statutes of Johannes-Gutenberg-Universität Mainz to ensure standard scientific practice.

Signed: 

Date: 18.07.2023

Abstract

Atmospheric measurements are important to determine climate change forcings and to assess the air quality in outdoor as well as indoor environments. Volatile organic compounds (VOCs) play an important role for both and are therefore monitored using various measurement devices. Two common techniques for the analysis of organic trace gases are gas chromatography-mass spectrometry (GC-MS) and proton transfer reaction-time of flight-mass spectrometry (PTR-ToF-MS). Unfortunately, several atmospheric constituents such as water vapour or ozone (O_3) can affect the measurements, leading to compromised data. Accurate measurements are crucial for correct data analysis, interpretation and data quality assurance.

In this doctoral project, the influence of relative humidity (RH), ozone and an ozone scrubber on GC-MS and PTR-MS analysis as well as some compound specific technical issues were investigated to assess their effect on the measurements and thus improve the experimental setup. Subsequently, the two techniques have been used to study the emission of VOCs from human body in the absence and presence of ozone, and at varying humidity, in a controlled-climate chamber.

The investigation of the effect of atmospheric constituents on simultaneous GC- and PTR-MS measurements showed that ozone can lead to increased signals for certain carbonyls and decreased signals for species with double bonds (isoprene, terpenes). Those interferences are either produced in the inlet line or inside the instrument. To reduce their effect, a sodium thiosulfate ozone ($Na_2S_2O_3$) scrubber was installed in the inlet line. It was found that the scrubber reduces the ozone concentration in the sample air effectively under tropospheric conditions, leading to elimination of the interferences for most species. However, highly ozone-reactive compounds such as sesquiterpenes were still impacted by the residual ozone in the lines. The scrubbing efficiency was dependent on ozone concentration, RH and flow rate and improved with relative humidity. Under typical tropospheric conditions, the scrubber endurance was 5 to 14 days. Stratospheric conditions (high O_3 and low RH) led to insufficient ozone scavenging and the investigated setup with one single $Na_2S_2O_3$ scrubber is therefore not suitable for measurements in the lower stratosphere.

During indoor experiments investigating VOC emissions from human body, extremely high signals on PTR *m/z* 69.07, which is usually assigned to isoprene, have been measured. Comparison with GC data showed that the PTR was suffering an interference from other compounds fragmenting on the same mass-to-charge ratio when ozone reacts with human skin oil or cotton clothing. The interferences on *m/z* 69.07 can stem from fragments of C_5 to C_{10} saturated aldehydes. Nonanal was the only species which could be

quantified reliably and which could be used to correct the *m/z* 69.07 signal. VOC emission from humans have been investigated in a controlled climate chamber at the Technical University of Denmark. When exercising, the emissions from human body (breath and skin) increase significantly compared to sedentary conditions. Comparison of the emission of two human volunteers showed that there are large inter individual differences for acetone and isoprene from human breath. Possible explanations for this phenomenon are differences in the cardiac output and metabolic state.

Zusammenfassung

Atmosphärische Messungen sind wichtig, um die treibenden Kräfte des Klimawandels zu verstehen und um die Luftqualität in Außen- und Innenräumen zu beurteilen. Flüchtige organische Verbindungen (VOCs) spielen in beiden Fällen eine wichtige Rolle und werden daher mit verschiedenen Messgeräten beobachtet. Zwei gängige Techniken für die Analyse organischer Spurengase sind die Gaschromatographie-Massenspektrometrie (GC-MS) und die Protonentransferreaktion-Flugzeit-Massenspektrometrie (PTR-ToF-MS). Verschiedene atmosphärische Bestandteile wie Wasserdampf oder Ozon (O_3) können die Messungen beeinträchtigen, was zu verfälschten Daten führt. Genaue Messungen sind entscheidend für eine korrekte Datenanalyse, Interpretation und Qualitätssicherung der Daten. In diesem Promotionsprojekt wurden der Einfluss der relativen Luftfeuchtigkeit (RH), des Ozons und eines Ozonfilters auf die GC-MS- und PTR-MS-Analyse sowie einige analytspezifische, technische Fragen untersucht, um ihre Auswirkungen auf die Messungen zu bewerten und somit den Versuchsaufbau zu verbessern. Anschließend wurden die beiden Techniken zur Untersuchung von VOC Emissionen des menschlichen Körpers in Abwesenheit und Anwesenheit von Ozon und unterschiedlicher Luftfeuchtigkeit in einer kontrollierten Klimakammer eingesetzt. Die Untersuchung der Auswirkungen von atmosphärischen Bestandteilen auf gleichzeitige GC- und PTR-MS-Messungen ergab, dass Ozon zu erhöhten Signalen für einige Carbonylverbindungen und verringerten Signalen für Verbindungen mit Doppelbindungen (Isopren, Terpene) führen kann. Diese Störungen werden entweder in der Einlassleitung oder im Gerät selbst erzeugt. Um ihre Wirkung zu verringern, wurde ein Natriumthiosulfat-Ozon-Filter ($Na_2S_2O_3$) in der Einlassleitung installiert. Es wurde festgestellt, dass der Filter die Ozonkonzentration in der Probenluft unter troposphärischen Bedingungen wirksam reduziert, was zur Eliminierung der Störungen bei den meisten Analyten führt. Allerdings wurde die Messung stark ozonreaktiver Verbindungen, wie Sesquiterpene, weiterhin durch das Restozon in den Leitungen beeinflusst. Die Reinigungseffizienz war von der Ozonkonzentration, der relativen Luftfeuchtigkeit und der Durchflussrate abhängig und verbesserte sich mit zunehmender relativer Luftfeuchtigkeit. Unter typischen troposphärischen Bedingungen betrug die Lebensdauer des Ozonfilters 5 bis 14 Tage. Stratosphärische Bedingungen (hoher O_3-Gehalt und niedrige Luftfeuchtigkeit) führten zu einer unzureichenden Ozonentfernung, so dass der untersuchte Aufbau mit einem einzigen $Na_2S_2O_3$-Ozonfilter für Messungen in der unteren Stratosphäre nicht geeignet ist. Bei Experimenten in Innenräumen zur Untersuchung von VOC Emissionen des menschlichen Körpers wurden extrem hohe Signale bei PTR *m/z* 69,07 gemessen, die normalerweise Isopren zugeordnet werden. Der Vergleich mit

GC-Daten zeigte, dass das PTR durch andere Verbindungen, die auf das gleiche Masse-zu-Ladungs-Verhältnis fragmentieren, gestört wird, wenn Ozon mit menschlichen Hautfetten oder Baumwollkleidung reagiert. Die Interferenzen bei *m/z* 69,07 können von Fragmenten gesättigter C5 bis C_{10} Aldehyde stammen. Nonanal war die einzige Spezies, die zuverlässig quantifiziert werden konnte und die zur Korrektur des Signals bei *m/z* 69,07 verwendet werden konnte. Die menschlichen VOC-Emissionen wurden in einer kontrollierten Klimakammer an der Technischen Universität von Dänemark untersucht. Bei sportlicher Betätigung sind die Emissionen des menschlichen Körpers (Atem und Haut) im Vergleich zu sitzenden Tätigkeiten stark erhöht. Der Vergleich der Emissionen von zwei Freiwilligen zeigte, dass es große individuelle Unterschiede bei Aceton und Isopren aus der menschlichen Atemluft gibt. Mögliche Erklärungen für dieses Phänomen sind Unterschiede in der Herzleistung und im Stoffwechselzustand.

Contents

List of Figures

List of Tables

List of Abbreviations

VOC	**V**olatile **O**rganic **C**ompounds
BVOC	**B**iogenic **V**olatile **O**rganic **C**ompounds
OH	**H**ydr**O**xyl radical
NO	**N**itrogen **O**xide
O_2	**O**xygen
OVOC	**O**xygenated **V**olatile **O**rganic **C**ompound
UV	**U**ltra**V**iolet
6-MHO	6-**M**ethyl-5-**H**epten-2-**O**ne
4-OPA	4-**O**xo**P**entan**A**l
SOA	**S**econdary **O**rganic **A**erosol
RO_2	Organic peroxides
PTR-ToF-MS	**P**roton **T**ransfer **R**eaction-**T**ime **o**f **F**light-**M**ass **S**pectrometer
SIM	**S**ingle **I**on **M**onitoring
m/z	Mass to charge ratio
LOD	**L**imit **O**f **D**etection
HO_2	Hydroperoxy radical

Chapter 1

Introduction

1.1 Reactive atmospheric trace gases

As the name implies, atmospheric trace gases are present at very low concentrations (<1%) in the atmosphere. Nevertheless, the more reactive species play important roles in atmospheric chemistry and therefore can have a profound effect on the global oxidation capacity and climate, thereby directly affecting human well-being and health (Pandis and Seinfeld, 2006). Volatile organic compounds (*VOC*s) have been defined as being those molecules possessing a maximum of 15 carbon atoms, a boiling point below 260 °C and a vapor pressure >10 Pa at room temperature (Koppmann, 2008). VOCs have direct and indirect impacts on the earth's climate. Depending on their light absorption properties, volatility and lifetime, they can act as greenhouse gases, lead to particle formation or participate in oxidative processes that can lead to the formation or loss of atmospheric ozone (Koppmann, 2008; Pandis and Seinfeld, 2006).

1.1.1 Sources

VOCs can be released into the atmosphere from various natural and anthropogenic sources. Current global emission inventories indicate that the sum of biogenic emissions is approximately five to ten times larger than the anthropogenic release (Duan et al., 2022; *Emissions Database for Global Atmospheric Research* n.d.; Sindelarova et al., 2014). The major source of global VOC is the terrestrial biomass, particularly in the tropic, with terpenes and isoprene being the most abundant and reactive of a multitude of species. They act as a means of communication for plants and plants, plants and insects, and insects and insects; and they are understood to protect plants against heat and oxidative stress, as well as herbivory (Hoffmann, Zetzsch, and Rossi, 2007). Emission of biogenic VOC (BVOC) from vegetation is dependent on light and temperature which leads to the largest global emission being from tropical forested regions. Within the group of natural VOC sources are also volcanoes and the ocean, which both emit considerable amounts of sulfur and halogenated species. Still, the contribution of anthropogenic emission to global VOC emission is not negligible. At temperate latitudes in winter they can exceed biogenic emissions, especially in populated areas. The major source of anthropogenic VOC is the processing and use of fossil fuels.

Large amounts of gaseous organic species are released from exploitation of fossil fuels, evaporation from industry, emission from transportation as well as from biomass burning (Hoffmann, Zetzsch, and Rossi, 2007; Koppmann, 2008; Pandis and Seinfeld, 2006). VOC release from human body has only a very small contribution to the global emission (Fenske and Paulson, 1999; Veres et al., 2013) but in more constrained indoor environments these too can influence human health and well-being through chemical exposure, just like emission from buildings, furniture and other indoor materials (Salthammer et al., 2018; Sundell, 2017; Wolkoff and Nielsen, 2001).

1.1.2 Sinks

Organic gases can be removed from the atmosphere physically by wet or dry deposition or through biological uptake, photolysis as well as with oxidants such as ozone or radical reactions such as OH or NO_3. VOC removal through chemical oxidation reactions can either lead to the formation of particles or produce diverse gaseous product species which can react further, ultimately to CO_2 and H_2O. The hydroxyl radical (HO) plays a major role as a sink for organic reactive species in the atmosphere. It is formed by the reaction of an excited oxygen atom (O^1D) with a water molecule in the presence of sunlight (Lelieveld et al., 2016; Levy, 1971).

$$O_3 \xrightarrow{h\nu} O_2 + O^* \tag{1.1}$$

$$O^* + H_2O \longrightarrow 2\,HO^\bullet \tag{1.2}$$

Other oxidative species such as ozone (O_3), nitrate (NO_3) and halogen (Cl, Br) radicals can also lead to gas phase oxidation of VOCs, but to a smaller extent (Atkinson, 1994; Koppmann, 2008; Pandis and Seinfeld, 2006).

$$RH + OH^\bullet \longrightarrow R^\bullet + H_2O \tag{1.3}$$

$$R^\bullet + O_2 \xrightarrow{M} RO_2{}^\bullet \tag{1.4}$$

$$NO + RO_2{}^\bullet \longrightarrow NO_2 + RO^\bullet \tag{1.5}$$

$$RO^\bullet + O_2 \longrightarrow R'CHO + HO_2{}^\bullet \tag{1.6}$$

$$NO + HO_2{}^\bullet \longrightarrow NO_2 + OH^\bullet \tag{1.7}$$

$$NO_2 \xrightarrow{h\nu} NO + O(^3P) \tag{1.8}$$

$$O(^3P) + O_2 \longrightarrow O_3 \tag{1.9}$$

$$RH + 3\,O_2 + NO \xrightarrow{h\nu} R'CHO + O_3 + NO_2 + H_2O \tag{1.10}$$

Reaction of OH with hydrocarbons in air (in Equation 1.4 described with M) leads to an organic radical (R) species and water (equation 1.3). Those organic radicals react further with O_2 to form organic peroxy radicals (RO_2), which are again a very reactive species that can react further with nitric oxide (NO) and O_2 to form carbonyls and other oxygenated species (Equations 1.4-1.6). Those OVOCs (oxygenated volatile organic compounds) usually have

different physical and chemical properties (e.g. solubility) than their precursor molecules due to their different chemical structure. Again, they can react, be removed through deposition processes or aggregate to secondary organic aerosol particles (SOA). (Finlayson-Pitts and Pitts Jr, 1999)

$$HO_2^{\bullet} + O_3 \longrightarrow OH^{\bullet} + 2\,O_2 \tag{1.11}$$

Hydroperoxy radicals (HO_2) are formed as a by-product of the OVOC formation and these can react to form ozone when NO is present (Equations 1.7-1.9). The reaction of HO_2 with NO or O_3 also serves to recycle the OH radial, allowing oxidation cycles to continue. As previously mentioned, ozone is another reactant for gas phase oxidation of VOCs, more details can be found in the next section. Without NO, O_3 is destroyed (Equation 1.11) while generating OH again. If NO is present at levels around 100 ppt or above then ozone will be photochemically formed. As we can see from the chemical reactions above, reactive VOCs are driving the chemistry of the atmosphere. With their atmospheric lifetimes ranging from minutes to several decades they influence oxidation chemistry on many scales, as well the Earth's radiative budget and climate.

1.2 Ozone chemistry

Within the earth's atmosphere, ozone has different roles depending on the atmospheric layer in which it is found. The troposphere contains only a small amount ($\sim$ 10%) of the total atmospheric ozone, mixing ratios in the boundary layer range from tens of ppb (*parts per billion*) to 200 ppb, with tropospheric background levels around 30 ppb. The presence of tropospheric O_3 has generally negative effects on humans and plants. It can cause inflammation in the human respiratory tract and oxidatively stress vegetation leading to reduced crop yields. Moreover, on a global scale it can act as a greenhouse gas absorbing outgoing radiation. In contrast, stratospheric ozone is essential for life on earth as it absorbs high energy ultraviolet (*UV*) radiation from the sun. About 90 % of the total ozone is located in the stratosphere, with concentrations up to 10 ppm in the ozone layer (20-30 km height) (Pandis and Seinfeld, 2006).
In outdoor as well as indoor air chemistry, ozonolysis of alkenes leads to the formation of carbonyl compounds. The reaction mechanism is shown in reaction 1.1. When ozone is added to a carbon-carbon double bond, a primary ozonide is formed, which decomposes to a carbonyl compound and a carbonyl oxide (Criegee intermediate), a bi-radical species. The Criegee intermediate can first isomerize, dissociate and rearrange or directly form carbonyls through further reaction. Hence, ozonolysis can lead to various carbonyl products.

In indoor environments, the reaction of ozone with human skin oil, clothing and building materials leads to a decrease in indoor ozone concentration

[1] Adapted from https://commons.wikimedia.org/w/index.php?curid=3472536 by RedAndr, CC BY-SA 4.0.

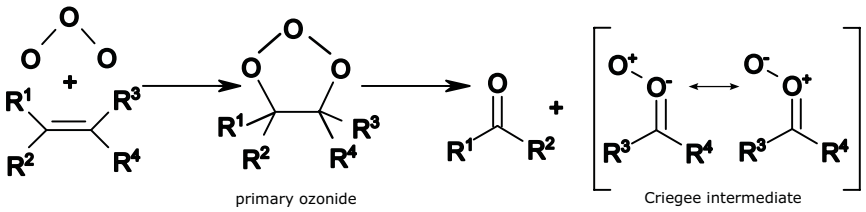

FIGURE 1.1: Alkene ozonolysis.[1]

(relative to outdoors) but an increase the amount of chemicals with functional groups in the indoor air. In occupied indoor environments, especially ozonolysis reaction with squalene plays an important role. Squalene is one of the main constituents of human skin oil. On a molar basis, roughly half of the unsaturated carbon bonds in human skin surface lipids are from squalene (Weschler, 2016). When reacting with ozone, several carbonyls with potential adverse health effects are produced (Weschler, 2016; Weng et al., 2009; Zhang, Lioy, and He, 1994). Primary carbonyl products such as acetone, 6-methyl-5-hepten-2-one (6-MHO) and geranyl acetone are generated in this first step. Furthermore, if these products still contain carbon-carbon double bonds, they can react further with O_3 to form secondary products. The most abundant secondary product of the reaction of squalene and ozone is 4-oxo-pentanal (4-OPA), which is known to be a pulmonary irritant (Weschler, 2016).

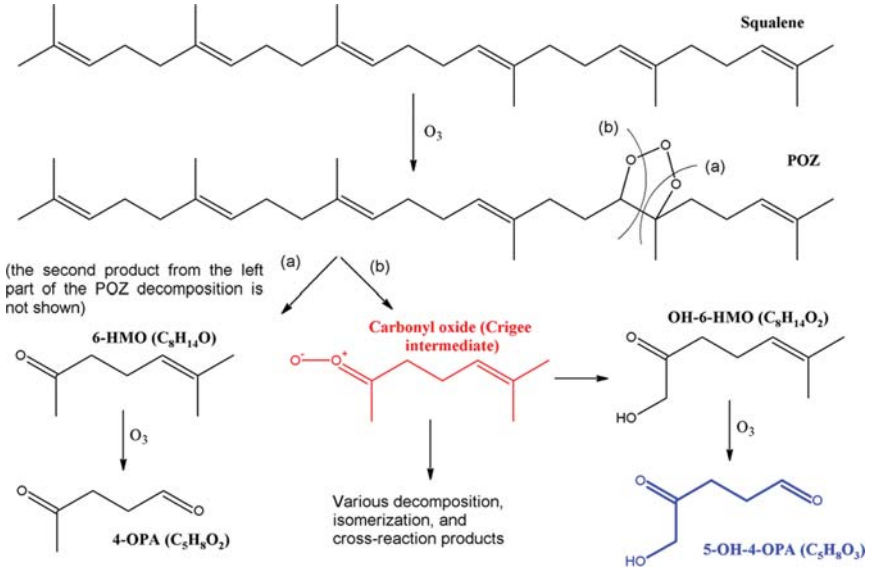

FIGURE 1.2: Scheme of squalene ozonolysis.[2]

[2]From Fooshee et al. (2015), page 2.

1.2.1 Influence of Ozone on VOC measurements

The presence of ozone can also adversely impact the quality of VOC measurements due to its highly oxidative nature. Besides reaction with compounds adsorbed to the walls of the instrument's inlet tubing, oxidation during pre-concentration or with the instrument's inner surfaces can occur and lead to positive and negative interference of the target analytes. (Apel et al., 2003; Ernle, Ringsdorf, and Williams, 2023; Koppmann et al., 1995; Northway et al., 2004; Pollmann, Ortega, and Helmig, 2005). For analytical techniques with pre-concentration, ozone scrubbers are commonly used to avoid ozone entering the sampling setup, reacting with the immobilized analytes during pre-concentration and compromising the measurement (Fick et al., 2001; Holfmann, 1995; Pollmann, Ortega, and Helmig, 2005). In contrast, for online techniques ozone scavenging is not often applied as it is assumed that the interference from ozone is negligible due to short reaction times in the gas phase inside the measurement device. However, Apel et al.2003 and Northway et al.2004 have independently shown that interference can be induced by ozonolysis reaction of compounds which are immobilized on the inner walls of the measurement system.

1.3 Indoor air

It is important to monitor the indoor air quality as humans spend most of their time indoors (Klepeis et al., 2001; Weschler, 2009). Additionally, pollutants in indoor air are much more likely to be inhaled at higher concentrations than outdoors. This is due to the usually low air change rate in typical indoor environments (ca. 0.7 h^{-1}) (Nazaroff, Weschler, and Corsi, 2003; Yamamoto et al., 2010). Besides emissions from building materials, furnishings and the chemical compounds entering from the outside, the occupants indoors have a considerable impact on the indoor air quality and chemistry. Human beings emit gases such as CO_2 but also several hundred VOCs via breath and skin. Additionally, they wear clothing and perform various actions indoors (such as cooking, cleaning, eating, exercising, etc.) all of which lead to further VOC emissions. Emitted species can react with oxidants such as ozone or the hydroxyl radical, creating oxidized species which can have adverse health effects: 6-MHO and 4-OPA are both gas phase products from squalene ozonolysis that are respiratory irritants (Anderson et al., 2012; Wolkoff et al., 2013). Literature reports huge differences in the human emission of some compounds emitted via breath such as isoprene or acetone (Anderson, 2015; King et al., 2010; Španěl et al., 2011). Those differences can be due to different metabolic state, food and drink, health or induced through actions like exercising or fasting (Anderson, 2015; King et al., 2009; Senthilmohan et al., 2000; Smith, Spanel, and Davies, 1999). The exact reasons for and the extent of those inter human differences are not yet completely understood. A detailed understanding of the indoor air chemistry is needed to predict indoor air quality and establish methods to keep it high, especially during occupancy.

1.4 Instrumentation

1.4.1 Fast GC-MS

Gas chromatography-mass spectrometry (GC-MS) is a standard technique for VOC measurements. The advantage of chromatographic techniques compared to other online methods (e.g. PTR-MS) is, that the compounds are separated before detection. Thus, isomeric compounds such as acetone and propanal can be identified individually. In gas chromatography, compounds are separated due to interaction with a stationary phase (immobilized on the chromatographic column) and according to their boiling point. More interaction with the stationary phase and higher boiling points lead to later elution from the separation column. The here presented fast GC-MS system was previously described in detail by Bourtsoukidis et al. A schematic picture of the main parts is shown in Figure 1.3. Enrichment of the target analytes is performed with a cryogenic pre-concentration unit prior to injection of the analytes onto the chromatographic column. The pre-concentration is a three-step process using stainless steel traps for (a) water removal, (b) enrichment and (c) focusing. Due to minimized thermal masses, the heating rate of the cryo trap is extremely fast (100°C/min) and assures rapid injection, leading to sharp peaks at the beginning of the chromatogram. The silico-steel transfer lines between the traps are heated to approximately 50-60°C to avoid condensation and line losses. Usually, for commercial GC-MS systems the following gas chromatographic separation takes between 15 and 120 min. The fast GC-MS used in the here presented studies has a separation time of 2.5 min (total cycle time 3 min). This could be achieved using a custom-built oven with minimized thermal masses able to generate rapid cooling rates (ca. 30°Cs^{-1}, a detailed description of the oven can be found in Bourtsoukidis et al.). After elution from the GC column, the analytes enter a quadrupole mass spectrometer which was operated in single ion monitoring (SIM) mode. In contrast to the full scan mode, in SIM mode, only a preset mass to charge ratio (m/z) range can be detected, but the sensitivity is much improved (Desiderio, Nibbering, and Kraj, 2008). The fast GC-MS instrument used in this thesis measures highly volatile organic compounds including alkenes, aldehydes, ketones halogenated and sulfur compounds as well as nitrogen containing species and small aromatic compounds like benzene and chlorobenzene.

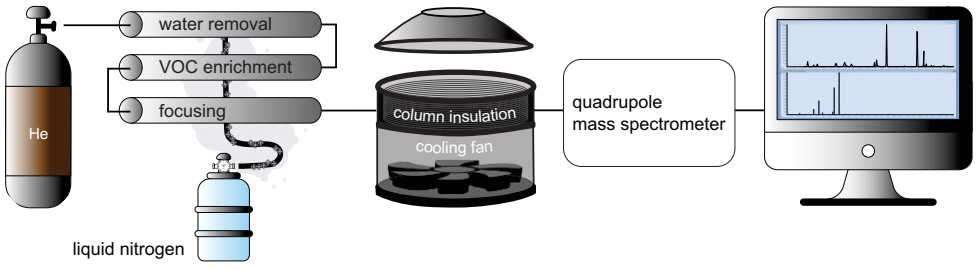

FIGURE 1.3: Schematic overview of the fast GC-MS system.

FIGURE 1.4: Fast GC-MS instrument while being filled with liquid nitrogen for pre-concentration prior to flight.

The mass range which can be measured by the instrument is limited by the short separation time of 2.5 min. Bromoform was the compound with the highest molecular mass that could be measured within 3 min cycle time. For the calibration, a multi-component gas cylinder (Apel-Riemer, USA) has been used. A five-point full calibration was usually performed before and after each experimental day. Additionally one-level calibration points have been measured every 2 h to monitor the instrument performance. Limits of detection (LOD) were in the lower ppt range (usually 2-50 ppt) and the total measurement uncertainty usually $\leq$ 10%. The total measurement uncertainty was calculated using error propagation and includes the uncertainties of the calibration gas standard, volumes and flows in the system, the calibration curve, the measured mixing ratio, and from the peak integration.

Data analysis

An in-house written software code for the data anlysis program IGOR (Wavemetrics) has been used for the automatic peak integration. It is based on the Igor-built-in Levenberg-Marquardt algorithm, (which is itself based on the least-squares method). The Igor software compares a reference (calibration gas) sample with the ambient sample using *m/z* ratio, retention time and peak shape from the reference chromatogram for peak identification and integration. As the fast GC-MS sometimes shows large retention time shifts, automatic retention time correction is an important feature. This correction is based on matching peak groups in calibration gas and ambient samples. For extreme shifts (usually only occurring when instrumental issues arise

due to some parts reaching the end of their lifetime (e.g. the extremely thin cold-trap thermocouples)) the automated retention time correction can be adjusted manually. The whole automatic integration process can be observed in the software, making it easy to spot any imperfect peak integration. For data analysis a custom-built Python code has been used which can be found in appendix A. First, the code extracts sample volume, sampling time, average calibration standard gas and zero air flows per sample from the instruments' log files (mergeV25Igor.py). This data is then merged with the results from the Igor peak integration. For both, calibration and sample data, the area from the peak integration is normalized by the sample volume. The code for the calibration data (CalOutlier.py) labels potential outliers by calculating a modified z-score (*Iglwicz and Hoaglin outlier test* n.d.), followed by a generalized extreme Studentized deviate (ESD) test for outlier identification (*generalized ESD test for outliers* n.d.). Average background mixing ratios and mixing ratios for the calibration points are calculated. Linear regression of the calibration data is performed, for each analyte, the data including the regression line is plotted with Python's matplotlib. Figure 1.5 shows as an example the linear regression plot for propanal. The results of the linear regression are also printed into a calibration output file, which is used by the code for the sample data (timeline.py) to calculate the ambient air mixing ratios. Additionally, the total measurement uncertainty is calculated, including the uncertainties of the linear regression, the measured mixing ratio, the volumes in GC and calibration system, the mixing ratio in the calibration gas cylinder, and from the peak integration (which is a built-in Igor function). For the timeline plot, the mixing ratio is plotted against the sampling time. Two separate plots are produced, one including ambient, zero, and calibration gas samples and a second one showing only the ambient data, but together with

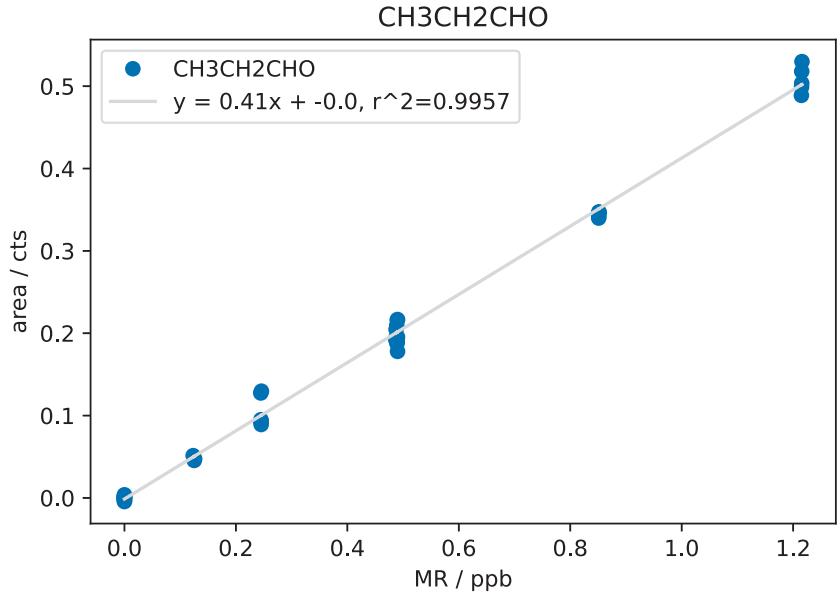

FIGURE 1.5: Linear regression plot from Python code for propanal.

its uncertainty (Figure 1.6).

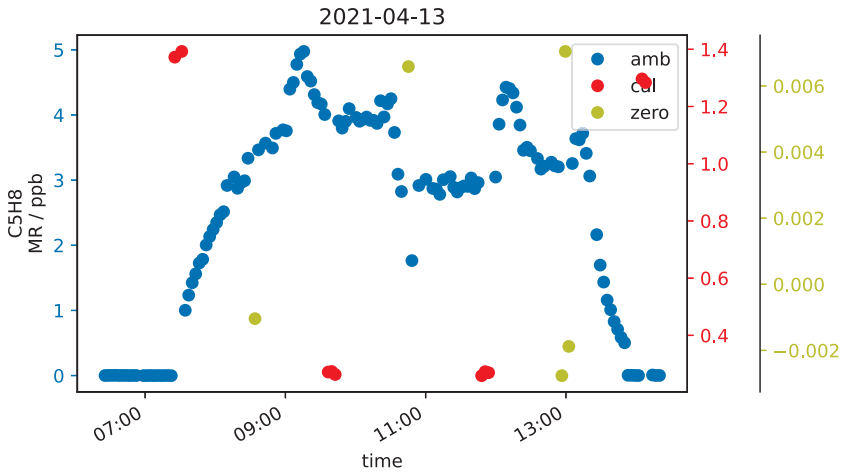

(A)

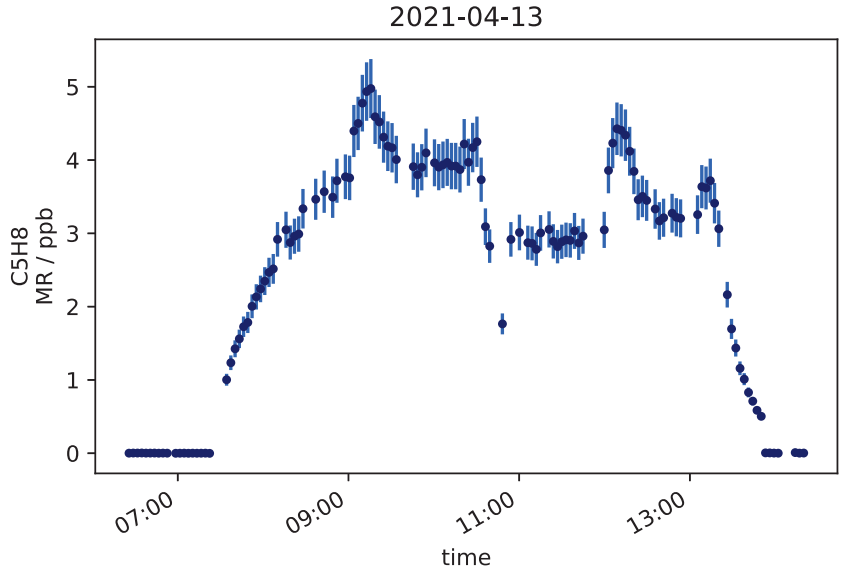

(B)

FIGURE 1.6: Timeline plots for isoprene from the Python data analysis (A) including ambient (blue dots), zero (yellow dots) and calibration (red dots) data and (B) only ambient data with error bars showing the total measurement uncertainty of the data points.

1.4.2 PTR-ToF-MS

Proton transfer reaction time-of-flight mass spectrometry (PTR-ToF-MS) is a technique commonly used for VOC analysis in indoor and outdoor environments. It uses a rather soft ionization technique, resulting in little fragmentation during the detection process. However, depending on the properties

of the analytes and the instrumental settings some fragmentation can still occur. The PTR-MS system used in the here presented studies (PTR-MS 8000, IONICON Analytik, Austria) was operated with H_3O^+ as the primary ions. It is possible to ionize compounds with a proton affinity higher than water (691 kJ mol^{-1}). During the ionization process a proton from the H_3O^+ ions is transferred to the analyte in the drift tube, usually resulting in a protonated molecular ion (MH^+). In the following reflectron time-of-flight area (see Figure 1.7), the ions need different times to reach the detector. In the ionization stage each iion is given the same amount of kinetic energy but because the ions have different masses, they also have different velocities. The time to reach the detector depends on the mass-to-charge ratio: smaller ions are faster than heavier ions. PTR-ToF-MS is a technique with high sensitivity, a wide range mass spectrum (*m/z* 1-500) and high time resolution ($\geq$ 10 Hz) (Graus, Müller, and Hansel, 2011; Jordan et al., 2009). In the presented studies, the mass resolution ($m/\Delta m$) was 4000-5000. With such high mass resolution, the exact mass can be used for identification, which helps identify nominally isobaric compounds with small exact mass differences. Calibrations using a multi-component standard gas cylinder (Apel-Riemer, USA) were usually performed at the beginning, in the middle and end of an experimental series. For VOCs which were absent in the standard gas mixtures, the mixing ratios were calculated with a theoretical method using the proton transfer rate coefficient (*k*-rate) (Cappellin et al., 2012). Raw ion signals were normalized by the sum of the primary ions (H_3O^+) and the first water cluster ($(H_2O)_2H^+$). LODs (3σ) were typically $\leq$ 0.015 ppb with a total measurement uncertainty $\leq$ 15%.

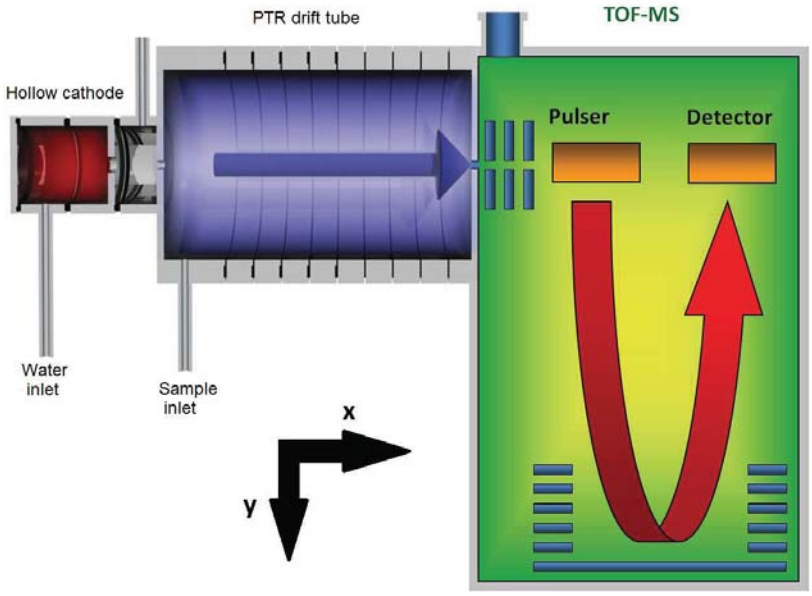

FIGURE 1.7: Schematic setup of a PTR-ToF-MS instrument (Müller et al., 2008).

1.5 Open research questions and thesis outline

Volatile organic compounds have an influence on the global climate, air quality and can also have adverse health effects (Crutzen and Lelieveld, 2001; Williams, 2004). Thus, accurate VOC measurements in indoor and outdoor environments are of great importance. The development of stable, accurate and reliable measurement techniques, as well as the identification of potential interferences can help improve data quality, comparability and interpretation. Technical studies contribute strongly to critical thinking about results and may help identify problems in datasets. GC-MS as well as PTR-MS are common techniques used for VOC identification and quantification. PTR-MS has a very high time resolution and sensitivity, perfectly suited for online measurements as real time changes in mixing ratio can be detected. However, PTR-MS with H_3O^+ as the primary ions cannot distinguish between isomeric compounds such as acetone and propanal. Fortunately, GC-MS is capable of separating isomers and compounds with the same (exact) mass before detection, albeit with lower time resolution. Hence, the two measurement techniques complement one another perfectly. PTR-ToF-MS and fast GC-MS are the two techniques mainly used in this PhD project. Due to their capability to (quasi) online monitor VOC mixing ratios, they have been used to measure human VOC emission indoors. However, some compounds show large day-to-day variations and differences in emission from various humans. This is the case especially for compounds which are abundant in human breath. Those inter human differences in emission are not yet well understood (Fenske and Paulson, 1999; King et al., 2009; Sun et al., 2017). They may be the result of exogenous factors such as what the person has eaten or drunk in the recent past, or be endogenous depending more on innate metabolic functions within the human body. The understanding can be improved with the amount of data collected, thus with an increased number of studies on human emissions.

Chapter 2 focuses on atmospheric (O_3 and RH) and technical influences ($Na_2S_2O_3$ scrubber) on measurements with PTR-MS in H_3O^+ mode and fast GC-MS. It is known, that ozone and humidity can affect the measurement of both instruments. Ozonolysis of the target analytes particularly affects techniques with pre-concentration prior to detection like for example GC-MS (Helmig, 1997; Koppmann et al., 1995). Furthermore, artifacts can be generated due to reaction with ozone in the instrument inlet lines (Apel et al., 2003; Northway et al., 2004) or due to water vapour in the sample gas which can condense inside the measurement setup and interfere especially with hydrophilic analytes. Both, ozone concentration and relative humidity vary in indoor and outdoor environments. Therefore, their influence on the measurement needs to be well known. In **Chapter 2** the influence of O_3 and RH on GC-MS and PTR-MS measurements is investigated. The removal of ozone with a sodium thiosulfate scrubber within the measurement setup has been tested at different relative humidity and it has been studied whether the scrubber itself also influences the VOC measurement. Additionally, the scrubber endurance has been tested under dry and humid conditions.

Based on the results a recommendation for the maximum usage time for the $Na_2S_2O_3$ scrubber is given.

Chapter 3 focuses on interferences on PTR *m/z* 69.071. This mass to charge ratio is usually used for isoprene detection in PTR with H_3O^+ primary ions. Isoprene is a reactive alkene which is abundant in outdoor and indoor environments. It is emitted by vegetation and via human breath. Isoprene plays an important role in the gas phase chemistry of the atmosphere as it can react with oxidant species such as OH and ozone, producing carbonyl species which may react further. PTR isoprene measurements can suffer interference by fragments of aldehydes with the same exact mass (*m/z* 69.071) (Ruzsanyi et al., 2013). These compounds are also present in indoor environments, especially when O_3 is present (Weschler, 2016). Chapter 3 studies the fragmentation patters of C5-C10 saturated aldehydes in our PTR-ToF-MS. The fragment ratios from the fragmentation experiment are compared with the same ratios in a study of occupied indoor air measurements, which was performed at the Technical University of Denmark (DTU). This comparison determined whether the aldehydes can be quantified in the presented indoor air measurements and whether the measured *m/z* 69.071 signal can be corrected for the aldehydes' interference. The effect of nonanal on the PTR-isoprene signal has been quantified and the nonanal corrected isoprene signal has been compared with GC-MS isoprene measurements.

Chapter 4 studies the emission of two human volunteers during different levels of physical exercise (walking and running) without ozone and under the presence of ozone. Emissions are higher during exercise due to factors like increased breathing rate, cardiac output and sweating. The results from the two subjects are compared and inter human differences in emission and between the different levels of ozone are discussed based on current knowledge. This study expands the data pool on human emission during exercise and inter individual differences. It can help interpret data from indoor environments where humans perform exercise, which is particularly interesting nowadays, as gyms and exercise at home (especially since the pandemic) are gaining popularity. The data shows how human emission during exertion affects the indoor air composition relative to the sedentary condition and how it can be influenced by inter individual differences, particularly from breath related compounds.

References

Anderson, Joseph C (2015).
"Measuring breath acetone for monitoring fat loss".
In: *Obesity* 23.12, pp. 2327–2334.

Anderson, Stacey E et al. (2012). "Irritancy and allergic responses induced by exposure to the indoor air chemical 4-oxopentanal".
In: *Toxicological Sciences* 127.2, pp. 371–381.

Apel, EC et al. (2003). "A fast-GC/MS system to measure C2 to C4 carbonyls and methanol aboard aircraft".
In: *Journal of Geophysical Research: Atmospheres* 108.D20.

Atkinson, Roger (1994).
"Gas-phase tropospheric chemistry of volatile organic compounds".
In: *J. Phys. Chem. Ref. Data Monog* 2, pp. 11–216.

Bourtsoukidis, Efstratios et al. (2017).
"An aircraft gas chromatograph–mass spectrometer System for Organic Fast Identification Analysis (SOFIA): design, performance and a case study of Asian monsoon pollution outflow".
In: *Atmospheric Measurement Techniques* 10.12, pp. 5089–5105.

Cappellin, Luca et al. (2012). "On quantitative determination of volatile organic compound concentrations using proton transfer reaction time-of-flight mass spectrometry".
In: *Environmental science & technology* 46.4, pp. 2283–2290.

Crutzen, Paul J and Jos Lelieveld (2001).
"Human impacts on atmospheric chemistry".
In: *Annual review of earth and planetary sciences* 29.1, pp. 17–45.

Desiderio, Dominic M, Nico M Nibbering, and Agnieszka Kraj (2008).
Mass spectrometry: instrumentation, interpretation, and applications.
John Wiley & Sons.

Duan, Chensong et al. (2022). "The research hotspots and trends of volatile organic compound emissions from anthropogenic and natural sources: A systematic quantitative review". In: *Environmental Research*, p. 114386.

Emissions Database for Global Atmospheric Research (n.d.).
https://edgar.jrc.ec.europa.eu/. Accessed: 2023-07-02.

Ernle, Lisa, Monika Akima Ringsdorf, and Jonathan Williams (2023).
"Influence of ozone and humidity on PTR-MS and GC-MS VOC measurements with and without a Na 2 S 2 O 3 ozone scrubber".
In: *Atmospheric Measurement Techniques* 16.5, pp. 1179–1194.
DOI: https://doi.org/10.5194/amt-16-1179-2023.

Fenske, Jill D and Suzanne E Paulson (1999).
"Human breath emissions of VOCs".
In: *Journal of the Air & Waste Management Association* 49.5, pp. 594–598.

Fick, Jerker et al. (2001).
"Ozone removal in the sampling of parts per billion levels of terpenoid compounds: An evaluation of different scrubber materials".
In: *Environmental science & technology* 35.7, pp. 1458–1462.

Finlayson-Pitts, Barbara J and James N Pitts Jr (1999). *Chemistry of the upper and lower atmosphere: theory, experiments, and applications*. Elsevier.

Fooshee, David R et al. (2015).
"Atmospheric oxidation of squalene: molecular study using COBRA modeling and high-resolution mass spectrometry".
In: *Environmental science & technology* 49.22, pp. 13304–13313.

generalized ESD test for outliers (n.d.).
https://github.com/bhattbhavesh91/outlier-detection-grubbs-test-and-generalized-esd-test-python/blob/master/generalized-esd-test-for-outliers.ipynb. Accessed: 2019-12-23.

Graus, Martin, Markus Müller, and Armin Hansel (2011). "High resolution PTR-TOF: quantification and formula confirmation of VOC in real time".
In: *Journal of the American Society for Mass Spectrometry* 21.6, pp. 1037–1044.

Helmig, Detlev (1997). "Ozone removal techniques in the sampling of atmospheric volatile organic trace gases".
In: *Atmospheric Environment* 31.21, pp. 3635–3651.

Hoffmann, T., C. Zetzsch, and M. J. Rossi (2007). "Chemie von Aerosolen".
In: *Chemie in unserer Zeit* 41.3, pp. 232–246.

Holfmann, T (1995).
"Adsorptive preconcentration technique including oxidant scavenging for the measurement of reactive natural hydrocarbons in ambient air".
In: *Fresenius' journal of analytical chemistry* 351, pp. 41–47.

Iglwicz and Hoaglin outlier test (n.d.). https://gist.github.com/Szuuuken/1c9fc3ab9d08d6a12bad5b929cbb5a46. Accessed: 2019-12-23.

Jordan, A et al. (2009).
"A high resolution and high sensitivity proton-transfer-reaction time-of-flight mass spectrometer (PTR-TOF-MS)".
In: *International Journal of Mass Spectrometry* 286.2-3, pp. 122–128.

King, Julian et al. (2009). "Isoprene and acetone concentration profiles during exercise on an ergometer".
In: *Journal of breath research* 3.2, p. 027006.

King, Julian et al. (2010). "Dynamic profiles of volatile organic compounds in exhaled breath as determined by a coupled PTR-MS/GC-MS study".
In: *Physiological measurement* 31.9, p. 1169.

Klepeis, Neil E et al. (2001).
"The National Human Activity Pattern Survey (NHAPS): a resource for assessing exposure to environmental pollutants". In: *Journal of Exposure Science & Environmental Epidemiology* 11.3, pp. 231–252.

Koppmann, R et al. (1995). "The influence of ozone on light nonmethane hydrocarbons during cryogenic preconcentration".
In: *Journal of Geophysical Research: Atmospheres* 100.D6, pp. 11383–11391.

Koppmann, Ralf (2008). *Volatile organic compounds in the atmosphere*. John Wiley & Sons.

Lelieveld, J. et al. (2016). "Global tropospheric hydroxyl distribution, budget and reactivity". In: *Atmospheric Chemistry and Physics* 16.19, pp. 12477–12493.

Levy, H (1971). "Normal atmosphere: Large radical and formaldehyde concentrations predicted". In: *Science* 173.3992, pp. 141–143.

Müller, M et al. (2008). *Cotributing Efforts to ASCOS using the Proton Transfer Reaction Technique for VOC Analysis*. EGU, ASCOS pre-expedition workshop. URL: https://slideplayer.com/slide/4792461/.

Nazaroff, William W, Charles J Weschler, and Richard L Corsi (2003). "Indoor air chemistry and physics". In: *Atmospheric Environment* 37, pp. 5451–5453.

Northway, MJ et al. (2004). "Evaluation of the role of heterogeneous oxidation of alkenes in the detection of atmospheric acetaldehyde". In: *Atmospheric Environment* 38.35, pp. 6017–6028.

Pandis, Spyros N and John H Seinfeld (2006). *Atmospheric chemistry and physics: From air pollution to climate change*. Wiley.

Pollmann, Jan, John Ortega, and Detlev Helmig (2005). "Analysis of atmospheric sesquiterpenes: Sampling losses and mitigation of ozone interferences". In: *Environmental science & technology* 39.24, pp. 9620–9629.

Ruzsanyi, Veronika et al. (2013). "Multi-capillary-column proton-transfer-reaction time-of-flight mass spectrometry". In: *Journal of Chromatography A* 1316, pp. 112–118.

Salthammer, Tunga et al. (2018). "Assessing human exposure to organic pollutants in the indoor environment". In: *Angewandte Chemie International Edition* 57.38, pp. 12228–12263.

Senthilmohan, Senti T et al. (2000). "Quantitative analysis of trace gases of breath during exercise using the new SIFT–MS technique". In: *Redox Report* 5.2-3, pp. 151–153.

Sindelarova, Katerina et al. (2014). "Global data set of biogenic VOC emissions calculated by the MEGAN model over the last 30 years". In: *Atmospheric Chemistry and Physics* 14.17, pp. 9317–9341.

Smith, David, Patrik Spanel, and Simon Davies (1999). "Trace gases in breath of healthy volunteers when fasting and after a protein-calorie meal: a preliminary study". In: *Journal of applied physiology* 87.5, pp. 1584–1588.

Španěl, Patrik et al. (2011). "Breath acetone concentration; biological variability and the influence of diet". In: *Physiological Measurement* 32.8, N23.

Sun, Meixiu et al. (2017). "Continuous monitoring of breath acetone, blood glucose and blood ketone in 20 type 1 diabetic outpatients over 30 days". In: *J. Anal. Bioanal. Tech* 8, pp. 2155–9872.

Sundell, J (2017). "Reflections on the history of indoor air science, focusing on the last 50 years". In: *Indoor Air* 27.4, pp. 708–724.
Veres, Patrick R et al. (2013). "Anthropogenic sources of VOC in a football stadium: Assessing human emissions in the atmosphere". In: *Atmospheric Environment* 77, pp. 1052–1059.
Weng, Mili et al. (2009). "Levels and health risks of carbonyl compounds in selected public places in Hangzhou, China". In: *Journal of Hazardous Materials* 164.2-3, pp. 700–706.
Weschler, Charles J (2009). "Changes in indoor pollutants since the 1950s". In: *Atmospheric environment* 43.1, pp. 153–169.
— (2016). "Roles of the human occupant in indoor chemistry". In: *Indoor air* 26.1, pp. 6–24.
Williams, Jonathan (2004). "Organic trace gases in the atmosphere: an overview". In: *Environmental Chemistry* 1.3, pp. 125–136.
Wolkoff, Peder and Gunnar D Nielsen (2001). "Organic compounds in indoor air—their relevance for perceived indoor air quality?" In: *Atmospheric Environment* 35.26, pp. 4407–4417.
Wolkoff, Peder et al. (2013). "Human reference values for acute airway effects of five common ozone-initiated terpene reaction products in indoor air". In: *Toxicology letters* 216.1, pp. 54–64.
Yamamoto, N et al. (2010). "Residential air exchange rates in three major US metropolitan areas: results from the Relationship Among Indoor, Outdoor, and Personal Air Study 1999–2001". In: *Indoor air* 20.1, pp. 85–90.
Zhang, Junfeng, Paul J Lioy, and Qingci He (1994). "Characteristics of aldehydes: concentrations, sources, and exposures for indoor and outdoor residential microenvironments". In: *Environmental science & technology* 28.1, pp. 146–152.

Chapter 2

Influence of O_3, RH and a $Na_2S_2O_3$ ozone scrubber on PTR-MS and GC-MS measurements

This chapter has been published as: Lisa Ernle, Monika Akima Ringsdorf, and Jonathan Williams (2023). "Influence of ozone and humidity on PTR-MS and GC-MS VOC measurements with and without a Na 2 S 2 O 3 ozone scrubber". In: *Atmospheric Measurement Techniques* 16.5, pp. 1179–1194. DOI: https://doi.org/10.5194/amt-16-1179-2023

Contribution to this publication by Lisa Ernle: *Designed the experiment, conducted the GC-MS measurements, performed the data analysis and prepared the manuscript.*

Abstract. The measurement of volatile organic compounds (VOCs) can be influenced by ozone (O_3), resulting in sampling artifacts that corrupt the data obtained. Published literature reports both, positive (false enhancements of signal) and negative (loss of signal) interference in VOC data due to ozonolysis occurring in the sample gas. To assure good data quality it is essential to be aware of such interfering processes, characterize them and try to minimize the impact with a suitable sampling setup. Here we present results from experiments with a sodium thiosulfate ozone scrubber ($Na_2S_2O_3$), which is a cost effective and easily applied option for O_3 scavenging during gas phase sampling. Simultaneous measurement of selected organic trace gases using gas chromatography- and proton transfer reaction-mass spectrometry was performed at different ozone levels (0-1 ppm) and different relative humidities (0-80 %). In this way both tropospheric and stratospheric conditions were examined. The measured data show that several carbonyl compounds including acetaldehyde, acetone and propanal show artificial signal enhancement when ozone is present at higher concentrations (>150 ppb) in dry air, while analytes with double bonds like isoprene (measured with GC-MS) and terpenes show lower signals due to reaction with ozone. Both effects can be eliminated or in the case of sesquiterpenes substantially reduced by using $Na_2S_2O_3$ impregnated quartz filters in the inlet line. With the chosen scrubbing material, relative humidity (RH) substantially improves the scrubbing efficiency. Under surface conditions between 50-80 % RH, the filter allows accurate measurement of all species examined.

2.1 Introduction

Volatile organic compounds (VOCs) are trace atmospheric constituents usually present at mixing ratios of parts per billion (ppb) or lower in the earth's atmosphere. Nevertheless, they can have a considerable impact on the global air chemistry, climate and influence the health of living organisms on the earth's surface (Crutzen and Lelieveld, 2001; Williams, 2004). Organic trace gases can act as greenhouse gases, contribute to particle formation and take part in photochemical oxidation processes that influence ozone. Additionally many VOCs are also considered to be contaminants of the indoor environment where human exposure to such chemicals can be high (Weschler and Carslaw, 2018). VOC sources can be of natural (plants, phytoplankton, volcanoes, etc.) or anthropogenic origin (e.g. fossil fuel combustion, agriculture, industry) (Koppmann, 2008; McDonald et al., 2018; Weschler and Shields, 1997). To understand the chemical reactions and processes in outdoor as well as indoor environments, it is essential to accurately quantify the VOCs in the air.

Common analytical techniques for sampling organic trace gases are proton-transfer-reaction mass spectrometry (PTR-MS) and gas chromatography-mass spectrometry (GC-MS). With these measurement techniques a wide range of volatile organic compounds can be measured including aliphatic and aromatic hydrocarbons, oxygenated and halogen containing species (Koppmann, 2008; Warneck and Williams, 2012). However, research has shown that due to

the reactivity of some analytes to ozone, measurements can be rendered inaccurate, as already reported by Helmig (1997) more than twenty years ago. Ozone can influence VOC measurements either due to reaction with the target analytes during sampling, which particularly affects techniques with preconcentration steps prior to analysis (Helmig, 1997; Koppmann et al., 1995; Pollmann, Ortega, and Helmig, 2005), or by generating sampling artifacts in the inlet of an online instrument. Northway et al. and Apel et al. reported for example increased mixing ratios for acetaldehyde in their systems for measurements in the lower stratosphere where ozone levels are high and humidity is low. Ozone and water are omnipresent in the troposphere with mixing ratios between 10 and 200 ppb (ozone) and humidities (10-100 %). Stratospheric O_3 is essential for life on planet earth as it absorbs high energy solar UV radiation. It is formed in the stratosphere through the photolysis of oxygen, which generates mixing ratios between 1-10 ppm. While such processes generate the protective ozone layer in the stratosphere, at ground level this oxidative gas is considered to be a pollutant as it is detrimental to the human respiratory tract and damages plants (Pandis and Seinfeld, 2006). Being present in both the troposphere and stratosphere, albeit at different concentrations, ozone can potentially affect VOC measurements made at the ground and from high flying aircraft. The two instruments examined in this study are regularly installed on an aircraft capable of reaching ca. 15 km which at mid-latitudes gives access to the lower stratosphere. Also in indoor environments where ozone is typically 3-5 times less than outside ambient levels, it may affect the measurement fidelity.
Sodium thiosulfate ($Na_2S_2O_3$) has been reported to have a good ozone scrubbing efficiency for VOC measurements (Lehmpuhl and Birks, 1996; Pollmann, Ortega, and Helmig, 2005) and was therefore chosen as the best test material for O_3 removal in the experiments described here. Like ozone, humidity varies strongly between the dry stratosphere and much more humid conditions of the earth's surface. Humidity is considered an important variable here as it can strongly influence chemistry occurring at surfaces. Measurement conditions were therefore examined that reflect the conditions likely to be met in these two environments. The aim of this study was to investigate the influence of different ozone levels and different relative humidity (RH) on two specific VOC measurement instruments, namely the fast GC-MS "SOFIA" described by Bourtsoukidis et al. (2017) and a PTR-ToF-MS described in Wang et al. (2022). We report on the effect of using the sodium thiosulfate impregnated quartz filters for multiple VOC species including carbonyls, alcohols and non-methane hydrocarbons. Additionally, the lifetime of the scrubber with respect to ozone exposure was determined under tropospheric and stratospheric conditions. This is essential to assure that the scrubber is working correctly when applied in the field, to determine optimum exchange times, and to avoid unnecessary exchange and waste. These results will define operational expectations of using $Na_2S_2O_3$ filter in field conditions, to improve organic trace gas measurement techniques, assure good data quality for smaller VOCs and therefore improve the data comparability between different studies.

2.2 Materials and methods

The influence of ozone on measurements from an online VOC instrument (PTR-ToF-MS 8000, Ionicon Analytik, Austria) and a custom built quasi-online fast gas chromatograph-mass spectrometer (GC-MS) (Bourtsoukidis et al., 2017) which collects, concentrates and measures within 3 minutes was investigated. Additionally, the effect of an implemented sodium thiosulfate ozone scrubber on those systems as well as the scrubber lifetime was examined at different relative humidity. A list with the measured species is shown in Table 2.2. It includes saturated and unsaturated halocarbons, non-methane hydrocarbons (NMHCs), small oxygenated VOCs (OVOCs), siloxanes and some nitrogen and sulfur containing molecules. Some species could be detected with both instruments simultaneously while other species could only be measured by one. The majority of the tubing used in this study was FEP (fluorinated ethylene propylene) Teflon which was found by Deming et al. to perform well in a comparison of inlet materials (including polyetheretherketone (PEEK) and stainless steel), as adsorption on FEP was found to be independent of humidity, concentration and functionality. The tubing was not new, but used previously for airborne measurements aboard a research aircraft. It was flushed with synthetic air for at least one hour prior to the experiments performed. When considering the ozone in the instrument inlet, one could consider passivating the inlet surfaces prior to measurement by the introduction of high (500 ppb) ozone mixing ratios. Northway et al. tested this possibility and noted a passivation that disappeared during further field measurements. As this will in effect generate a shifting background to the subsequent measurements, and as 6 hour flushing is impractical prior to flight measurements we chose not to follow this procedure.

2.2.1 Experimental setup

The experimental setup includes both PTR-ToF-MS and fast GC-MS as shown in Figure 2.1. Synthetic air from a gas cylinder (synthetic air, hydrocarbon free, T50, Westfalen, Germany) was connected to the ozone generator which was set to generate O_3 at levels between 25 and 1000 ppb. This corresponds to tropospheric and lower stratospheric levels, similar to those encountered by the HALO aircraft on which the instruments are certified to fly. Thereafter, the air stream was led through ultra-pure water for humidification. Ozone as a non-polar molecule has a very low solubility in water and will therefore not be lost during the humidification process. Two different calibration gas cylinders (40L, Apel Riemer, USA) were connected through a junction (T-piece) to the sampling line. These cylinders contained a gravimetrically prepared mixture of VOCs at known mixing ratios, which could be added to the system air. The VOC enriched synthetic air could then be directed through the ozone scrubber or directly to the two mass spectrometers, which both drew circa 200 sccm air from the sampling line each. At the end of the Teflon tubing inlet line the ozone monitor was connected to measure the O_3 concentration after the scrubber. Several exhaust lines and pressure gauges were installed in the

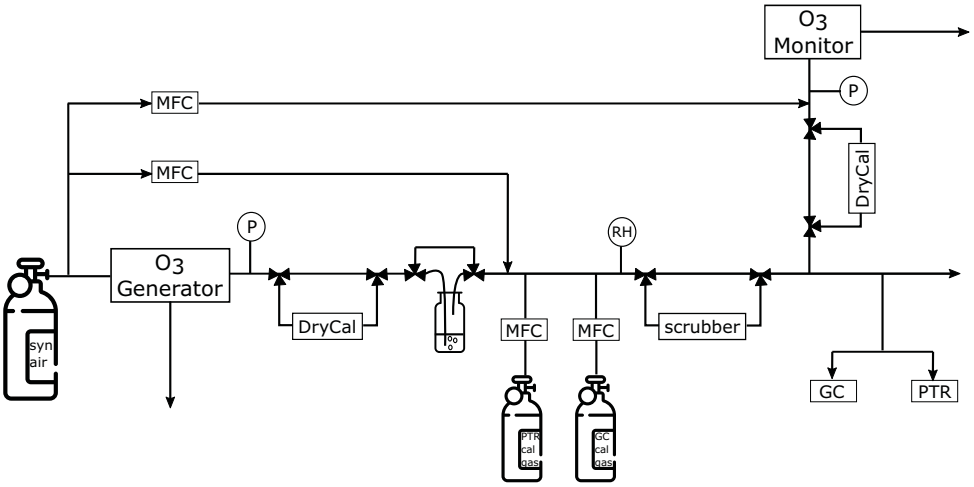

FIGURE 2.1: Experimental setup, abbreviations stand for: MFC - mass flow controller; RH - relative humidity sensor; P - pressure gauge; DryCal - flow meter.

setup to ensure a system pressure close to ambient pressure (ca. 1000 hPa). This is required for the operation of the ozone instruments. To make sure that the monitor was always operated within the required flow range, a dilution flow could be added shortly before the instrument. Gas flows were checked regularly with a flow meter (DryCal, Mesalabs, USA) after the ozone generator and monitor. All the lines were made of FEP and heated to approximately 45 °C to avoid condensation in the tubing. This simulates conditions on the research aircraft aboard which the measurement devices have been installed. The total tubing length between ozone generator and scrubber was approximately 2 m, the outer diameter was 1/4", again equivalent to the aircraft set-up. During the ozone experiment series various tests were performed (cf. Table 2.1): VOC mixtures were measured at several levels, adding 0, 50 and 1000 ppb of ozone to investigate the measurement performance at ambient background ozone levels on the ground and in the lower stratosphere. Additionally, one VOC level was measured at seven different ozone levels up to 1000 ppb (0, 25, 50, 150, 400, 750, 1000 ppb). The tests also included experiments without added VOCs to see if any of the analytes are produced in the pre-used inlet line. Note that during the very first experiment performed, flows were measured every time the VOC level was adjusted. It turned out that some compounds were emitted from the flow meter resulting in elevated terpene masses. When switching to a new calibration gas level as well as in the first hour of the experiment, there were spikes in the

TABLE 2.1: Conditions of the different experiments performed in this study.

Condition	O_3 levels / ppb	Calgas MR / ppb	RH / %
Effect of O_3 on VOCs	0, 50, 1000	0, 0.5, 1, 2, 4	0
Effect of O_3 on tubing	0, 25, 50, 100, 150, 400, 750, 1000	0, 0.5	0
Effect of RH on VOCs / scrubber	0, 50, 150	0, 0.5, 2	0, 50, 80
Scrubber endurance	50, 150, 1000	0	0, 80

VOC signal. These were judged to be mechanical flow related anomalies and therefore removed to assure better visibility of the mixing ratio in the plots. To investigate the influence of sodium thiosulfate impregnated quartz filters as an ozone scrubber, VOC levels at 0.5 and 2 ppb were measured at different ozone levels (0, 50 and 150 ppb) and different relative humidities (0 %, 50 % and 80 % RH) with and without scrubber in the flow path. For scrubber endurance tests, another exhaust line was installed after the ozone generator to reduce the flow through the sodium thiosulfate impregnated quartz filter in order to simulate field conditions. The flow through the filter was set to 200-600 sccm to replicate either typical field measurement conditions or the experiments focusing on the influence on the VOC measurements. For those experiments the flow through the scrubber was higher to provide enough air for both of the instruments. Before each single longevity experiment the $Na_2S_2O_3$ impregnated filter was exchanged and left in the flow path until an abrupt increase in ozone concentration was detected with the O_3 monitor. This rise marks the end of the scrubber lifetime. Further details on the preparation of the filter scrubber can be found in section 2.2.3. Scrubber performance was tested under three different ozone concentrations: 50, 150 and 1000 ppb at 0 % RH. These are the same ozone levels used for the experiment focused on the effect of O_3 on the VOC measurements, which correspond to ambient ground and lower stratospheric ozone levels. Additionally, the influence of 80 % relative humidity on the scrubber lifetime was tested. This RH level was chosen as an extreme to see whether or not it changes the scrubber performance. Relative humidity was measured with a humidity sensor that includes a temperature sensor (MSR145, MSR, Switzerland; indicated with "RH" in Figure 2.1).

2.2.2 Instrumentation

Ozone instruments

An ozone generator as well as an ozone monitor (49iQPS and 49iQ, both Thermo Fisher Scientific, USA) were installed in the experimental setup. Each instrument's supply air stream is divided into a reference and a sample gas channel. In the generator the sample gas flows through an ozonator, while the reference gas of the monitor flows through a scrubber to eliminate existing ambient ozone. Both instruments use a spectroscopic approach to determine the mixing ratio: as the O_3 molecule absorbs UV light of 254 nm the difference of light intensity of this wavelength in both channels is used to calculate the ozone concentration in the sample stream based on Beer's Law (ThermoFisherScientific, 2020a; ThermoFisherScientific, 2020b).

PTR-MS

An Ionicon PTR-ToF-MS with a drift tube pressure of 2.2 hPa, drift temperature 60 °C and E/N 137 Td was operated with H_3O^+ as primary ions. It is a soft ionization technique and therefore causes little fragmentation of the analytes during the detection process. This is the case for most analytes in

this study. However, some species (e.g. terpenes, siloxanes) do fragment during ionization (Pagonis, Sekimoto, and Gouw, 2019). Fragments can impact the measurement of target species such as isoprene if they have exactly the same mass. Identification of the analytes was performed using the exact mass of the most abundant fragment, usually the protonated molecular mass, which does not exclude simultaneous measurement of isomeric compounds. The mass range of the system was 0-500 amu and the mass resolution approximately 3500. The PTR used a FEP inlet tubing (OD 1/4" (0.635 cm), inner diameter (ID) 1/8″ (0.3175 cm)) with an inlet flow of 200 sccm. The distance between ozone scrubber and PTR was 1.85 m, resulting in an inlet residence time t_{res} of ca. 4 s. In order to regulate the pressure in the drift tube during flight measurements, the sample air passes and adjustable O-ring (fluorinated propylene monomer (FPM) or nitrile butadiene rubber (NBR), $t_{res} \leq$ 30 ms). The influence of the O-ring on VOC measurements was found to be zero without O_3 present, but has not been tested separately under ozone exposure. Inside the instrument, a 1 m line (ID 0.1 cm) made of polyetheretherketone (PEEK) is used (ca. 70 sccm, $t_{res} \leq$ 1 s, depending on the flow rate). limits of detection (LOD) were <0.05 ppb, with a total uncertainty of 15-20 %. Measured species included alkenes, siloxanes and OVOCs. For measurements at RH>0 a humid calibration was applied: The calibration was performed at the same relative humidity as the corresponding experiment.

GC-MS

The fast GC-MS system has been described in detail by Bourtsoukidis et al. (2017). In this study it was used to measure halocarbons, small NMHCs and OVOCS as well as some sulfur containing compounds and small organic nitrates. Due to its chromatographic column it is capable of separating isomeric compounds prior to detection (e.g. acetone and propanal). The custom-built instrument uses a cryogenic three step pre-concentration to collect air samples, followed by gas chromatographic separation in a custom-built oven and detection with a quadrupole mass spectrometer which was operated in selected ion monitoring mode (SIM). With a time resolution of 3 min it is currently not possible to measure high molecular mass compounds (e.g. sesquiterpenes) as those would need more time to elute from the GC-column. Bromoform is the largest analyte detected with the currently applied method. The system's inlet flow was 200 sccm, tubing length between GC inlet and ozone scrubber 2 m (OD 1/4" (0.635 cm), ID 1/8″ (0.3175 cm)), which results in an inlet residence time of ca. 5 s. Inside the system, the sample air is exposed to silicosteel tubing (OD 1/16″ (0.1588 cm), ID 0.02″ (0.0508 cm), 40 sccm, t_{res} < 1 s) and stainless-steel surfaces in the traps (t_{res} 1.5 min). LODs were typically <0.03 ppb (acetaldehyde, acetone and acrolein <0.2 ppb) and the total measurement uncertainty approximately 10 %.

2.2.3 Ozone scrubbing

Various materials have been tested to eliminate interferences from ozone on VOC measurements. Helmig (1997) compiled an overview of widely used O_3 scrubbing techniques for the sampling of atmospheric organic compounds. Several groups have reported satisfactory results of sodium thiosulfate as an ozone scavenger for VOC analysis (Helmig, 1997; Lehmpuhl and Birks, 1996; Pollmann, Ortega, and Helmig, 2005; Strömvall and Petersson, 1992). In this study the scrubbers were prepared by soaking quartz fiber filters (37 mm, GE Healthcare Life Sciences, USA) in a 10 % (w/w) aqueous solution for 1 h followed by drying under a nitrogen flow of approximately 100 sccm at room temperature. This quartz filter was placed under a 47 mm PTFE-filter (Sartorius, Germany) in a Teflon filter holder. The smaller quartz filter was selected to avoid leaks at the filter holder (ID 47 mm, Reichelt Chemie Technik, Germany) previously caused due to the thickness of the quartz filter. The volume of the filter housing is ca. 55 mL, resulting in a residence time of ca. 6 s with a flow rate of $\sim$600 sccm.

2.2.4 Scrubber lifetime calculation

The time that the scrubber remains effective at removing ozone, here termed the scrubber lifetime is important information for field measurement practitioners. In order to improve data quality and keep cost and work load low, the ozone scrubbers need to be exchanged before their efficiency is compromised, while still using them as long as possible. Assuming that the scrubber lifetime is a function of ozone mixing ratio and flow, the data from the scrubber lifetime experiment was plotted and fitted with a power function. Additionally the influence of relative humidity on the scrubber lifetime was tested.

2.2.5 Potential effects causing interference

VOC measurements performed by the PTR-ToF-MS and the fast GC-MS may in the presence of ozone, suffer interference through various effects. Surface reactions on the inner walls of the tubing can lead to ozonolysis of compounds previously absorbed on the FEP inlet tubing. The ozonolysis of alkenes, which are either present on the tubing surface or in the gas phase (sample air) can lead to production of carbonyl compounds which cause positive artifacts on the carbonyl masses. Another potential source of interference is fragmentation during the ionization process in the PTR-MS. Several groups reported for example fragments on PTR *m/z* 69.07 from C5-C10 aldehydes (Buhr, Ruth, and Delahunty, 2002; Ruzsanyi et al., 2013; Wang et al., 2022). The instrument-internal fragmentation process itself is independent of ozone, but the presence of the aldehyde species in the sample air is likely to be caused by the release of those species from the sample line surface due to ozonolysis reaction. Not only the PTR, but also the GC-MS can suffer interference caused by ozone inside the instrument. It has been reported previously, that O_3 induced emission from rotor material of multiposition valves

TABLE 2.2: Measured species and effect of ozone. X: no effect; ↓: negative interference; ↑: positive interference.

Analytes and effect of O_3 on measured MR					
X	Dichlorodifluoromethane	X	Trichloroethene	X	Hydroxyacetone
X	Trichlorofluoromethane (CFC-11)	X	Chlorobenzene	X	Isopropyl nitrate
X	Tetrachloromethane	X	Benzene	X	Acetonitrile
X	1,1,2-Trichloro-1,2,2-Trifluoroethane (CFC-113)	X	m-Xylene	X	Acrylonitrile
X	Bromomethane	X	1,2,4-Trimethylbenzene	X	Carbon disulfide
X	Bromoform	X	3-Methylfuran	X	DMS
X	Chloromethane	X	2-methyl-3-buten-1-ol	X	D3
X	Dichloromethane	↑	Acetaldehyde	X	D4
X	Chloroform	↑	Propanal	X	D5
X	Iodomethane	↑	Acetone	X	n-butane, i-butane
X	Bromodichloromethane	↑	Butanal	X	Propene
X	1,1,1-Trichloroethane	X	MEK	↓	Isoprene
X	1,1,2-Trichloroethane	X	MTBE	↓	Monoterpenes
X	Vinylchloride	X	Acrolein	↓	Sesquiterpenes
X	Tetrachloroethene	↓	Methacrolein		

can lead to positive artifacts when measuring C2-C4 aldehydes (Apel et al., 2003).

2.3 Results and discussion

2.3.1 Influence of ozone on VOC measurements

For most of the analytes, mainly saturated NMHCs and halocarbons, no ozone interference of the measurement through reactive loss due to ozone was expected. This is because such species do not contain a double bond with which ozone can react, nor do they contain oxygen atoms so are unlikely to be produced by surface oxidation processes. However, due to the different molecular structures and physical properties of some analytes, it was potentially possible to obtain negative interference for some unsaturated species like isoprene and terpenes as well as artificial signal enhancement on the aldehyde masses. Table 2.2 shows whether ozone had an effect on the measured mixing ratio of the VOCs.

No effect on VOC measurements

In accordance with the expectations no interference from reactions with ozone were observed for most of the measured species, namely saturated and unsaturated halocarbons, alkanes, aromatics, nitriles, methyl tert butyl ether (MTBE), ethanol, hydroxyacetone, methyl ethyl ketone (MEK), isopropyl nitrate, the two sulfur containing species carbon disulfide and dimethyl sulfide (DMS) as well as siloxanes. As an example of the VOCs where ozone did not influence the measurements Figure 2.2 shows the mixing ratios of chlorobenzene applied and measured by GC- and PTR-MS as well as the ozone mixing ratio. In this experiment no ozone scrubber was applied. While the instruments observe slightly different mixing ratios owing to differences in sensitivity, the relative change in chlorobenzene mixing ratios remain unchanged when ozone is present.

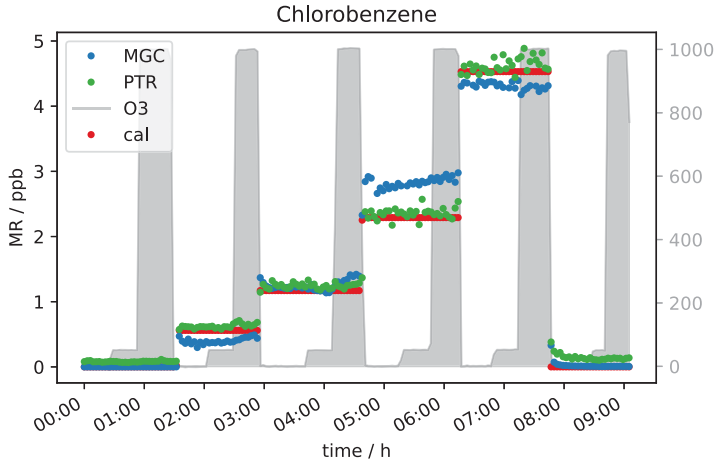

FIGURE 2.2: Effect of Ozone (0, 50, 1000 ppb) on GC- and PTR-MS measurements of chlorobenzene under different standard gas levels (0-4 ppb).

Ozone causing positive interference

Based on current literature, some carbonyl compounds such as aldehydes and ketones do have the potential to show higher mixing ratios when ozone is present. Northway et al. and Apel et al. observed positive artifacts under ozone presence for acetaldehyde. Additionally, Apel et al. observed artifact formation for propanal, acetone and butanal in their fast GC-MS system, which were emitted by parts of their system when ozone was present. Lehmpuhl and Birks found positive interference also for larger carbonyl compounds. Acetaldehyde measurements in this study under dry conditions agree with the results reported by Northway et al., Apel et al. and others. The VOC signal increases with ozone concentration. Both, the PTR- and GC-MS measured higher acetaldehyde mixing ratios when O_3 was above 150 ppb (see Figure 2.3). This indicates that the interference is not instrument specific but more likely a function of the common inlet tubing exposure to ozone. Note that the inlet lengths to GC and PTR were roughly the same. The higher enhancement of the GC acetaldehyde could be due to emission of oxidation products from the material of multiposition valves as described by Apel et al. In contrast to the PTR data, the ozone induced enhancement of the GC signal increases with acetaldehyde concentration. This effect can be due to the different materials used for the tubing inside the instruments: Deming et al. showed, that in glass and metal tubing competitive adsorption occurs, which depends on humidity, concentration and functionality of the analyte, while polymer tubing shows independent absorption. Our fast GC instrument is equipped with heated silico-steel tubing, which allows competitive adsorption, while the PTR is equipped with PFA (perfluoroalkoxy alkanes) tubing. Additionally, with increasing O_3 mixing ratios ozonolysis reactions during trapping are gaining importance. It seems, that the interferences on the VOC measurements caused by high ozone exposure are an effect of both,

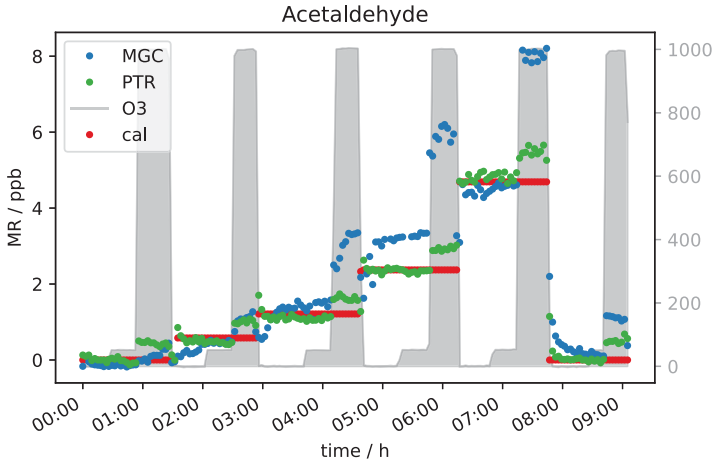

FIGURE 2.3: Five different standard gas levels between 0 and approx. 4 ppb at ozone mixing ratios of 0, 50 and 1000 ppb.

inlet line and instrument's surfaces. The higher GC-signals at 2 ppb of calibration gas are again assigned to the difference in sensitivity (due to filament degradation) already mentioned in the previous section. In Figures 2.3 and 2.4a, the acetaldehyde signals rise significantly when 1000 ppb of ozone was present. For the zero air sample (Figure 2.4b) the signal rose after increasing ozone from 150 ppb where the effect was negligible to 400 ppb. The acetaldehyde signal increased further between 400 and 1000 ppb O_3 to about 0.4 ppb (GC) to 0.5 ppb (PTR). Interestingly, the GC signal in Figure 2.4b did not drop when the standard gas level dropped to 0 ppb. This is an interesting observation that we currently cannot explain. No abnormal behavior in the GC-MS could be ascertained at this time including retention time shifts, tuning anomalies or changes in RH. We conclude that most likely it was an unlogged flow switching issue. Nevertheless, it does not interfere with our general observation, that the acetaldehyde signal is suffering positive interference under high ozone exposure, most likely due to ozonolysis reactions at the tubing surface.

Besides acetaldehyde, C3 and C4 aldehydes and ketones have also been measured, namely propanal, acetone, butanal and MEK. Unfortunately, for those compounds the results were not as clear as for the C2 carbonyl described above. The PTR-ToF-MS in H_3O^+ mode cannot separate the aldehyde from the ketone as they have exactly the same mass, i.e. the PTR-Tof-data presented here always shows the sum of propanal and acetone (C3), and butanal and MEK (C4) respectively and should be therefore double the GC signals for the separated species. When measuring zero air, ozone increases the signal of the C3 and C4 carbonyls (cf. Figure 2.5), starting at O_3 mixing ratios of 400 ppb, similar to acetaldehyde. This is most likely due to the reaction of ozone with species attached/adsorbed at the walls of the instrument sampling systems or to unmeasured ozone reactive species in the zero air. While butanal (measured by GC-MS) shows a strong increase, MEK does not show significant increase in the GC data.

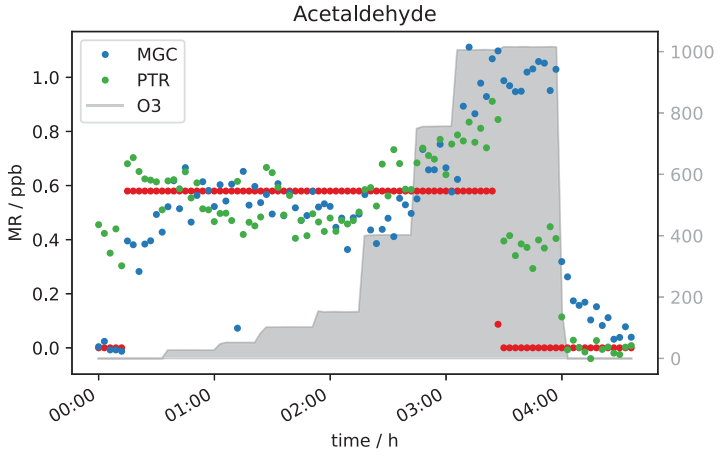

(A)

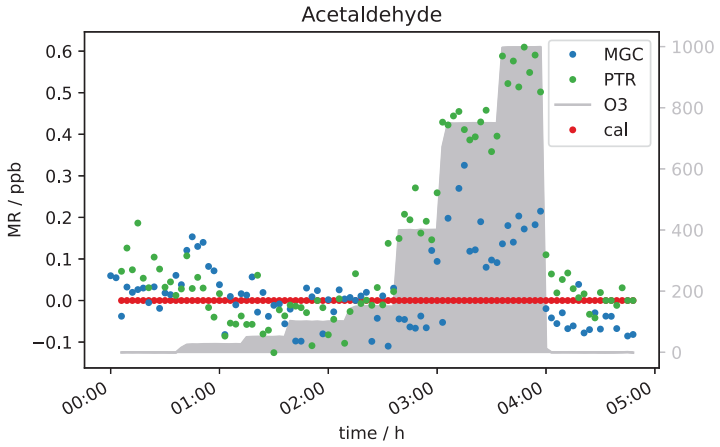

(B)

FIGURE 2.4: Acetaldehyde mixing ratios at seven different ozone levels between 0 and 1000 ppb and one standard gas level. VOC levels are 0 ppb (a) and 0.5 ppb (b).

Interestingly, the aldehyde mixing ratios are relatively stable with a tendency to decrease with ozone when the standard gas was added. Figure 2.6 shows this phenomenon. Propanal and butanal mixing ratios do not show a substantial increase under the same O_3 conditions where they increase in the zero air measurement, while the sum of C3 carbonyls (PTR signal) and GC acetone again increase (as in the zero air measurement). As propanal slightly decreases and acetone strongly increases with ozone, the PTR measurements shows a positive net ozone effect for the C3 carbonyls. For C4 carbonyls, the GC quantification during this experiment was compromised (too low mixing ratio) for unknown reasons. However, the qualitative results match the rest of our observations: butanal decreases slightly, while MEK increases slightly, leading to a stable signal for the sum of butanal and MEK, which is shown by the PTR data presented in Figure 2.6b. Additionally, the qualitative results of butanal and MEK are in line with the qualitative results of C2-C3 carbonyls:

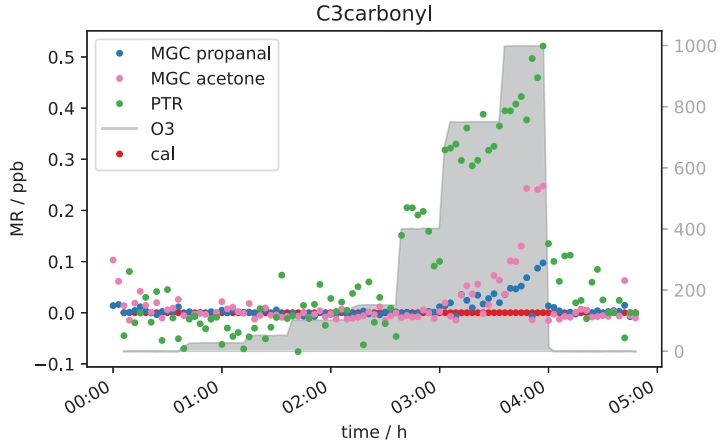

(A)

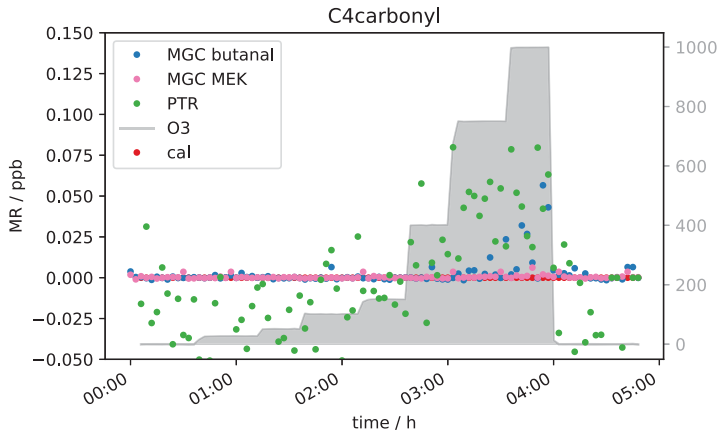

(B)

FIGURE 2.5: C3- and C4 carbonyl mixing ratios of a zero air sample at different ozone levels.

The signals for the ketones (acetone (C3), MEK (C4)) increase with O_3 mixing ratios $\geq$ 400 ppb and the signals for the aldehydes (acetaldehyde (C2), propanal (C3) and butanal (C4)) are relatively stable with a tendency to decrease between 200 and 400 ppb O_3 and increase as well with O_3 mixing ratios $\geq$ 400 ppb. Between 3.5 and 4 h after start of the experiment (cf. Figure 2.6), not all signals dropped to background levels. They finally drop once ozone was switched off. This is consistent with the results from the zero air measurement (Figure 2.5) and the acetaldehyde data (Figure 2.4b). It shows that exposure of the inlet tubing to high ozone does not rapidly clean the lines of the interfering compounds. Apel et al. reported carbonyl generation in the presence of ozone from the rotor material of VICI valves and a KNF Teflon pump included in their system (Apel et al., 2003). Positive artifacts were reported for acetaldehyde, propanal, acetone and butanal, they did not find any interference for MEK. This matches our results. We assume that C2-C4 carbonyl compounds are generated inside the setup inlet tubing and were measured by the GC as otherwise the signal would have dropped when measuring zero air with 1000 ppb O_3. However, at 0.5 ppb of calibration gas

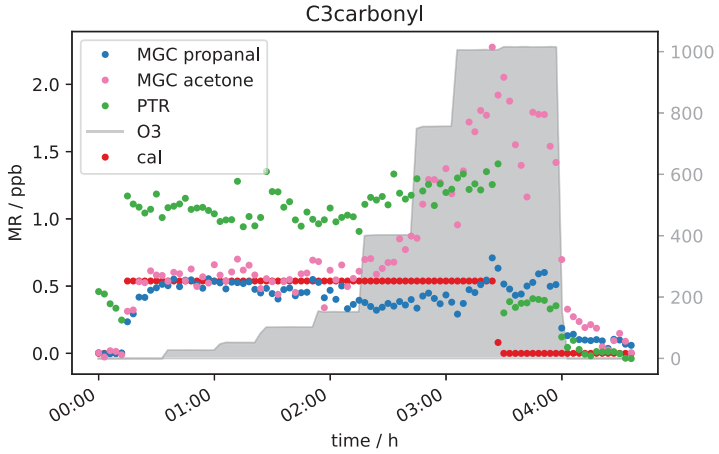

(A)

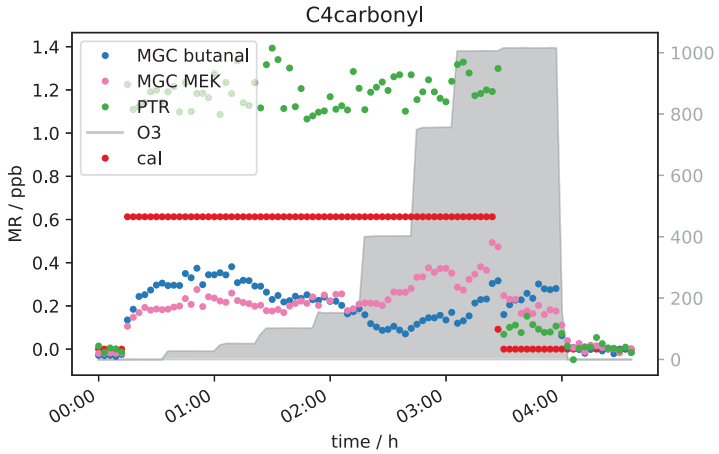

(B)

FIGURE 2.6: C3- and C4 carbonyl mixing ratios at approximately 0.5 ppb per VOC at different ozone levels.

we observed a C3 and C4 aldehyde loss under high ozone exposure in the GC measurements. A possible explanation for this is the effect is due to OH radicals produced via Criegee intermediates from the ozonolysis reaction of alkenes present in the standard gas. OH radicals react preferentially with aldehydes rather than ketones. Apparently, these reactions are faster than the C3 and C4 aldehyde generation within the sampling setup. All the experiments show the same trend: under dry conditions, at tropospheric ozone levels ($\leq$ 150 ppb O_3), no interference from the oxidant can be observed, while under stratospheric conditions (> 400 ppb O_3) there is a strong interference. This leads to the conclusion, that both instruments can measure C2 to C4 carbonyls in the troposphere without being restricted by the amount of ozone present. No reliable results can be achieved when ozone is above 150 ppb under dry conditions. Hence, the current setup is not suitable for stratospheric measurements of these oxygenated species.

Ozone causing negative interference

Due to the presence of reactive double bonds, terpenes (isoprene, alpha pinene and beta caryophyllene) were expected to show a decrease in mixing ratio with increasing ozone concentration. This was indeed observed. In Figure 2.7 it can be seen that the monoterpene signal at 50 ppb of O_3 is ten to twenty percent lower for each VOC level compared to the signal without ozone present. The signal drops by almost the same percentage when O_3 was increased to 1000 ppb. For sesquiterpenes the effect is even stronger. With 50 ppb O_3, the signal drops by roughly 80 %, while the signal is close to or below detection limit at an ozone level of 1000 ppb depending on the terpene mixing ratio applied. This behavior can be explained with reference to the different reaction rate constants k of the mono- and sesquiterpenes in the calibration gas with ozone. α-pinene, which is the monoterpene included in the standard gas mixture, has a reaction rate constant with ozone of 9.6×10^{-17} $cm^3 molecules^{-1} s^{-1}$ while k for β-caryophyllene is 1.2×10^{-14} $cm^3 molecules^{-1} s^{-1}$ (IUPAC, 2021). With a reaction rate more than three orders of magnitude larger, the reaction is fast enough to remove 1 ppb of β-caryophyllene within the short time the sample air needs to travel through the inlet line (< 10 s). Furthermore, it can be seen that the sesquiterpene needs considerable time (more than an hour) to reach a steady state level in the beginning of the experiment (∼ 03:00 in Figure 2.7), even with lines heated to 45 °C. This could be due to independent absorption of the FEP tubing of these less volatile species (Deming et al., 2019). Another compound which was expected to show a decreasing mixing ratio with increasing ozone concentration due to its double bonds was isoprene. It was measured simultaneously with PTR- and GC-MS. As can be seen in Figure 2.8, the signal is not measurably affected by adding 50 ppb of O_3. At an ozone level of 1000 ppb, the GC detects roughly 50 % less isoprene. This fits with expectations as isoprene ozonolysis is rather slow, the reaction rate coefficient being close to the one for α-pinene (1.3×10^{-17} $cm^3 molecules^{-1} s^{-1}$), which results in only partial

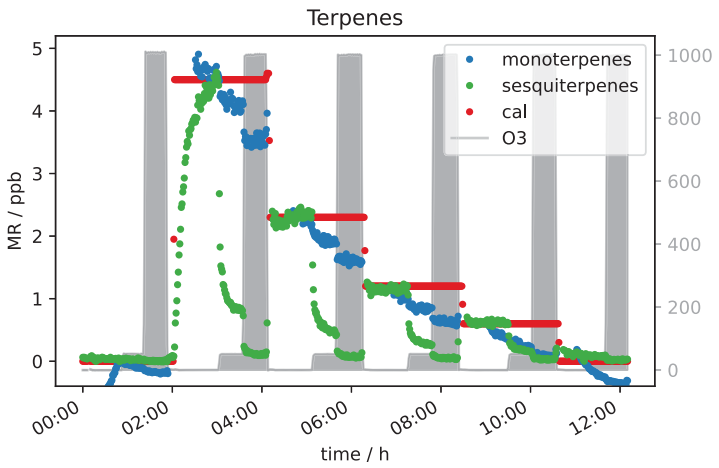

FIGURE 2.7: Different terpene levels at 0, 50 and 1000 ppb O_3 measured with PTR-MS.

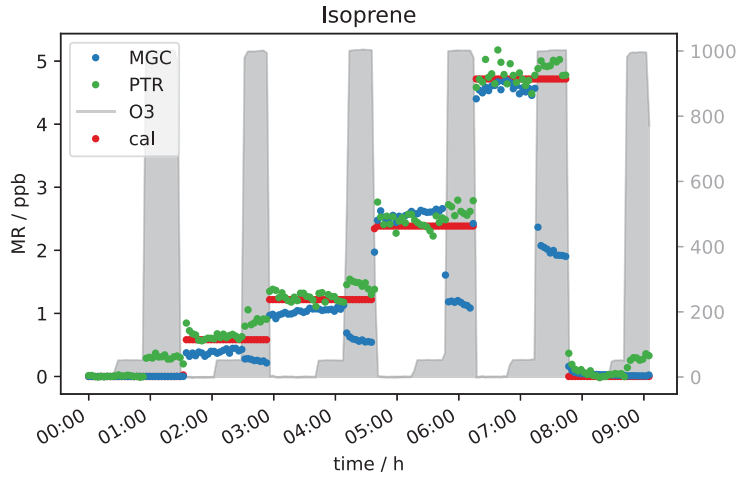

FIGURE 2.8: Different isoprene levels at 0, 50 and 1000 ppb O_3.

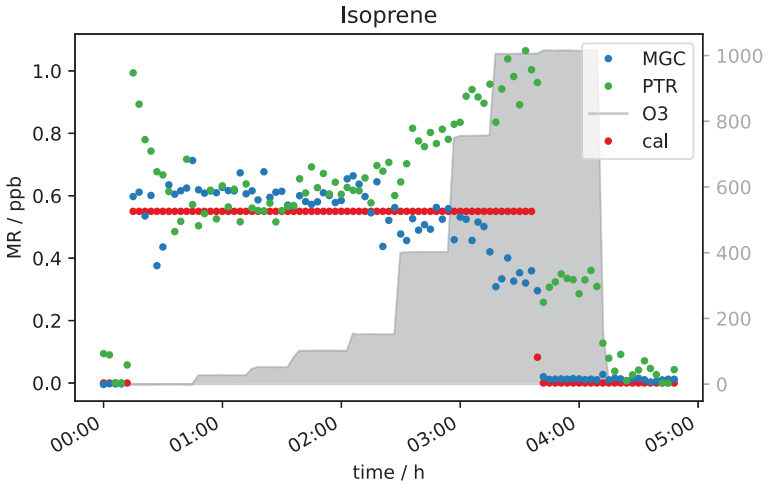

(A)

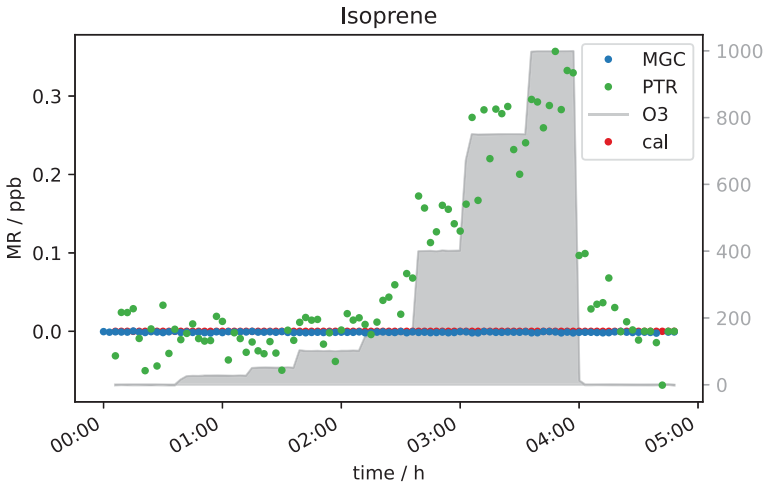

(B)

FIGURE 2.9: Isoprene mixing ratio at different ozone levels.

depletion of the isoprene present. Interestingly the PTR-ToF shows slightly higher mixing ratios of the isoprene mass (*m/z* 69) when ozone is present. The elevated signal on this mass can be caused by carbonyl compounds present in sample air or inlet line. Literature reports the same exact mass commonly used for isoprene detection in PTR systems to be a fragment of certain aldehydes (Buhr, Ruth, and Delahunty, 2002; Ruzsanyi et al., 2013). Most likely the PTR *m/z* 69 signal in the present study is elevated because under the experimental conditions the positive offset from the carbonyl compounds is higher than the isoprene depletion. For the GC-MS, aldehydes do not interfere as the analytes are separated in the chromatographic system prior to detection. The assumption is supported by the measurement of a zero air sample (no standard gas added into the system) at different ozone levels (see Figure 2.9a). The GC does not detect any isoprene in the zero air sample regardless of the ozone concentration, while the PTR-MS shows an increasing m/z 69 signal at O_3 levels between 150 and 1000 ppb. Apparently the PTR-ToF-MS signal correlates with the oxidant's concentration. At 150 ppb O_3 the PTR-MS detects approximately 100 ppt of signal at the isoprene mass, at 400 ppb of ozone PTR measurements show around 150 ppt and with the highest tested O_3 concentration (1000 ppb) roughly 350 ppt.
Figure 2.9b shows data obtained from the measurement of one isoprene level ($\sim$0.6 ppb) at seven different ozone mixing ratios and without ozone. GC-isoprene is stable until 100 ppb of O_3. Somewhere between 150 and 400 ppb the isoprene signal starts to decrease until it reaches approximately two thirds of the real value at 1000 ppb O_3. The two analytical instruments show reverse effects of ozone being present: the PTR-isoprene mass signal is increasing over the same range as the GC signal decreases. This is in line with the measurement of the zero air. The PTR-signal increase is probably due to fragments of other compounds on the same exact mass. In literature, increased PTR *m/z* 69 signals have been reported in high ozone environments in indoor and outdoor air studies which could not be attributed to isoprene (Colomb et al. (2006), Wang et al. (2022)). Those studies might have been influenced by the same interference we observed.

Effect of sodium thiosulfate scrubber on VOC measurements

Generally, when the sodium thiosulfate impregnated quartz filters were added to the sampling system (see Figure 2.1), no influence on the VOC measurements was seen for the selected VOCs. The literature also reports that this scrubbing material is suitable for measurement of many VOCs without causing interferences (Helmig, 1997; Pollmann, Ortega, and Helmig, 2005). In Figure 2.10 the measured terpene mixing ratios 0 and 2 ppb VOC with and without scrubber are shown. It can be seen, that the scrubber performed as expected and removed the ozone effectively. α-pinene levels reach the same concentration with the scrubber as before ozone was applied. The measurement of this compound is not affected by the sodium thiosulfate filters and if the scrubber is applied, there is no interference on the measurement with up to 170 ppb of ozone. As mentioned before β-caryophyllene again needed

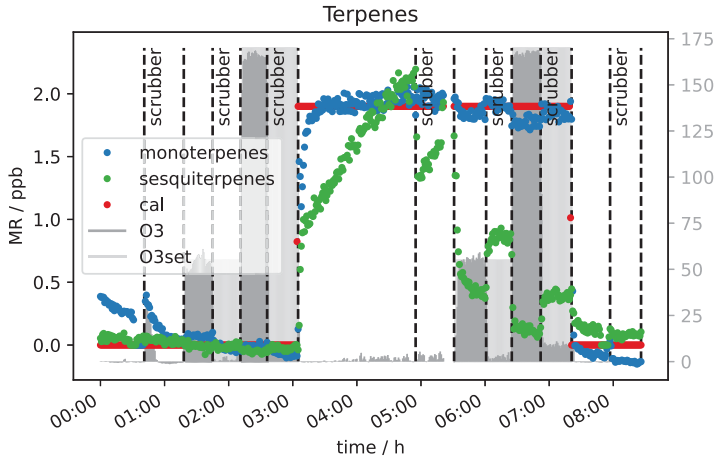

FIGURE 2.10: Terpene mixing ratios measured by PTR-MS with and without scrubber at 50 and 170 ppb O_3.

a long time to reach steady state when 2 ppb of the VOC were applied to the system (inlet line temperature 45 °C, cf. section 2.2.1). Steady state is reached after almost two hours when the scrubber was introduced (∼04:30). For the 30-40 min when the thiosulfate filters were introduced (∼4:50-5:30) steady state is not even reached. Sesquiterpene adsorption by the tubing material would again explain this effect. The scrubber was connected using Teflon tubing and a filter holder of the same material. The first time when the terpene-rich air was directed through the scrubber (50 ppb O_3, five hours after start of the experiment, (∼4:50-5:30)) the sesquiterpene mixing ratio increased within half an hour, while later (170 ppb O_3, (∼6:00-7:30)) this was not the case. In other words, in the first half hour the sesquiterpenes appeared to be absorbed by the tubing (∼4:50-5:30), while afterwards the material was conditioned and the concentration could reach steady state (∼6:00-7:30). Steady state mixing ratios decrease with increasing O_3 mixing ratio as the scrubber was installed roughly half way between the junction where the standard gas was connected and the analytical instruments. On their way to the scrubber, the sesquiterpenes are depleted by ozonolysis. Furthermore, at the applied flow rate of approximately 650 sccm, there is already about 10 ppb of ozone passing the scrubber (cf. section 2.3.2) which allows the oxidant to further react with β-caryophyllene on the way between the scrubber and the detector. An improved filter assembly or several scrubbing filters as suggested by Pollmann, Ortega, and Helmig could improve the sesquiterpene sampling. For all other compounds including isoprene no interference from the scrubber itself could be observed. Furthermore, interferences from ozone on the measurements of analytes like isoprene or acetaldehyde could be eliminated with the filter scrubber in line. The effect on sesquiterpenes could probably also be eliminated if the scrubber was placed at the inlet's front end and the flow through the scrubber was lower. However, it cannot be excluded that the sesquiterpene signal is affected by the scrubber material. Therefore, a longer time span with the scrubber in the sampling line would be required for the signal to reach steady state and the instrument would be

unresponsive to rapid changes.

2.3.2 Scrubber endurance

Figure 2.11 shows the O_3 mixing ratio measured with the ozone monitor behind the sodium thiosulfate scrubber under the dry condition at approximately 200 sccm. Results from the experiment at 1000 ppb O_3 can be seen in Figure 2.11a. The ozone concentration behind the filter never reached 0 ppb, already at the beginning 100 ppb of the oxidant could pass the scrubber. That means 1000 ppb of ozone result in an overload of the scrubber capacity, and it was not suitable to remove the oxidant completely from the dry sample air - not even for short time periods. The concentration increases slightly in the beginning, while after 15 h a sudden signal rise can be observed where the mixing ratio increases from roughly 200 ppb to 500 ppb. After 55 h no ozone was scavenged anymore, the concentration before the scrubber is the same as after. Despite inefficient scrubbing under these conditions, the scrubber lifetime would be 15 h as after this time period a strong increase in the signal of the ozone monitor can be observed. In total it can be concluded that the sodium thiosulfate impregnated quartz filters made in the way described in the method section are not suitable for measurements at these flow rates and such high ozone levels as encountered in the lower stratosphere due to insufficient O_3 removal and relatively fast depletion of the scrubbing material. However, at lower flow rates it might be more efficient and effective.
Figure 2.11b presents the result from a similar experiment but with 150 ppb of ozone applied, which corresponds to high ozone levels at ground level, and typical for the upper troposphere. In the very beginning, the O_3 concentration was already 20 ppb. It can be excluded that the filter is not able to remove the O_3 completely as the experiment was started twice under these conditions. The first time the ozone mixing ratio was zero at the beginning, but unfortunately the experiment had to be stopped after 50 h. There was no sudden signal increase visible within that time. This 20 ppb offset during the second experiment might be caused by the filter not being perfectly centered in the filter holder. It is possible that a tiny stream of air bypassed the filter inside the filter holder as the 37 mm quartz filter was placed under a 47 mm Teflon filter as described in section 2.2.3. With 150 ppb of ozone applied, the measured mixing ratio increased by 20 ppb within 40 h and up to 50 ppb within 80 h. As previously shown even isoprene was not affected by 50 ppb of ozone. The only compounds affected by such low O_3 levels were mono- and sesquiterpenes. Therefore, it is concluded that the ozone scrubber can be used up to 80 h (3.3 days) at a flow of 255 sccm. The scrubber lifetime test for the lowest ozone concentration used here (50 ppb) took in total more than 20 days. During the first 300 h (12.5 days) the signal didn't change and was below or close to the limit of detection of 0.5 ppb. Around 300 h the measured mixing ratio started to be above detection limit, but still below 5 ppb O_3. A sudden increase occurred after approximately 350 h (14.5 days), where the mixing ratio climbed up to 20 ppb within 1.5 days. After the total

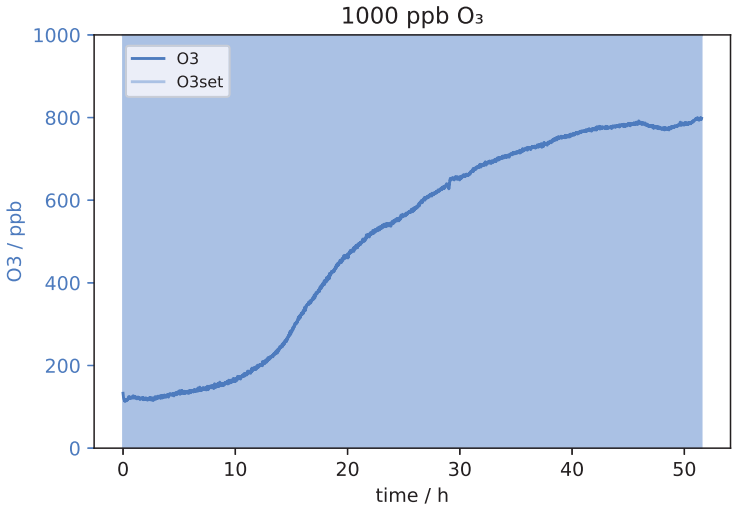

(A)

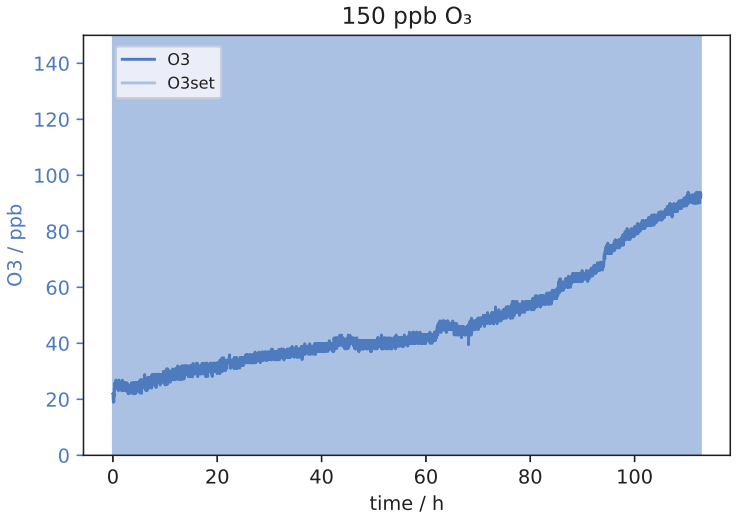

(B)

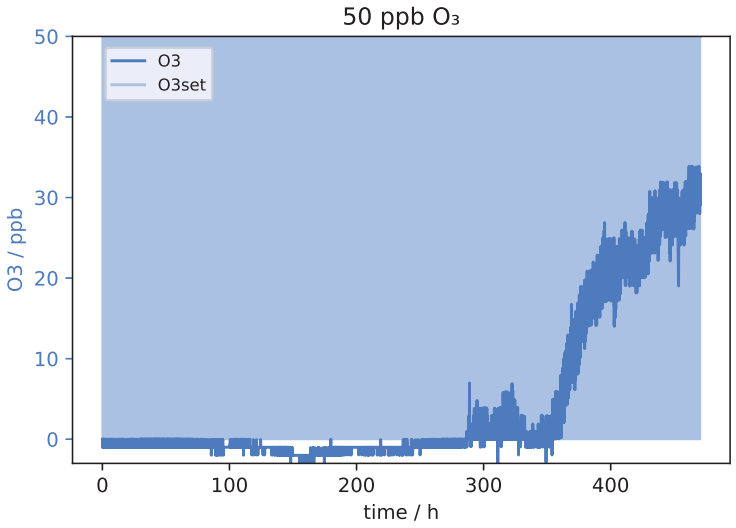

(C)

FIGURE 2.11: O_3 mixing ratio after $Na_2S_2O_3$ scrubber at 0 % RH. Flows and O_3 levels before scrubber: (a) 220 sccm, 1000 ppb; (b) 255 sccm, 150 ppb; (c) 230 sccm, 50 ppb.

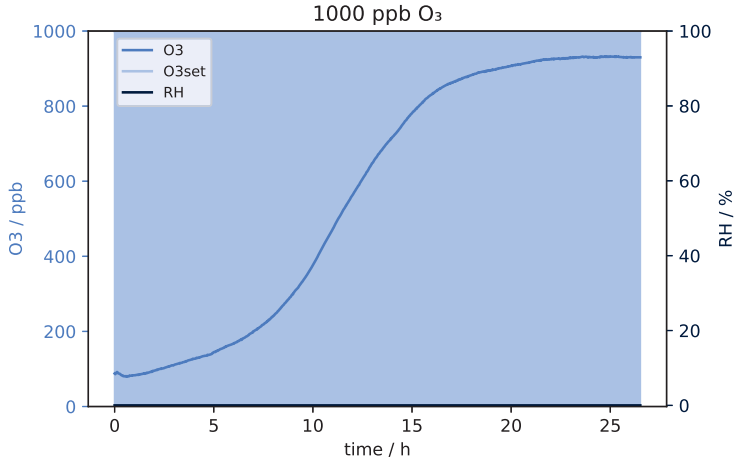

(A)

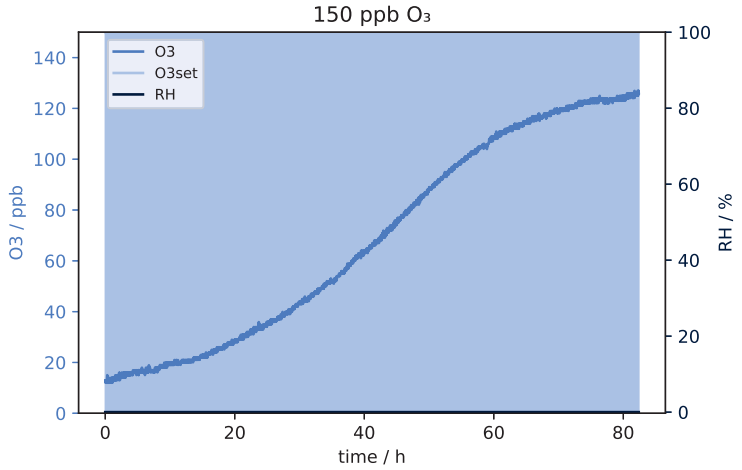

(B)

FIGURE 2.12: O_3 mixing ratio after $Na_2S_2O_3$ scrubber at 0 % RH. Flows and O_3 levels before scrubber: (a) 550 sccm, 1000 ppb; (b) 620 sccm, 150 ppb.

time of 477 h (almost 20 days) the experiment was stopped, the mixing ratio after the scrubber reached more than 30 ppb. The breakthrough point of the $Na_2S_2O_3$ impregnated filter after 350 h was determined as the end of the scrubber lifetime i.e. at background O_3 mixing ratios of 50 ppb the scrubber lasts more than 14 days. Results of the test at a flow of 550 sccm, which corresponds approximately to the flow used for the experiments to investigate the effect of ozone on the VOC measurements (section 2.3.1) are presented in Figure 2.12. Please note that for the average and minimum scrubber lifetimes only measurements at O_3 levels 150 and 1000 ppb have been included as for 50 ppb there was no measurement at approximately 550 sccm. For quality assurance it is considered important to have a real measurement which can be compared with the calculated results.
The scrubber lifetime is 8 h at 550 sccm and 1000 ppb O_3 according to Figure 2.12a. At the lower ozone level (150 ppb), the actual flow was 620 sccm. From

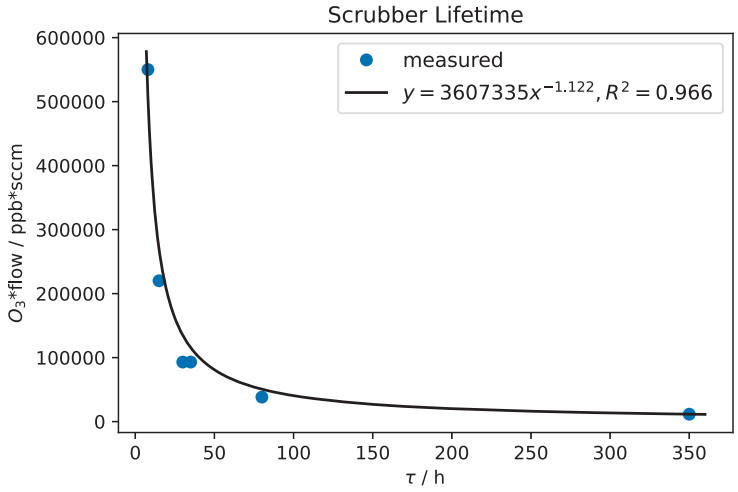

FIGURE 2.13: Measured data from the scrubber endurance test.

TABLE 2.3: Ozone mixing ratio and corresponding flows through the scrubber during scrubber endurance tests as well as resulting lifetimes τ.

	measured		
O_3 / ppb	flow / sccm	τ / h	τ / days
1000	220	15	0.6
150	255	80	3.3
50	230	350	14.6
1000	550	8	0.3
150	620	35	1.5

the plot a lifetime of 30 h has been determined. Scrubber lifetime τ highly depends on ozone concentration and flow rate. In Table 2.3 measured flows and lifetimes can be found. The data was fitted with a power function ($y=ax^b$, cf. Figure 2.13) being the best fit with R^2 close to 1. Additionally, the lifetimes for exactly 200 and 550 sccm were calculated with equation 2.1 and can be found in Table 2.4. The factors *a* and *b* obtained from the fit were rounded to 3500000 and -1 respectively as small changes are attributed to measurement uncertainties.

$$\tau = \frac{3500000}{O_3 * flow} \tag{2.1}$$

The ozone levels were chosen to correspond to those experienced in the troposphere (50 and 150 ppb O_3) and stratosphere (1000 ppb O_3) so that replacement times of the scrubber under field conditions could be determined. Flows correspond to the inlet flows of the mass spectrometers (200 sccm) and to the flow used for the experiments described in section 2.3.1.

The calculated lifetime at 200 sccm and 1000 ppb of ozone is 18 h. Hence,

TABLE 2.4: Calculated scrubber lifetimes τ at exactly 200 and 550 sccm.

	calculated		
O_3 / ppb	flow / sccm	τ / h	τ / days
1000	200	18	0.7
150	200	117	4.9
50	200	350	14.6
1000	550	6	0.3
150	550	42	1.8

this is the time after which the filter should be exchanged under these conditions if reducing ozone to 100-200 ppb is enough for the compounds of interest. If the background ozone mixing ratio does not exceed 150 ppb and the flow is the same as used for the here applied mass spectrometers (200 sccm), the scrubber needs to be replaced after 117 h to avoid interference from ozone for analysis of most VOCs except terpenes. However, on many ground based measurement sites in the troposphere the ozone mixing ratio rarely exceeds 50 ppb, which would result in a scrubber exchange every 14 days to assure efficient ozone removal. The lifetime calculation at 550 sccm and stratospheric ozone concentration results a scrubber lifetime of 6 days and is slightly lower than the measured lifetime (8 days, cf. Figure 2.12a). With 150 ppb O_3 and the same flow τ would be 42 h and filter replacement due in less than 2 days. The determination of the lifetime is approximate as we use the time at which a sudden increase in ozone concentration after the scrubber was observed. Exchanging the filter earlier does not affect the data quality and is therefore recommended. The filter assembly could be improved by using a filter housing which fits perfectly to the filter diameter in order to avoid any small air stream bypassing the filter. In this study, we did not examine the effect of several filters placed in series in the line as it was done by Pollmann, Ortega, and Helmig They found that with additional filters the scrubbing efficiency and scrubber endurance could be improved, but we adopted single filters to test their efficacy and endurance while minimizing potential uptake losses.

However, in section 2.3.1 the presented experiments were all performed in less than one day and the maximum ozone concentration (1000 ppb) was applied for only several hours. Thus, the ozone concentration was stable throughout each experiment.

2.3.3 Effect of humidity

Field measurements can take place in various locations and environmental conditions. Relative humidity may influence the analysis of water soluble compounds. However, the presence of water may also affect the behaviour of VOC molecules when interacting with surfaces. The scrubber material used here is inorganic and water soluble and has therefore been tested under dry and humid conditions. For the measurements performed within this

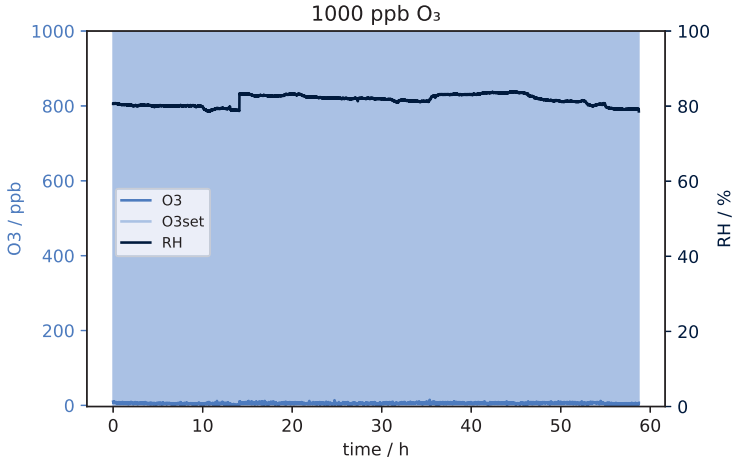

FIGURE 2.14: O_3 mixing ratio after $Na_2S_2O_3$ scrubber at 80 % RH, 230 sccm.

study, humidity did not have any influence on the GC- and PTR-ToF-MS instrument measurement capability as these dried the air before detection (GC-MS) or used humid calibrations (PTR-ToF-MS). Thus any effects observed can be ascribed to the inlet system. Interestingly, the scrubber lifetime increased dramatically at 80 % relative humidity. The test was done twice to double check the results obtained. Figure 2.14 shows the ozone mixing ratio and relative humidity measured at 1000 ppb O_3 and a flow of 230 sccm. RH was relatively stable throughout the whole experiment. As mentioned in section 2.3.2, under similar dry conditions the sodium thiosulfate scrubber was able to remove only 90 % of the ozone and filter performance dropped drastically after 15 h. In contrast, at 80 % RH the ozone could be removed completely from the sample air. The O_3 mixing ratio did not change over 65 h of experiment, it was always below 10 ppb. After 65 h the experiment was stopped.

The only signal that was still influenced by ozone when the filter scrubber was in the sample line, was the sesquiterpene signal. Consequently the corresponding mixing ratio can be used to investigate whether or not relative humidity changes the results compared to the dry condition. Figure 2.15 shows the sesquiterpene mixing ratio under dry (2.15a) and humid (2.15b) conditions when ca. 2 ppb standard gas was introduced to the system. In the first plot the signal with scrubber at 50 ppb of ozone (approx. 06:00-06:30) comes back to 50 % of the original signal, while in the second plot it comes back to approx. 80 % (approx. 08:00-09:00) of the original height. This is consistent with the results from the scrubber lifetime tests at 80 % RH and suggest that scrubber performance benefits from increased humidity.

Sodium thiosulfate reacts with ozone to tetrathionate, water and oxygen:

$$2\,S_2O_3{}^{2-} + O_3 + 2\,H^+ \longleftrightarrow S_4O_6{}^{2-} + O_2 + H_2O \tag{2.2}$$

As it is an equilibrium reaction, the equilibrium will shift to the left if there is an excess of water, recovering the thiosulfate from the $S_4O_6{}^{2-}$ produced.

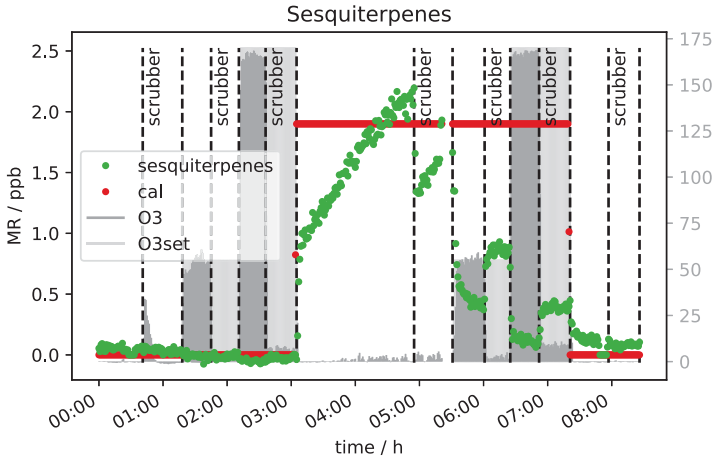

(A)

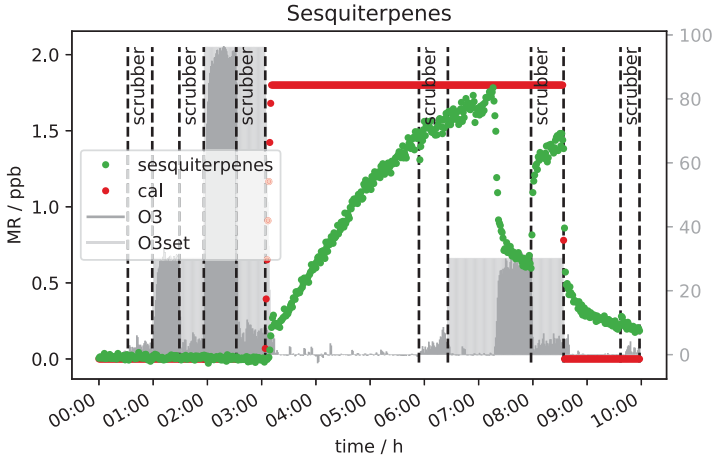

(B)

FIGURE 2.15: Sesquiterpene mixing ratio with and without scrubber different O_3 mixing ratios when 2 ppb of sesquiterpenes were introduced to the system; (a) 0 % RH, (b) 50 % RH.

This could explain why the ozone level during the scrubber performance test at a relative humidity of 80 % was relatively stable throughout the whole measurement time which was almost 3 days and why all the oxidant can be scavenged at an O_3 level of 1000 ppb.

2.4 Conclusions

Most species tested were not affected by ozone being present. Nevertheless, higher mixing ratios were observed for carbonyl compounds indicating an ozone interference. Signals for acetaldehyde, propanal, acetone and butanal increased with ozone levels above 150 ppb in zero air measurements with GC as well as PTR. Thus, it can be concluded, that there are positive artifacts generated in the experimental setup i.e. in the tubing, inside the ozone generator or within both of the mass spectrometers. As we observed the same

during stratospheric measurements before, the ozone generator cannot be the only source. Apel et al. originally conducted ozone sensitivity tests on their airborne GC-MS system due to anomalous acetaldehyde observations in the stratosphere. Our experiments also show acetaldehyde to be the species most affected by ozone interference. When our PTR encountered a stratospheric intrusion in flight as on 2nd June 2020 we found 0.88 ppb acetaldehyde (altitude 13000 m, O_3 465 ppb), extremely suspect for such a short-lived molecule under otherwise clean conditions. Unfortunately, the fast GC-MS did not measure acetaldehyde during this flight campaign. When 0.5 ppb of VOC standard gas was measured, the signals for propanal and butanal decreased due to the reaction with the OH radical, generated from ozonolysis of terpenes. For MEK no ozone interference could be observed. Decreasing signals were found for monoterpenes (α-pinene), sesquiterpenes (β-caryophyllene) and GC-isoprene as expected due to the direct reaction with ozone. The PTR-ToF-MS measured increasing "isoprene" mixing ratios on *m/z* 69 with increasing ozone concentration due to aldehyde fragments on the same exact mass. Those fragments are most likely ozonolysis products from some adsorbed species inside the FEP tubing or the instrument itself from some former measurements. Therefore caution should be applied when interpreting the isoprene mixing ratios provided by PTR-ToF-MS in high ozone environments. Generally the scrubber lifetime under tropospheric conditions (O_3 mixing ratios between 50 and 150 ppb) and a flow of 200 sccm is between five and fourteen days. The inlet flow of both instruments is the same (200 sccm), therefore the result can directly be used for ground based field measurements with the here employed PTR-ToF-MS and fast GC-MS systems. Sodium thiosulfate impregnated quartz filters are a very convenient means of ozone scavenging as the filters can be prepared in advance easily, at low cost and can be stored in a dry, dark and clean place. The preparation as well as the application are simple and the usage time for the filters is with several days long enough to allow measurement of complete diel cycles without stopping the measurements in between to open the inlet line for scrubber exchange. Nevertheless, the scrubbing technique as applied here is not suitable for sesquiterpene measurement. The observed loss of these analytes could be reduced with a $Na_2S_2O_3$ scrubber in line, but it could not be eliminated completely. Similar results have been reported earlier. Pollmann, Ortega, and Helmig (2005) found ozone concentrations in the sampling air reduced to 0.4 % when using a thiosulfate scrubber at an ozone mixing ratio of 100 ppb and 255 sccm. Unfortunately they did not report how long these conditions were measured. Nevertheless, their finding is comparable to that reported here, at 150 ppb O_3 and at the same flow the scrubber could reduce ozone to almost zero while at 50 ppb the oxidant's mixing ratio was below the limit of detection for more than 14 days. The tests have shown that the scrubbing technique used in this study performs well for most ground based operations of the VOC instruments, as inlet flows and ozone levels are usually low enough to stay within range of good performance of the sodium thiosulfate filter scrubber. Nonetheless, it is not possible to completely avoid sesquiterpene loss due to reaction with ozone during sampling. The current setup is not suitable for

measuring highly ozone reactive compounds such as sesquiterpenes or under high ozone conditions like in the lower stratosphere. Fortunately, since sesquiterpenes are emitted from the surface, they are extremely unlikely to be present in the stratosphere. In general it can be concluded that higher humidity has a positive influence on the VOC measurements performed here with a sodium thiosulfate filter scrubber, when ozone was present and no interference from the humidity on the gas analysis itself could be observed. Still, the O_3 removal is not sufficient to measure sesquiterpenes when ozone is present, not even at low mixing ratio such as 50 ppb. Implementing a stable humidification to the measurement system is non-trivial and additional effects for other analytes could develop. It is important to continue the development and characterization of reliable techniques which are cheap and easy to implement for lab as well as field experiments.
In summary we can say that insertion of the ozone scrubber resulted in the removal of most of the interferences observed. This implies that most of the effects observed were initiated in the inlet and any residual effects were produced within the instruments being therefore different and specific for each instrument. It is important to note that these improvements apply to the suite of gases tested here, and presumably also to those with comparable vapor pressures and ozone reactivities. The filter system could be further improved with a low dead volume filter housing to avoid any tiny air streams bypassing the filter inside the assembly and by the installation of multiple scrubbing filters in series as was tested by Pollmann, Ortega, and Helmig However, it is important to consider that the introduction of a filter into the system can also induce some negative effects. For example, highly oxygenated low volatility species are likely to suffer losses on such a filter assembly. Such compounds may need entirely different approaches such as inlet-less collection onto adsorbent filled cartridges or ozone removal at the inlet entrance by the addition of nitric oxide (NO). Furthermore, the filter itself can introduce flow rate limits to the inlet due to its physical restriction of flow. Generally, for field studies, our current recommended strategy is to use a high-volume, constant temperature, flow from inlet tip to close to the instrument and then subsample that flow, through the ozone scrubber, into the instrument at a lower rate. The inlet material should be Teflon in agreement with the findings of Deming et al. VOC emitting materials such as silicone should be avoided and during high local pollution events (such as in an aircraft taxiing on the ground) inlets should be stoppered or back flushed to avoid strong contamination.

Data availability: The data are published at https://doi.org/10.5281/zenodo.7576413 (Ernle and Ringsdorf, 2022).

Author contributions: LE and MAR designed the experiment; LE and MAR performed the measurements; LE and MAR analyzed the data; LE wrote the manuscript draft; MAR and JW reviewed and edited the manuscript.

Competing interests: The contact author has declared that neither they nor their co-authors have any competing interests.

Acknowledgements: We would like to acknowledge our lab technicians Thomas Klüpfel and Rolf Hofmann for exchanging gas bottles during long experiments.

References

Apel, EC et al. (2003). "A fast-GC/MS system to measure C2 to C4 carbonyls and methanol aboard aircraft".
In: *Journal of Geophysical Research: Atmospheres* 108.D20.

Bourtsoukidis, Efstratios et al. (2017).
"An aircraft gas chromatograph–mass spectrometer System for Organic Fast Identification Analysis (SOFIA): design, performance and a case study of Asian monsoon pollution outflow".
In: *Atmospheric Measurement Techniques* 10.12, pp. 5089–5105.

Buhr, Katja, Saskia van Ruth, and Conor Delahunty (2002).
"Analysis of volatile flavour compounds by Proton Transfer Reaction-Mass Spectrometry: fragmentation patterns and discrimination between isobaric and isomeric compounds".
In: *International Journal of Mass Spectrometry* 221.1, pp. 1–7.

Colomb, Aurélie et al. (2006).
"Airborne measurements of trace organic species in the upper troposphere over Europe: the impact of deep convection".
In: *Environmental Chemistry* 3.4, pp. 244–259.

Crutzen, Paul J and Jos Lelieveld (2001).
"Human impacts on atmospheric chemistry".
In: *Annual review of earth and planetary sciences* 29.1, pp. 17–45.

Deming, Benjamin L et al. (2019).
"Measurements of delays of gas-phase compounds in a wide variety of tubing materials due to gas–wall interactions".
In: *Atmospheric Measurement Techniques* 12.6, pp. 3453–3461.

Ernle, Lisa, Monika Akima Ringsdorf, and Jonathan Williams (2023).
"Influence of ozone and humidity on PTR-MS and GC-MS VOC measurements with and without a Na 2 S 2 O 3 ozone scrubber".
In: *Atmospheric Measurement Techniques* 16.5, pp. 1179–1194.
DOI: https://doi.org/10.5194/amt-16-1179-2023.

Helmig, Detlev (1997). "Ozone removal techniques in the sampling of atmospheric volatile organic trace gases".
In: *Atmospheric Environment* 31.21, pp. 3635–3651.

IUPAC (2021). *Atmospheric Chemical Kinetic Data Evaluation*.
URL: https://iupac-aeris.ipsl.fr/ (visited on 07/26/2021).

Koppmann, R et al. (1995). "The influence of ozone on light nonmethane hydrocarbons during cryogenic preconcentration".
In: *Journal of Geophysical Research: Atmospheres* 100.D6, pp. 11383–11391.

Koppmann, Ralf (2008). *Volatile organic compounds in the atmosphere*.
John Wiley & Sons.

Lehmpuhl, David W and John W Birks (1996).
"New gas chromatographic-electron-capture detection method for the determination of atmospheric aldehydes and ketones based on cartridge sampling and derivatization with 2, 4, 6-trichlorophenylhydrazine".
In: *Journal of Chromatography A* 740.1, pp. 71–81.
McDonald, Brian C et al. (2018). "Volatile chemical products emerging as largest petrochemical source of urban organic emissions".
In: *Science* 359.6377, pp. 760–764.
Northway, MJ et al. (2004). "Evaluation of the role of heterogeneous oxidation of alkenes in the detection of atmospheric acetaldehyde".
In: *Atmospheric Environment* 38.35, pp. 6017–6028.
Pagonis, Demetrios, Kanako Sekimoto, and Joost de Gouw (2019).
"A library of proton-transfer reactions of H3O+ ions used for trace gas detection". In: *Journal of the American Society for Mass Spectrometry* 30.7, pp. 1330–1335.
Pandis, Spyros N and John H Seinfeld (2006).
Atmospheric chemistry and physics: From air pollution to climate change.
Wiley.
Pollmann, Jan, John Ortega, and Detlev Helmig (2005).
"Analysis of atmospheric sesquiterpenes: Sampling losses and mitigation of ozone interferences".
In: *Environmental science & technology* 39.24, pp. 9620–9629.
Ruzsanyi, Veronika et al. (2013). "Multi-capillary-column proton-transfer-reaction time-of-flight mass spectrometry".
In: *Journal of Chromatography A* 1316, pp. 112–118.
Strömvall, Ann-Margret and Göran Petersson (1992). "Protection of terpenes against oxidative and acid decomposition on adsorbent cartridges".
In: *Journal of Chromatography A* 589.1-2, pp. 385–389.
ThermoFisherScientific (Apr. 2020a).
49iQ Instruction Manual, Ozone Analyzer.
— (Apr. 2020b). *49iQPS Instruction Manual, Ozone Primary Standard*.
Wang, Nijing et al. (2022).
"Emission rates of volatile organic compounds from humans".
In: *Environmental Science & Technology* 56.8, pp. 4838–4848.
Warneck, Peter and Jonathan Williams (2012). *The atmospheric Chemist's companion: numerical data for use in the atmospheric sciences*.
Springer Science & Business Media.
Weschler, Charles J and Nicola Carslaw (2018). "Indoor chemistry".
In: *Environmental Science & Technology* 52.5, pp. 2419–2428.
Weschler, Charles J and Helen C Shields (1997).
"Potential reactions among indoor pollutants".
In: *Atmospheric environment* 31.21, pp. 3487–3495.
Williams, Jonathan (2004).
"Organic trace gases in the atmosphere: an overview".
In: *Environmental Chemistry* 1.3, pp. 125–136.

Chapter 3

Assessment of aldehyde contributions to PTR-MS *m/z* 69.07 in indoor air measurements

This chapter has been accepted as: Lisa Ernle et al. (2023). "Assessment of aldehyde contributions to PTR-MS *m/z* 69.07 in indoor air measurements". In: *Environmental Science: Atmospheres*. Accepted

Contribution to this publication by Lisa Ernle: *Designed the experiment, conducted the GC-MS measurements, performed the data analysis and prepared the manuscript.*

Abstract Proton transfer reaction-mass spectrometry (PTR-MS) has been widely used for monitoring outdoor and indoor volatile organic compounds. For outdoor air, mass-to-charge-ratio *m/z* 69.070 is usually assigned to isoprene. Isoprene is also a major component of human breath and therefore abundant in occupied indoor environments. Mass 69.07 as an indicator of indoor isoprene can suffer interference resulting from fragmentation of aldehydes [Ruzsanyi *et al., Journal of Chromatography A*, 2013, **1316**, 112-118], which are also abundant indoors, especially when ozone is elevated [Weschler C. J. *Indoor air*, 2016, **26**, 6-24]. As part of the Indoor Chemical Human Emission and Reactivity (ICHEAR) campaign we examined this effect in human-occupied chamber studies, in the absence and presence of ozone. We find that such interferences do occur when ozone reacts with both human skin oil and cotton-based clothing. In the presence of humans and 35 ppb ozone, PTR-mass 69.07 was three times higher than the isoprene mixing ratio measured independently by GC-MS. To investigate this effect, we measured the fragmentation patterns of aldehydes and examined the contribution of different aldehydes to *m/z* 69.07 in the ICHEAR experiments. Nonanal, and its contribution to *m/z* 69.07, could be quantified reliably for clothing and human dermal emissions under the experimental conditions. In contrast, decanal is difficult to quantify, since compounds other than decanal fragment to *m/z* 157, its MH^+ peak, which also makes it difficult to estimate decanal's contribution to *m/z* 69.07.

3.1 Introduction

The measurement of volatile organic compounds (VOCs) in air is often performed using proton transfer reaction–mass spectrometry (PTR-MS) and gas chromatography–mass spectrometry (GC-MS). Generally, these techniques can generate high quality in-situ measurement data down to ppt (parts per trillion) detection limits with a time resolution of minutes (GC) or seconds (PTR). PTR-MS uses a rather soft ionization technique, which usually results in little fragmentation of the analytes after protonation so that the signal is usually detected at the analyte compound mass plus the mass of one proton. But, depending on the chemical structure of the analyte and the settings of the instrument, fragmentation can occur. Therefore, care must be taken to minimize measurement artifacts.

Ozone can play an important role in measurement artifacts indoors (e.g. Ernle, Ringsdorf, and Williams, 2023). It is ubiquitously present in outside tropospheric air and is transferred to indoor environments through passive or active ventilation. Indoors, ozone reacts rapidly, both on surfaces and in the gas phase, with compounds containing a double bond. Consequently, indoor concentrations tend to be 3-5 times lower than co-occuring outdoor concentrations (Nazaroff and Weschler, 2022). Humans are known to be a strong sink for indoor ozone, in particular through reactions with constituents of skin oils such as squalene and sapienic acid (Arata et al., 2019; Weschler, 2016; Weschler and Nazaroff, 2023). Such reactions have the potential to interfere

with mass spectrometric measurements of key reactive indoor compounds such as isoprene by generating additional signal on the target masses either directly or through fragmentation within the measurement device (as is the case for nonanal and decanal).

Isoprene is one of the most abundant reactive VOCs measured indoors when people are present (Wang et al., 2022). It is present in exhaled human breath (Buhr, Ruth, and Delahunty, 2002; Fenske and Paulson, 1999) and reacts rapidly with OH radicals and much less rapidly with ozone (O_3). The isoprene loss due to OH and O_3 depends on the reaction rate coefficient and the oxidant concentration. For typical indoor O_3 concentrations, and for the conditions used in our experiments, the isoprene loss due to OH and O_3 differs by at least one order of magnitude. Due to its large contribution to total indoor OH reactivity (Wang et al., 2020), isoprene needs to be accurately measured in studies of indoor OH dynamics. For a PTR-MS operating in the standard H_3O^+ mode, *m/z* 69.07 is usually assigned to isoprene (Yáñez-Serrano et al., 2021). Early iterations of PTR-MS were equipped with a quadrupole detector allowing only 1 amu mass resolution, so that any species generating signals between 69 and 70 amu were potential interferents with the accurate quantification of isoprene. Prior outside air studies noted the potential of cyclopentene, furan, 2-methyl-3-buten-ol(Williams et al., 2001) and even the minor constituent carbon suboxide (C_3O_2(Keßel et al., 2017)) to contribute to *m/z* 69. More recent versions of the PTR-MS have been equipped with a time of flight mass spectrometer capable of higher mass resolution allowing identification of the exact molecular formula; they are therefore less prone to interference through fragmentation. Nevertheless, compounds that can fragment onto the exact mass of protonated isoprene (*m/z* 69.07) can compromise the measurement.

Buhr, Ruth, and Delahunty investigated volatile flavour compounds and found that C_5 to C_9 saturated aldehydes fragment onto mass 69.07, while their isomeric ketones do not. Ruzsanyi et al. studied fragmentation patterns with a multi-capillary-column PTR-ToF-MS and reported that the most abundant ion for C_8 to C_{10} saturated aldehydes as well as for 3-methylbutanal was *m/z* 69.07. According to Gueneron et al. and Yuan et al. several cycloalkane species also produce fragments of the same mass.

In recent years, PTR-MS has been widely applied in indoor air research that involves VOC measurements (Coffaro and Weisel, 2022; Farmer et al., 2019; Rizk et al., 2018; Wang et al., 2022; Wisthaler et al., 2005). Aldehydes are common VOCs indoors (Salonen et al., 2009). When ozone is present in a human occupied indoor environment, nonanal and decanal can be formed from the oxidation of cooking oils and human skin oils, which coat indoor surfaces, furnishings and clothing (Rai et al., 2014; Weschler et al., 2007; Weschler and Nazaroff, 2023). Both aldehydes can contribute to *m/z* 69.07. Therefore, it is important to understand to what extent *m/z* 69.07 can originate from fragments when using PTR-MS (H_3O^+) to measure isoprene in occupied environments.

This study aims to assess the importance of potential interference effects in occupied indoor environments using data from both a PTR-MS and a GC-MS

system. We have measured potential interferents from human beings under controlled climatic conditions in the absence and presence of ozone. A separate fragmentation test of several aldehydes was performed with the PTR-ToF-MS used during the ICHEAR campaign. The experiments were designed to a) identify aldehydes that contribute to PTR *m/z* 69.07 in the ICHEAR studies, b) quantify their contributions to this mass fragment and c) determine if PTR-ToF-MS measurements of aldehydes and their fragments can be used to correct for their interference in indoor isoprene measurements.

3.2 Materials and methods

3.2.1 PTR-ToF-MS

VOC measurements were performed with the PTR-Tof-MS 4000 (IONICON Analytik, Austria). It was operated with standard operational settings in the ICHEAR study and the fragmentation experiment. The applied settings were: drift tube pressure p_{drift} 2.2 mbar, energy level in drift tube *E/N* 137 Td , and a drift temperature T_{drift} of 60°C. The fragmentation test was performed under a similar temperature (ca. 21°C) than the ICHEAR experiments (25°C, 31°C), but different relative humidity (dry condition for fragmentation experiment, RH 25% and 65% during ICHEAR). The instrument was operated at 1 s time resolution. For the fragmentation experiment C_5 to C_{10} aldehydes, which were all detected within the course of the ICHEAR experiment (Wang et al., 2020; Wang et al., 2022), were measured with PTR-ToF-MS in order to find the fragment masses of those compounds. Due to a lack of calibration gas standards, the VOC mixing ratio was calculated with the theoretical method described by Cappellin et al. where the measured counts were corrected by mass-dependent duty cycle. As C_5 to C_{10} aldehydes are target compounds in this study, we used the proton transfer rate coefficient of those aldehydes (k-rate) proposed in Cappellin et al. for more accurate quantification. The uncertainty of the theoretic calculation is mainly from the calculated *k*, which is considered to be 10-15% from quantum chemical calculations (Cappellin et al., 2012). For the isoprene quantification during the ICHEAR experiments, using PTR-ToF-MS, the total uncertainty is 6%, including signal precision and calibration accuracy (gas standard uncertainty, flow measurement accuracy and calibration curve fitting uncertainty). Limits of detection (LOD, 3σ) were <0.043 ppb, with a total uncertainty of 15% during ICHEAR. For the fragmentation test, raw ion signals (counts per second, cps) were normalized by the sum of the primary reagent ion (H_3O^+) and the first water cluster ($(H_2O)_2H^+$) and reported as normalized counts per second (ncps). The same normalization approach was also performed for the ICHEAR experiments for quantification. The total measurement uncertainty for the fragmentation test was usually $\leq$34%.

3.2.2 Fast GC-MS

Isoprene was measured with a custom-built fast GC-quadrupole-MS system previously described by Bourtsoukidis et al. The instrument includes a three-step cryogenic pre-concentration unit, which first collects the analytes before rapidly injecting them from the last trap into the GC-system (heating rate 100° C/s^{-1}). The instrumental setup is equipped with an internal calibration system, which is used to perform calibrations with up to five different standard gas levels. A 4-5 point calibration was performed every day. With a chromatographic separation time of 2.5 minutes and a total GC-cycle time of 3 min the system is considered a quasi-online measurement device. Due to the high time resolution, the fast GC-MS currently cannot measure larger aldehydes ($\geq$ C_7). Isoprene was detected in single ion monitoring (SIM) mode on *m/z* 68 and was nicely separated from adjacent peaks. The total measurement uncertainty was usually $\leq$10%. The propagation of uncertainty was calculated including the uncertainties of the calibration curve, the measured mixing ratio, the volumes in GC and calibration system, the isoprene mixing ratio in the calibration gas cylinder, and from the peak integration.

3.2.3 Experimental setup for the fragmentation test

A synthetic air flow was connected to a mass flow controller (MFC) which was set to 1 slpm. Shortly after the MFC, an injection T-piece was installed. It was made of Nylon connections with a septum, through which the needle of a gas syringe could be inserted. 5 to 25 µL gas phase headspace samples of the aldehydes were injected manually in the PTR-ToF-MS at least five times. Different volumes were chosen for different aldehydes due to their different vapor pressures. The goal was to get a reasonably high signal. Chemicals used for the aldehyde fragmentation test are shown in Table 3.1. This fragmentation test was performed under dry conditions and the results were used to determine the contribution of fragmentation to *m/z* 69.07 for the chamber experiments. A later set of fragmentation experiments were performed under different RH conditions (RH30 and RH60) for reference but not applied to the calculations because the detection efficiency for heavier compounds cannot be compared due to the replacement of the detector of the PTR-ToF-MS.

3.2.4 ICHEAR setup

Four human subjects were sitting in a stainless steel chamber with an air change rate of 3.2 h^{-1}. The temperature and relative humidity set points in these experiments were ca. 25°C/25% and 31°C/65%. After three hours of measurement without ozone present, ozone was introduced with a target concentration in the occupied chamber of 35 ppb. The subjects were asked to use a provided set of fragrance-free personal care products and laundered, new cotton clothing. VOC emissions were measured with PTR-ToF-MS and

TABLE 3.1: Chemicals used for aldehyde fragmentation with PTR-ToF-MS. Concentrations were between 95 and 99%.

Chemical compound	Supplier
pentanal	Merck
hexanal	Aldrich
heptanal	Aldrich
octanal	Aldrich
nonanal	Aldrich
decanal	Alfa Aesar

GC-MS. In order to simplify the analysis, experiments without breath emissions (and therefore without isoprene) were first examined from the ICHEAR data set. These experiments included the investigation of four new and worn shirts, with and without ozone as well as experiments with human dermal and clothing emissions. The latter were obtained by having the exhalations from four human volunteers wearing masks transferred into a neighboring chamber so that the occupied chamber air was only influenced by dermal emissions. To investigate the humidity dependence, worn shirts were additionally measured in one experiment with three levels of RH (set points 30, 50, and 70%), each lasting at least 1.5 h. An overview of the here used ICHEAR experiments can be found in Table 3.2. From this data we identified possible aldehydes which fragment on PTR-ToF mass 69.07. More detailed information on the ICHEAR setup can be found in Bekö et al.

TABLE 3.2: Overview of the experiments performed during the ICHEAR campaign.

Experiment	Ozone	Temp. / ° C	RH
ICHEAR dermal	No	25	25
		31	65
	Yes	25	25
		31	65
ICHEAR shirts new	No	25	25
	Yes	25	25
ICHEAR shirts worn	No	25	25
	Yes	25	25, 30, 50, 70
ICHEAR whole body	No	25	25
	Yes	25	25

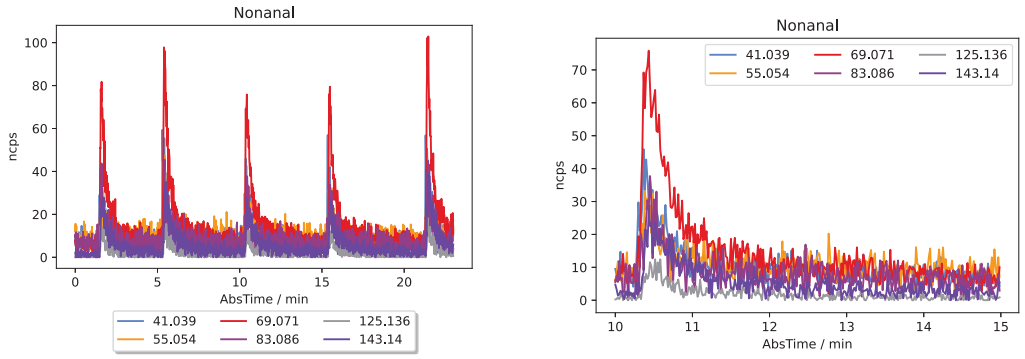

(A) (B)

FIGURE 3.1: Signals of masses detected after injection of nonanal headspace samples (a) and a zoomed-in plot of one signal (b).

3.2.5 Calculation of aldehyde signals for ICHEAR experiments

The laboratory determined fragment ratios measured with the PTR-ToF-MS were compared with ratios obtained from ICHEAR data and used to calculate the contribution from aldehyde emission to measured mass 69.07 during ICHEAR. Additionally, an experiment with human whole-body emission (dermal and breath) has been added as a more complicated example. In PTR-MS the mass used for carbonyl detection is the mass of the protonated carbonyl compound (MH^+). This mass actually includes the sum of aldehydes and ketones (e.g. pentanal and pentanone). Due to the fact that aldehydes are much more likely to lose a water molecule during ionization than ketones, the parental mass minus 18 is usually considered as a fragment of that aldehyde, which needs to be considered in quantification unless there are other interferences on this mass (Buhr, Ruth, and Delahunty, 2002). In this study these masses will be called MH^+-H_2O. The fragment fractions *f* reported in this study are an average from five replicate measurements (see Figure 3.1a exemplarily for nonanal). Peak integration was used to calculate the fraction of the specific fragment mass (see Figure 3.1b for a more detailed plot of the nonanal fragment masses after injection): Integration was performed between the two time points that define twice the detection limit (LOD=3*noise) of the *m/z* ratio with the lowest fraction (but $\geq$5% fragment fraction; for nonanal this is the grey line, *m/z* 125.136). The fragment fraction f_{frag} is described by the ratio of counts on the fragment (s_{frag}) and the sum of counts on all designated fragments (s_{CHO}, see Equation 3.1) of the same aldehyde (see Equation 3.2).

$$s_{CHO} = \sum_{i=1}^{n} s_{frag_i} \tag{3.1}$$

Where s_{frag_i} is the signal (ncps) for fragment i of n fragments. For example, we chose n=6 for the six observed fragments of nonanal (143.14, 125.14, 83.09,

69.07, 55.05 and 41.04).

$$f_{\text{frag}} = \frac{s_{\text{frag}}}{s_{\text{CHO}}} \tag{3.2}$$

Using the fragment fraction f_{frag} of one aldehyde, the signal for mass 69.07 from a specific aldehyde (s_{m69}) can be calculated with Equation 3.3 using the signal of the protonated aldehyde MH^+ (s_{MH^+}) and the fraction of mass 69.07 (f_{m69}) and MH^+ (f_{MH^+}) as shown in Equation 3.3. The calculated *m/z* 69.07 signal can be used to estimate the contribution of the specific aldehyde to the total measured *m/z* 69.07 signal.

$$s_{\text{m69}} = s_{\text{MH}^+} * \frac{f_{\text{m69}}}{f_{\text{MH}^+}} \tag{3.3}$$

3.2.6 Evaluation of the fragment fractions

The fragment ratio R_{CHO} has been calculated with Equation 3.4. It describes the ratio of the aldehyde's parental ion signal (s_{MH^+}) and the signal of its second mass fragment ($s_{MH^+\text{-}H_2O}$).

$$R_{\text{CHO}} = \frac{s_{\text{MH}^+}}{s_{\text{MH}^+\text{-}\text{H}_2\text{O}}} \tag{3.4}$$

The ratio is used to estimate whether or not there is an interference on MH^+ or MH^+-H_2O. It is not used in the calculation of the contribution of an aldehyde to *m/z* 69.07. If the ratio of those two fragment signals from the same aldehyde is the same in real world measurements than in the fragmentation test (where a single measurement of the aldehyde was performed without other compounds interfering), it can be assumed that there is no interference on neither MH^+ nor MH^+-H_2O. In case of interference of other compounds, it is unlikely that the ratio of the two fragments will stay the same. This ratio for the ICHEAR experiments discussed in the present paper has been compared to the ratio from the fragmentation test (see Table 3.4, Section 3.3.2). Additionally, the coefficient of determination R^2 has been used to estimate the reliability of R_{CHO}. The Pearson correlation coefficient r was obtained for the correlation of the signals on MH^+ with MH^+-H_2O for each single ICHEAR experiment. The average of all the squared correlation coefficients (average of the coefficients of determination R^2) is used for the estimation of the reliability of R_{CHO}. If the correlation is strong (coefficient of determination $R^2 \geq 0.90$) and the ratio is the same over several experiments including the fragmentation test, it can be assumed that there is no interference on the masses used for aldehyde detection. Please note that for experimental setups with different RH (e.g. ICHEAR shirts worn), an average ratio has been used.

TABLE 3.3: Measured fragment masses and their fractional contribution to the total, ±standard deviations, for C_5 to C_{10} aldehydes as measured in the fragmentation test (this study) or reported in the literature.

Aldehyde	Reference	Fragment masses [amu] and percent of total							
		MH^+	MH^+-H_2O						
Decanal		**157.16**	**139.15**	**97.11**	**83.09**	**69.07**	**55.05**		
	this study	12.9 ± 4.4	2.8 ± 1.1	11.2 ± 2.0	33.1 ± 3.9	10.8 ± 2.1	29.1 ± 3.8		
	Ruzsanyi et al.	4	-	12	66	18	-		
Nonanal		**143.14**	**125.14**	**85.08**	**83.09**	**69.07**	**55.05**	**41.049**	
	this study	12.9 ± 3.9	5.4 ± 2.0	-	13.8 ± 3.9	34.7 ± 4.2	15.1 ± 3.2	18.1 ± 4.5	
	Buhr et al.	19	11	-	15	36	3	3	
	Ruzsanyi et al.	22	-	14	23	40	-	-	
Octanal		**129.13**	**111.12**	**69.07**	**55.05**	**41.04**			
	this study	8.3 ± 1.7	17.7 ± 3.6	46.2 ± 2.8	9.8 ± 1.3	18.0 ± 3.6			
	Buhr et al.	11	38	40	2	3			
Heptanal		**115.11**	**97.11**	**69.07**	**55.05**	**41.04**			
	this study	4.8 ± 1.1	47.2 ± 2.5	4.8 ± 0.6	40.8 ± 2.8	2.4 ± 0.6			
	Buhr et al.	5	61	4	26	-			
Hexanal		**101.10**	**83.09**	**69.07**	**59.05**	**57.07**	**55.05**	**45.03**	**41.03**
	this study	4.1 ± 1.1	37.4 ± 6.7	1.5 ± 1.2	5.0 ± 3.6	1.7 ± 1.3	40.2 ± 5.9	7.3 ± 5.2	2.7 ± 1.3
	Buhr et al.	-	63	-	-	-	29	-	-
Pentanal		**87.08**	**69.07**	**45.03**	**41.04**				
	this study	5.1 ± 1.3	58.7 ± 3.6	7.4 ± 0.7	25.6 ± 3.0				
	Buhr et al.	-	71	4	15				

3.3 Results and Discussion

3.3.1 Aldehyde fragmentation fractions

Table 3.3 shows the fragment fractions for C_5 to C_{10} saturated aldehydes obtained from the fragmentation test of the present study and other studies using PTR-MS. If Buhr, Ruth, and Delahunty or Ruzsanyi et al. observed fragments which were not observed in the present study, only masses with fractions $\geq$ 10% are listed. Ruzsanyi et al. reported only the most abundant fragments. The fractions of mass 69.07 are similar, while generally the studies of Buhr, Ruth, and Delahunty and Ruzsanyi et al. report higher fractions for masses larger than 69.07 amu. The probability of fragmentation increases with the *E/N* value. Ruzsanyi et al. measured at *E/N* 140 Td which is comparable to our value of 137 Td. Unfortunately, Buhr, Ruth, and Delahunty did not report their *E/N* value. According to Schwarz, Filipiak, and Amann, the water concentration in the ion source also influences the fragmentation. Additionally the ratio of the water cluster to protonated water (*m/z* 37/*m/z* 19) should be comparable when comparing fragmentation patterns. This information was not available for the studies of Buhr, Ruth, and Delahunty and Ruzsanyi et al. Therefore, care must be taken when interpreting the values in Table 3.3.

3.3.2 Comparison of fragment fractions

Our own tests indicate that the fraction of mass at MH^+ and MH^+-H_2O does increase with relative humidity, while their ratio (R_{CHO} as defined in Equation 3.4) showed no clear humidity dependence. Therefore, the R_{CHO} from the fragmentation test can be compared with R_{CHO} from ICHEAR. For hexanal, heptanal and decanal the average R_{CHO} from ICHEAR are not in line

TABLE 3.4: Ratio R_{CHO} of the signals of MH^+ over MH^+-H_2O, as well as average coefficient of determination (R^2) between MH^+ and MH^+-H_2O, for C_5-C_{10} aldehydes as measured in the fragmentation test and ICHEAR experiments (see Table 3.2). Average values are displayed with their standard deviation.

Experiment	$R_{pentanal}$	$R_{hexanal}$	$R_{heptanal}$	$R_{octanal}$	$R_{nonanal}$	$R_{decanal}$
fragmentation	**0.10±0.01**	**0.11±0.00**	**0.10±0.01**	**0.47±0.02**	**2.38±0.15**	**4.68±0.57**
ICHEAR shirts new	0.10±0.07	0.13±0.06	0.28±0.12	0.65±0.25	2.12±0.67	-
ICHEAR shirts worn	0.08±0.03	-	0.16±0.02	0.48±0.02	2.36±0.35	9.48±0.29
ICHEAR dermal	0.12±0.00	0.16±0.01	0.19±0.02	0.31±0.14	2.19±0.07	8.36±0.69
ICHEAR whole body	0.09±0.09	-	0.19±0.20	0.48±1.50	2.31±6.13	9.62±20.66
average	**0.10±0.02**	**0.15±0.02**	**0.19±0.04**	**0.45±0.14**	**2.26±0.10**	**9.06±0.74**
average R^2	0.65±0.25	0.94±0.02	0.57±0.33	0.81±0.14	0.94±0.07	0.89±0.07

with R_{CHO} from the fragmentation test. This indicates that there are fragments from other compounds on MH^+ or MH^+-H_2O. The highest difference of R_{CHO} from ICHEAR compared to the fragmentation test is obtained for decanal and heptanal, where $R_{decanal}$ is 4.68±0.57 and $R_{heptanal}$ is 0.10±0.01 for the fragmentation test while it is 9.06±0.74 and 0.19±0.04 for the ICHEAR data respectively. Possible candidates responsible for this difference are isomeric compounds as well as $C_{10}H_{20}OH^+$ and $C_7H_{14}OH^+$fragments from larger compounds. It is more likely that other compounds fragment on mass 157.16 and 115.11 under the experimental conditions of ICHEAR as indicated by the high R_{CHO} values. Thus, assigning 157.16 to decanal alone would result in an artifactually high concentration. Possible fragments on *m/z* 157.16 can be ketones with ten carbon atoms, as well as menthol (Spanel and Smith, 1997) and dihydromyrcenol (Campbell et al., 2013), which are used as fragrance ingredients in soaps and detergents. For heptanal, fragments could potentially come from ketones with seven carbon atoms.

The difference in R_{CHO} between ICHEAR and the fragmentation test is below the standard deviation for pentanal, octanal and nonanal. But, the coefficients of determination R^2 for pentanal, heptanal and octanal are lower (between 0.57 and 0.81) than R^2 of the other aldehydes, indicating a rather weak correlation of MH^+ with MH^+-H_2O.

The only compound where R_{CHO} from the ICHEAR experiments is in line with the fragmentation experiment and the coefficient of determination is $\geq$ 0.90 is nonanal (ICHEAR $R_{nonanal}$ 2.26±0.10 compared to fragmentation test $R_{nonanal}$ 2.38±0.15, R^2=0.94±0.07). This means that for nonanal interference of other compounds on MH^+ or MH^+-H_2O (*m/z* 143.14, *m/z* 125.14) is unlikely. In summary, we consider the results of nonanal reliable, while those of the other C_5-C_{10} aldehydes are likely to be defective.

The fragmentation test was not performed under perfect conditions as there were possible impurities in the head space sample from other chemicals. For quality assurance, zero air was injected after several injections of each aldehyde. These syringe background samples have not shown a substantial increase in the monitored aldehyde masses. The fragmentation test delivered quite similar results for the five injections made per compound with the

standard deviation usually below 25% and the fragment fractions are comparable to those reported by other groups (Buhr, Ruth, and Delahunty, 2002; Ruzsanyi et al., 2013). Therefore, the fragmentation test is considered to be accurate enough for the results presented in Table 3.3 to be considered reliable.

3.3.3 Measured and calculated signals of nonanal in indoor air

During the ICHEAR campaign, we measured emissions in the absence and presence of ozone, from i) human body excluding breath (dermal), ii) new t-shirts, iii) worn t-shirts and iv) human bodies including breath (whole body). Results from these separate experiments, for steady-state conditions, are shown in Figure 3.2. The yellow bars show the percent of the total measured signal for *m/z* 69.07 due to nonanal as calculated using Equation 3.3. Generally, for dermal and shirt experiments in the absence of ozone, nonanal contributes between 40 and 60% to the measured signal resulting from all gas-phase compounds with fragments at *m/z* 69.07. For the experiment on human whole body emission, nonanal contributes only about 5%. In contrast, in the presence of ozone, nonanal contributes between 55% and 100% to the measured signal from all compounds at *m/z* 69.07 for dermal and shirts experiments and ca. 35% for the whole body conditions. In other words, during periods of elevated ozone, nonanal is the dominant contributor to the mass-to-charge-ratio which is commonly used to quantify isoprene under conditions excluding human breath and it is still contributing more than one 3rd to the total *m/z* 69.07 during measurement of human whole body emissions.

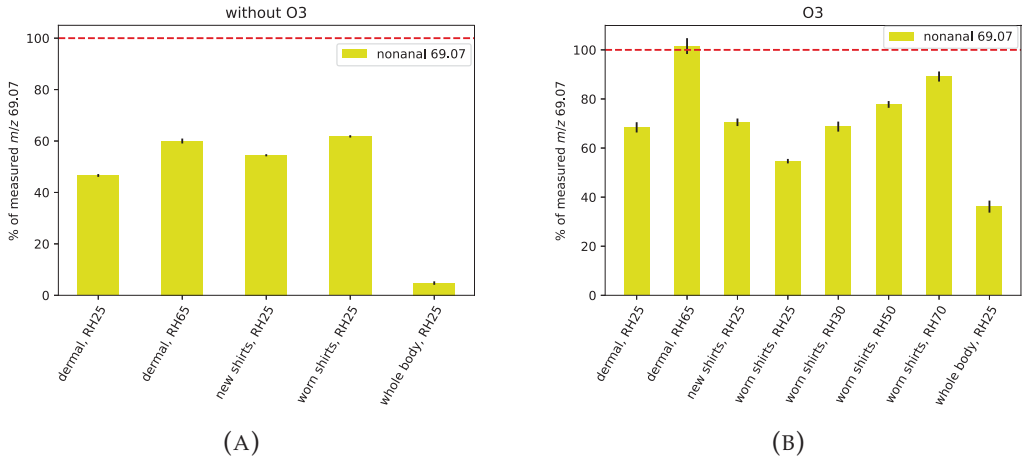

(A) (B)

FIGURE 3.2: For different ICHEAR experiments (see 3.2), the yellow bars indicate the percent of the total measured signal for *m/z* 69.07 due to nonanal as calculated using Equation 3.3. (a) In the absence of ozone; (b) in the presence of ozone. The small black lines indicate the standard deviation.

Influence of relative humidity

The nonanal signal increases with relative humidity. In the case of emissions from human bodies excluding breath (dermal experiments in Figure 3.2), *m/z* 69.07 from nonanal was a larger fraction of the total measured *m/z* 69.07 at 65% RH than at 25% RH. Both, for absent and present ozone. This is consistent with observations that humidity suppresses formation of stable secondary ozonides in triolein (Zhou, Zhou, and Abbatt, 2019); triolein and related unsaturated fats are an important source of ozone-derived nonanal. Relatedly, Arata et al. observed increased concentrations of carbonyls for the squalene ozone reaction with increased humidity. It is also consistent with the results summarized in the critical review by Coffaro and Weisel of ozone/squalene chemistry. Besides changes in ozonolysis chemistry with RH, the humidity dependence of a PTR-MS system can also play a role. It is known that signals from a PTR-MS using H_3O^+ ions are humidity dependent for some VOCs. Trefz, Schubert, and Miekisch reported increasing signal intensities for aldehydes as humidity increased. This is in line with our own tests, which showed increasing intensities for high fragment masses (including MH_+) and lower intensities for smaller fragment masses of the same compound. It is unclear to what extent the observed relative humidity effects are attributable to ozonolysis chemistry or less fragmentation with increasing humidity. In the ICHEAR study, the measured signals of nonanal were not corrected for the humidity dependence due to a lack of single component gas standards. Therefore, aldehydes' RH-dependency could lead to an overestimation of *m/z* 69.07 from nonanal. Both, RH-dependent ozonolysis experiments and the aldehydes' RH-dependency should be investigated to better estimate the relative contribution of these two effects. Note: the calculated contribution of nonanal to *m/z* 69.07) may be high, since the ratio of the fragment fractions (f_{m69}/f_{MH^+}) used for the Equation 3.3 calculation are from the fragmentation test, which was performed under dry conditions. Although $R_{nonanal}$ does not show a humidity dependence, $f_{m69}/f_{m143.14}$ decreases with RH. Based on our tests, the expected maximum decrease of this fraction is ca. 30%.

Human dermal and clothing emission

Focusing on the clothing experiments in which isoprene from breath emissions is absent (Figure 3.2a), it can be seen that with and without ozone, *m/z* 69.07 from nonanal at RH $\leq$ 30% accounts for roughly 50-60% of the measured *m/z* 69.07. For the experiment on human dermal emission at RH 25%, which excludes breath emissions by design, the contribution from nonanal is ca. 45% at the lower RH and 60% at the higher RH. In Figure 3.2b it can be seen clearly that the presence of 35 ppb of ozone leads to the emission of aldehydes in all experimental setups. Nonanal and decanal are primary products of the reaction of skin oil and clothing fabric with ozone. The mixing ratios of those products depend on the difference between inlet and outlet ozone mixing ratio (100-35 ppb = 65 ppb). Therefore, if we assume a much smaller

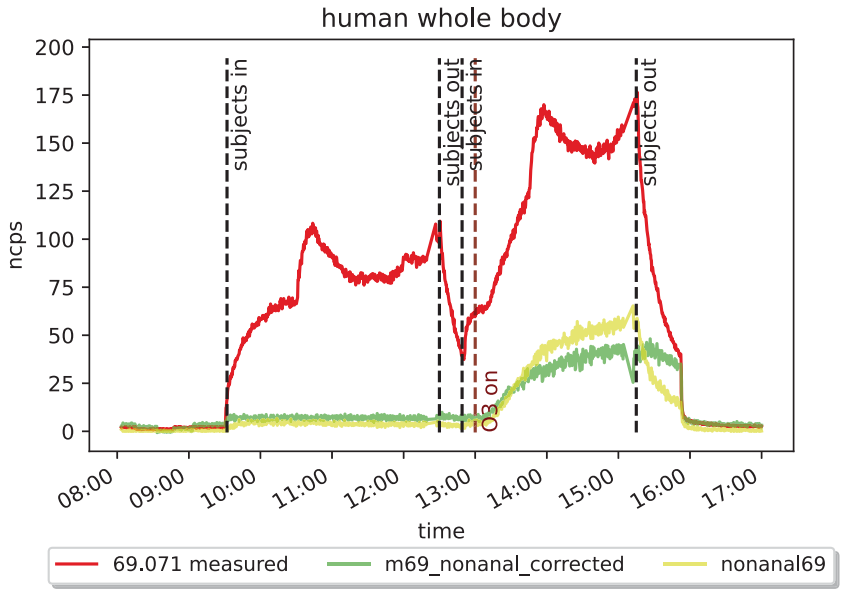

FIGURE 3.3: Signals of measured *m/z* 69.07 (red), calculated *m/z* 69.07 from nonanal (yellow) and *m/z* 69.07 corrected by the contribution of nonanal (green) from the ICHEAR whole body experiment (dermal and breath emission).

difference that may occur during the evening, such as 10 ppb of O_3, the contribution of the aldehydes would be approximately seven times lower than what we found in this study. In measurements of soiled t-shirts emissions absent and present ozone, Rai et al. found that nonanal and decanal emissions increased with ozone, RH and the soiling level of t-shirts.

Human whole body emission (dermal and breath)

The fraction of fragmentation signal on *m/z* 69.07 from nonanal without ozone present is significantly lower for the whole body experiment compared to other experiments. This is mainly due to isoprene, a component of human breath, which contributes to *m/z* 69.07 in the whole body emissions experiments, but not in the dermal-only or clothing experiments.

A timeline from the whole body (both, dermal and breath emissions) experiment, without and with ozone, is shown in Figure 3.3. In the morning (09:30-12:30), the red line (measured *m/z* 69.07) is mainly from isoprene in breath. The contribution of nonanal (yellow) to the *m/z* 69.07 signal is negligible. Aldehydes are not expected to be present in large amounts without ozone. In the afternoon (13:00-16:00) somewhat similar isoprene mixing ratios as in the morning would be expected, and this was the case for measurements by the fast GC-MS system. However, in the case of PTR-MS measurements, after ozone was switched on the green line (measured *m/z* 69.07 minus contribution from nonanal) is roughly 20 ncps higher than the morning signal. The results from the whole body experiment, which includes isoprene from breathing, show that the interpretation of the *m/z* 69.07 signal becomes more difficult with an increasing number of VOC sources, especially when

ozone is present.
Ozonolysis of VOCs from different sources including skin oils, cooking oils and colorants for fabric produces many different compounds including aldehydes (Coleman et al., 2008; Rai et al., 2014; Weschler et al., 2007; Wisthaler et al., 2005). This leads to additional compounds which were not considered in this study that may also fragment onto *m/z* 69.07, MH^+-H_2O or MH^+. Ozonolysis of compounds coming from the clothing fabric (cotton in the present case) can result in emission of nonanal and we can quantify nonanal's contribution to *m/z* 69.07. However, our results show, that if we consider only nonanal, we are missing other sources of *m/z* 69.07 fragments. Numerous studies have reported the production of decanal from the reaction of O_3 with skin oil (Weschler and Nazaroff, 2023). For this reason, decanal is also found on soiled clothing (Coleman et al., 2008; Weschler et al., 2007; Wisthaler et al., 2005). In the present study we measured ions which are usually assigned to decanal (MH^+ *m/z* 157.16 and MH^+-H_2O *m/z* 139.15), but our experiments have shown interference from other compounds on those masses. Hence, we cannot reliably quantify the contribution of decanal to *m/z* 69.07.

3.3.4 Comparison of GC-isoprene with PTR-*m/z* 69.07

Results from human whole body emission experiments in the presence of ozone show large discrepancy in isoprene emission measured by GC-MS and PTR-Tof-MS even after accounting for the interference from nonanal on PTR isoprene mass (*m/z* 69.07) as can be seen in Figure 3.4. In the morning, when O_3 was not present in the chamber, the signals agree well, while after ozone was switched on at around 13:00 (reaching ∼35 ppb), they differ substantially. The PTR-ToF-MS detects roughly 40% higher "isoprene" mixing ratio compared to the GC. Before subtracting the amount of *m/z* 69.07 which was produced from nonanal, the PTR-ToF-MS measured more than double the GC measured mixing ratio when O_3 was present. For our conditions, 1 ppb nonanal contributes to *m/z* 69.07 equivalent to approximately 1.45 ppb isoprene. However, there are still missing contributors for a reliable quantification of isoprene in the presence of ozone (e.g. decanal as discussed in section 3.3.3). The inlet and outlet O_3 mixing ratios in the ICHEAR experiments result in a difference of about 65 ppb. For a hypothetical night-time indoor-outdoor difference of 10 ppb, the interference would be approximately $1/7^{th}$ of that measured in this study. This would still result in ca. 0.5 ppb of "false isoprene" as the real isoprene mixing ratio was 3.5 ppb with four people in the chamber during the human whole body experiment.

3.4 Conclusions

Our experiments have shown that for an occupied indoor environment, isoprene cannot be quantified reliably with PTR-MS in H_3O^+ mode, since there are other compounds which can fragment on *m/z* 69.07. This is the case with humans as the primary emission source - other emission sources such as furniture, cooking or cleaning products were not present in this study. The same

applies if aldehydes or cycloalkanes from other sources are expected to be present in the sample air, since these compounds are known to fragment on the mass commonly attributed to isoprene in the PTR-MS community. If outdoor ozone concentrations are much lower, resulting in lower indoor product formation rates, the interference on *m/z* 69.07 due to products of ozone chemistry would be lower. Therefore, for the quantification of isoprene indoors, it is recommended to use PTR-MS with NO^+ as the primary reagent ion or a different, more specific measurement technique such as GC-MS, which preseparates the chemicals prior to mass spectrometric detection. However, for low ozone conditions and absent aldehyde emission sources, the contribution of compounds other than isoprene to *m/z* 69.07 may be negligible.
From the data it can be seen that for nonanal, the ratio $R_{nonanal}$ (i.e. MH^+ over MH^+-H_2O) from ICHEAR experiments agrees with the fragmentation test. Hence, those masses could be used for quantification of nonanal under the ICHEAR conditions and they can be used to quantify the contribution of nonanal to PTR *m/z* 69.07. In contrast, decanal from the ICHEAR data set shows an $R_{decanal}$ value that is almost double the value obtained from direct injection of the analyte. This leads to the conclusion that there might be a significant amount of C_{10} ketones produced or other compounds such as menthol or dihydromyrcenol that fragment on mass 157.16 within the context of indoor human emissions. Hence, the contribution of decanal to *m/z* 69.07 in indoor air measurements cannot be accurately quantified. The ratios R_{CHO} for hexanal and heptanal are also not in line with the ratio from the fragmentation test experiment and can therefore not be used to calculate these aldehydes' contribution to *m/z* 69.07 due to other compounds interfering on MH^+

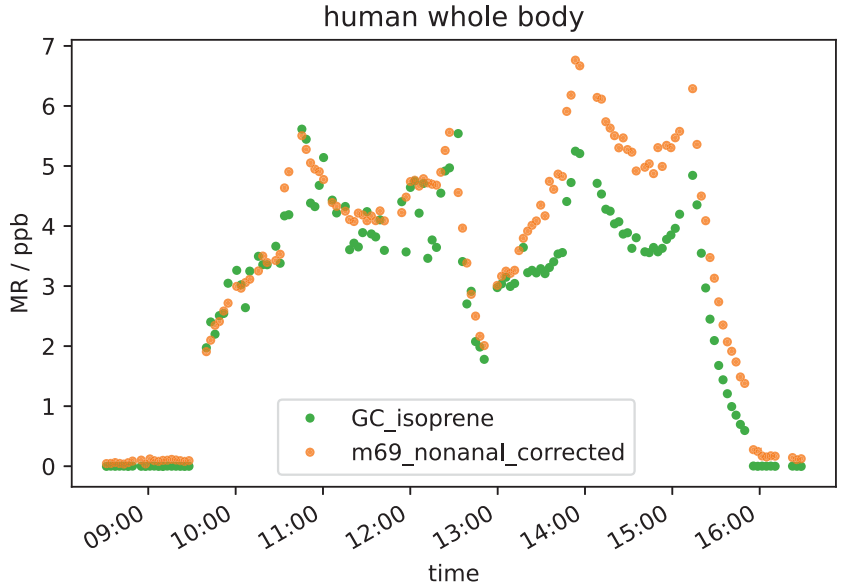

FIGURE 3.4: Mixing ratios (MR) of isoprene from the ICHEAR whole body experiment measured with GC-MS (green circles) and PTR-ToF-MS (orange circles). The PTR-ToF-MS values have been corrected for the interference produced from nonanal.

or MH^+-H_2O. The ratio of pentanal and octanal fit the fragmentation test, but the standard deviation for $R_{octanal}$ is very high (±0.13 for an average of $R_{octanal}$ of 0.45) and the coefficient of determination indicates a weak correlation for both, pentanal and octanal. The majority of the human-derived interferences to *m/z* 69.07 stem from the ozonolysis of human skin oil and cotton clothing (prewashed in fragrance free detergent) that generates nonanal. Most likely, significant additional interference was provided by decanal which was almost exclusively generated from ozone reactions with skin oil.
Further experiments and calculations should be performed to better determine under which conditions the aldehyde contribution to m/z 69.07 can be quantified with PTR-MS in H_3O^+ mode. The humidity dependence of fragmentation needs to be studied in detail to better understand the change in fragmentation pattern induced by change in humidity. This information would further improve the accuracy of the calculated contribution of nonanal to *m/z* 69.07, as well as the quantification of nonanal itself. Additionally, it would be helpful to estimate an ozone guideline value below which isoprene can still be measured reliably with PTR-MS in H_3O^+ mode since this is a standard measurement technique used for indoor measurements.

Author Contributions

LE and NW designed the experiment, performed the measurements and analyzed the data. LE wrote the manuscript draft, NW, GB, GCM, PW, CJW and JW reviewed and edited the manuscript.

Conflicts of interest

There are no conflicts of interest to declare.

Acknowledgements

The ICHEAR experiment was funded by the Alfred P. Sloan Foundation.

Data availability

The data are published at https://doi.org/10.5281/zenodo.8102656 (Ernle and Wang, 2023).

Notes and references

Arata, Caleb et al. (2019). "Heterogeneous ozonolysis of squalene: gas-phase products depend on water vapor concentration". In: *Environmental science & technology* 53.24, pp. 14441–14448.

Arata, Caleb et al. (2021). "Volatile organic compound emissions during HOMEChem". In: *Indoor air* 31.6, pp. 2099–2117.

Bekö, Gabriel et al. (2020). "The Indoor Chemical Human Emissions and Reactivity (ICHEAR) project: Overview of experimental methodology and preliminary results". In: *Indoor Air* 30.6, pp. 1213–1228.

Bourtsoukidis, Efstratios et al. (2017). "An aircraft gas chromatograph–mass spectrometer System for Organic Fast Identification Analysis (SOFIA): design, performance and a case study of Asian monsoon pollution outflow". In: *Atmospheric Measurement Techniques* 10.12, pp. 5089–5105.

Buhr, Katja, Saskia van Ruth, and Conor Delahunty (2002). "Analysis of volatile flavour compounds by Proton Transfer Reaction-Mass Spectrometry: fragmentation patterns and discrimination between isobaric and isomeric compounds". In: *International Journal of Mass Spectrometry* 221.1, pp. 1–7.

Campbell, Dahlia I et al. (2013). "Chemical analysis and chemical imaging of fragrances and volatile compounds by low-temperature plasma ionization mass spectrometry". In: *Rapid Communications in Mass Spectrometry* 27.16, pp. 1828–1836.

Cappellin, Luca et al. (2012). "On quantitative determination of volatile organic compound concentrations using proton transfer reaction time-of-flight mass spectrometry". In: *Environmental science & technology* 46.4, pp. 2283–2290.

Coffaro, Breann and Clifford P Weisel (2022). "Reactions and Products of Squalene and Ozone: A Review". In: *Environmental Science & Technology* 56.12, pp. 7396–7411.

Coleman, Beverly K et al. (2008). "Ozone consumption and volatile byproduct formation from surface reactions with aircraft cabin materials and clothing fabrics". In: *Atmospheric Environment* 42.4, pp. 642–654.

Ernle, Lisa, Monika Akima Ringsdorf, and Jonathan Williams (2023). "Influence of ozone and humidity on PTR-MS and GC-MS VOC measurements with and without a Na 2 S 2 O 3 ozone scrubber". In: *Atmospheric Measurement Techniques* 16.5, pp. 1179–1194. DOI: https://doi.org/10.5194/amt-16-1179-2023.

Ernle, Lisa et al. (2023). "Assessment of aldehyde contributions to PTR-MS *m/z* 69.07 in indoor air measurements".
In: *Environmental Science: Atmospheres*. Accepted.
Farmer, Delphine K et al. (2019). "Overview of HOMEChem: House observations of microbial and environmental chemistry".
In: *Environmental Science: Processes & Impacts* 21.8, pp. 1280–1300.
Fenske, Jill D and Suzanne E Paulson (1999).
"Human breath emissions of VOCs".
In: *Journal of the Air & Waste Management Association* 49.5, pp. 594–598.
Gueneron, Mylene et al. (2015).
"PTR-MS fragmentation patterns of gasoline hydrocarbons".
In: *International Journal of Mass Spectrometry* 379, pp. 97–109.
Keßel, Stephan et al. (2017).
"Atmospheric chemistry, sources and sinks of carbon suboxide, C 3 O 2".
In: *Atmospheric chemistry and physics* 17.14, pp. 8789–8804.
Nazaroff, William W and Charles J Weschler (2022).
"Indoor ozone: Concentrations and influencing factors".
In: *Indoor air* 32.1, e12942.
Rai, AC et al. (2014). "Ozone reaction with clothing and its initiated VOC emissions in an environmental chamber". In: *Indoor air* 24.1, pp. 49–58.
Rizk, Malak et al. (2018). "Impact of material emissions and sorption of volatile organic compounds on indoor air quality in a low energy building: Field measurements and modeling".
In: *Indoor air* 28.6, pp. 924–935.
Ruzsanyi, Veronika et al. (2013). "Multi-capillary-column proton-transfer-reaction time-of-flight mass spectrometry".
In: *Journal of Chromatography A* 1316, pp. 112–118.
Salonen, Heidi J et al. (2009). "Airborne concentrations of volatile organic compounds, formaldehyde and ammonia in Finnish office buildings with suspected indoor air problems".
In: *Journal of Occupational and Environmental Hygiene* 6.3, pp. 200–209.
Schwarz, K, W Filipiak, and A Amann (2009). "Determining concentration patterns of volatile compounds in exhaled breath by PTR-MS".
In: *Journal of Breath Research* 3.2, p. 027002.
Spanel, Patrik and David Smith (1997). "SIFT studies of the reactions of H3O+, NO+ and O2+ with a series of alcohols". In: *International Journal of Mass Spectrometry and Ion Processes* 167, pp. 375–388.
Trefz, Phillip, Jochen K Schubert, and Wolfram Miekisch (2018).
"Effects of humidity, CO2 and O2 on real-time quantitation of breath biomarkers by means of PTR-ToF-MS".
In: *Journal of breath research* 12.2, p. 026016.
Wang, Nijing et al. (2020). "Total OH reactivity of emissions from humans: in situ measurement and budget analysis".
In: *Environmental Science & Technology* 55.1, pp. 149–159.
Wang, Nijing et al. (2022).
"Emission rates of volatile organic compounds from humans".
In: *Environmental Science & Technology* 56.8, pp. 4838–4848.

Weschler, Charles J (2016).
"Roles of the human occupant in indoor chemistry".
In: *Indoor air* 26.1, pp. 6–24.
Weschler, Charles J and William W Nazaroff (2023).
"Human skin oil: a major ozone reactant indoors".
In: *Environmental Science: Atmospheres* 3.4, pp. 640–661.
Weschler, Charles J et al. (2007).
"Ozone-initiated chemistry in an occupied simulated aircraft cabin".
In: *Environmental Science & Technology* 41.17, pp. 6177–6184.
Williams, J et al. (2001). "An atmospheric chemistry interpretation of mass scans obtained from a proton transfer mass spectrometer flown over the tropical rainforest of Surinam".
In: *Journal of Atmospheric Chemistry* 38.2, pp. 133–166.
Wisthaler, Armin et al. (2005). "Products of ozone-initiated chemistry in a simulated aircraft environment".
In: *Environmental Science & Technology* 39.13, pp. 4823–4832.
Yáñez-Serrano, Ana María et al. (2021). "GLOVOCS-Master compound assignment guide for proton transfer reaction mass spectrometry users".
In: *Atmospheric Environment* 244, p. 117929.
Yuan, Bin et al. (2014). "Interpretation of volatile organic compound measurements by proton-transfer-reaction mass spectrometry over the deepwater horizon oil spill".
In: *International Journal of Mass Spectrometry* 358, pp. 43–48.
Zhou, Zilin, Shouming Zhou, and Jonathan PD Abbatt (2019).
"Kinetics and condensed-phase products in multiphase ozonolysis of an unsaturated triglyceride".
In: *Environmental Science & Technology* 53.21, pp. 12467–12475.

Chapter 4

Human VOC emission during physical exercise

Abstract Different activities do influence the VOC emission from the human body. Literature reports increased mixing ratios from both, human breath and skin emission during exercise. This is an important observation as with rising popularity of indoor sports the impact of exercise on the indoor air quality may be significant. Some decades ago, mainly indoor ball games and fight sports have been popular. In recent years, the popularity of gyms as well as the number of people exercising at home did rise significantly. Especially during the pandemic this was the only option to do sports during lockdown situations at many places. In this chapter results from two male volunteers performing moderate (walking) and intense exercise (running) on a treadmill under ozone-free and ozone present (35 ppb) conditions are presented. These are common indoor exercises (as part of indoor ball games as well as performed as a separate discipline in gyms). In accordance with literature, increasing mixing ratios were observed with exercise intensity. The two volunteers emitted similar amounts of CO_2 and DMS but large inter individual differences were observed for breath acetone and isoprene as well as for several skin oil oxidation products (e.g. 6-MHO). Depending on the compound, inter human differences can arise from different cardiac output or metabolic state. For the skin related emission personal hygiene can also play a role.

4.1 Introduction

A major source of volatile organic compounds (VOCs) in indoor environments are the occupants themselves. Human beings emit several hundred VOCs to the air around them through breath and skin. It is known, that bioeffluents can have a negative impact on the indoor air quality (IAQ) and can react with indoor pollutants. Therefore, occupant emissions can directly affect the personal exposure to certain compounds with potential health effects. Early indoor air chemistry studies tended to focus on the emissions from building materials, furniture, furnishings and heat sources rather than from the occupants themselves. Indeed, most were performed in the unoccupied environment as this was well controlled and no ethical issues could arise. One of the earliest studies including occupants was performed by Bako-Biro

et al. This study found lower levels of oxygenated VOCs (OVOCs) in the occupied compared to the unoccupied environment when ozone (O_3) was present. In order to fully characterize the human contribution to the indoor chemical environment a large-scale measurement project was initiated. During this Indoor Chemical Human Emissions And Reactivity (ICHEAR) campaign, occupant emissions were studied in a controlled climate chamber in the absence and presence of O_3. Additional factors such as clothing coverage, temperature and humidity were also investigated. Most of the data collected was from sedentary people. The key factor which was most affecting the speciation and the amount of VOCs generated by humans was ozone. (Bekö et al., 2020; Wang et al., 2020; Wang et al., 2022; Zannoni et al., 2022). With increasing popularity of gyms and exercise at home (for example on exercise bikes), the impact of human emissions during exercise on indoor air chemistry and air quality is gaining importance especially since such emissions are expected to be significantly higher during exertion compared to those from sedentary people. Here we report on the effect of two levels of exercise (walking and running).

4.2 Methods

4.2.1 Experimental setup

z This experiment on human VOC emission during physical exercise was part of the aforementioned ICHEAR project. It is described in detail by Bekö et al. Experiments were performed in a 22.5 m^3 stainless steel chamber at the Technical University of Denmark (DTU) with an air change rate of 3.2 h^{-1}. A schematic of the experimental setup is shown in Figure 4.1. The chamber air was drawn through a 1/2" main inlet line positioned at the chamber ceiling with a flow of ca. 13 lpm. From this main inlet line, the instruments drew bypass flows of 200 sccm (GC-MS (1/4") and PTR-MS (1/8")) and 230 sccm (Picarro (1/4"')). All inlet lines were made of flourinated ethylene propylene (FEP). For human VOC emission during physical exercise quantification, the data has been background corrected: the mean mixing ratio of the empty chamber before each experiment has been subtracted.
The emission of two male volunteers (age 21, BMI 23.6 and age 27, BMI 20.7) were measured in two separate experiments. They each did two levels of exercise consecutively, one hour of walking ($\sim$90 bpm)) and one hour of running ($\sim$130 bpm). The experiments were performed without ozone present and in the presence of 35 ppb O_3. VOCs in the chamber air were measured with a gas chromatograph-mass spectrometer (GC-MS) and a proton transfer reaction-mass spectrometer (PTR-MS), carbon dioxide (CO_2) has been measured with a CO_2 gas analyzer (G2401 Analyzer, Picarro, USA). Additionally, direct breath measurements with the PTR-MS have been performed 10 min before start and after stopping the exercise.

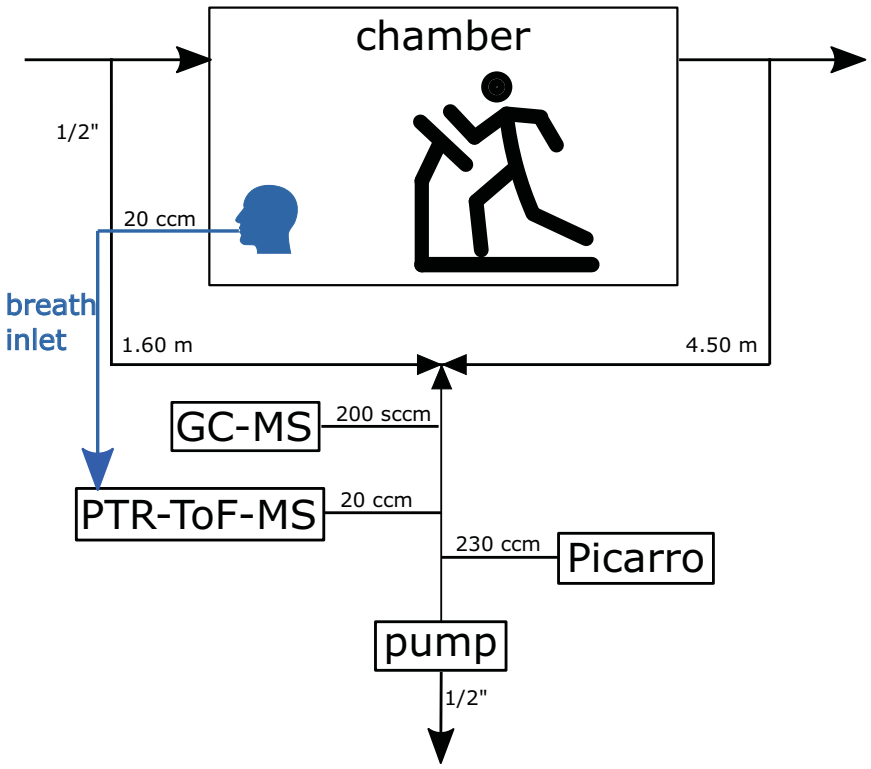

FIGURE 4.1: Schematic measurement setup of the experiment on human VOC emission during physical exercise.

4.2.2 Instrumentation

GC-MS

The GC-MS system used in the current study is a custom-built fast measurement device, previously described by Bourtsoukidis et al. It is equipped with a cryogenic pre-concentration system containing single traps for each of the three purposes: water removal, concentration and focusing. Separation in the GC column takes only 2.5 min, resulting in a total cycle time of only 3 min. Compared to standard GC systems (cycle time ca. 30-120 min), this is extremely fast and therefore suitable to measure the emitted VOCs in the chamber quasi-online. The instrument is equipped with a quadrupole mass analyzer usually running in single ion monitoring (SIM) mode. In the current study, small VOCs including isoprene and its oxidation products methacrolein (MACR) and methyl vinyl ketone (MVK), propanal, butanal, methylethyl ketone (MEK) and dimethylsulfide (DMS) were measured by the fast GC-MS. LODs were in the lower ppt range (2-40 ppt).

PTR-MS

The PTR-MS (8000, IONICON Analytik, Austria) was operated with H_3O^+ as primary ions. Operational settings were: drift tube pressure 2.2 hPA, drift temperature 60°C and E/N 137 Td. The mass range was 0-500 amu and the mass resolution 3500. PTR-MS uses a rather soft ionization technique which usually results in little fragmentation of the target molecules. For compound

identification the exact mass was used. The raw ion signal was normalized by the sum of the primary reagent ion (H_3O^+) and the first water cluster ((H_2O2H^+). In this study acetone, 6-methyl-5-heptene-2-on (6-MHO) and 4-oxopentanal (4-OPA) have been measured by PTR-MS. A multi-component gas standard (Apel-Riemer, USA) was used for acetone quantification, while 6-MHO and 4-OPA were quantified using the proton transfer rate coefficient (k-rate) due to a lack of gas standards. For acetone, the results from the experiments on human VOC emission during physical exercise, PTR *m/z* 59 which includes the sum of acetone and propanal, has been subtracted by the GC-measured mixing ratio for propanal. LODs were <75 ppt and the total measurement uncertainty was 7%.

Picarro CO_2 analyzer

The Picarro CO_2 analyzer (G2401 Analyzer, California, USA) uses wavelength-scanned cavity ring-down spectroscopy (WS-CRDS). This technique uses the absorption of a specific wavelength of the target gas for quantification. The light absorption is proportional to the gas concentration and and the path length the light travels through the sample. In cavity ring-down spectroscopy, the light circulates in the sample gas, resulting in a extremely long effective path. This is the key to reaching much higher sensitivity (parts per trillion (ppt) to parts per billion (ppb) level) compared to a conventional infrared spectrometer (LODs in ppm level) (Inc., 2015). The LOD for CO_2 in this study was 0.032 ppm with a total measurement uncertainty of ca. 3%.

4.3 Results and discussion

In this study CO_2 and several VOCs which are released through breath or dermal emission have been analyzed. This includes namely DMS, isoprene, 6-MHO, 4-OPA, acetone, propanal, MEK, butanal, MVK and MACR.

4.3.1 CO_2, DMS, isoprene

Figure 4.2 shows the measured mixing ratios in the chamber for CO_2, DMS and isoprene during the ICHEAR experiment. It should be noted that figure 4.2a shows the data collected with no ozone present while ozone was present in the Figure 4.2b data. As expected, the emission of CO_2 is similar for both subjects and independent from the presence of ozone. This is because both subjects were of similar age and BMI, and CO_2 does not react with ozone. CO_2 emissions increased by 600 ppb (factor of 250) from background CO_2 level (400 ppb) to 1000 ppb while walking and by another 700 ppb from walking to running (1700 ppb, increase by a factor of 170 walking to running and by a factor of 425 from background CO_2 level to running).
Another breath related compound is DMS, which is known to be produced in enzymatic processes that serve to remove toxic sulfur species from the body (King et al., 2010). Like CO_2, DMS does not react with O_3, so again

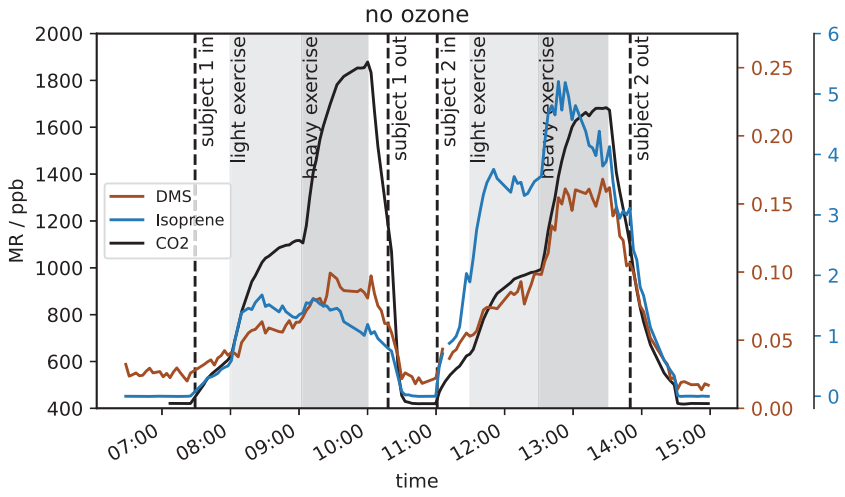

(A)

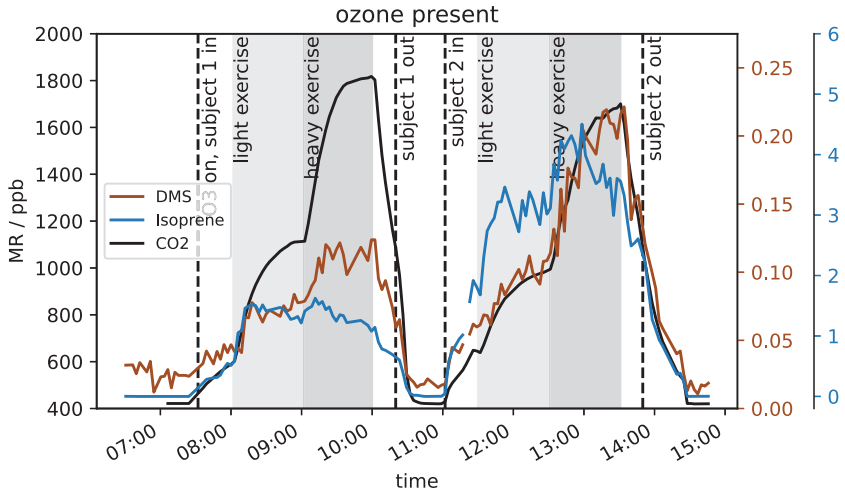

(B)

FIGURE 4.2: Mixing ratios of CO_2, DMS and isoprene for the two male subjects (A) without O_3 and (B) with O_3 present.

measured mixing ratios for the experiment with or without ozone are comparable. The DMS mixing ratio in the chamber increased by a factor of 1.7 (like CO_2, from 0.07 ppb walking to 1.2 ppb running). The similar increase in chamber mixing ratio for CO_2 and DMS from walking to running indicates that the increase is mainly due to an increase in breathing rate.
An interesting and reactive compound emitted via human breath is isoprene. Its putative metabolic origin as a byproduct of the mevalonate pathway has recently been falsified by Sukul et al. The origin of breath isoprene still remains unclear and is subject of further research (Sukul et al., 2021). Several studies have reported large differences in the human isoprene emission for different subjects (Fenske and Paulson, 1999; King et al., 2009; Senthilmohan et al., 2000; Stönner, Edtbauer, and Williams, 2018; Turner, Španěl, and Smith, 2005). The same can be observed in our limited dataset. Subject 2 (afternoon, 11:30-14:00) generates more than double the amount of isoprene (ca. 3-5 ppb) compared to subject 1 (morning, 08:00-11:00, ca. 1.5 ppb). This difference can be seen on both days, the one without ozone (Figure 4.2a) and on the day with 35 ppb of ozone being present (Figure 4.2b) and is probably due to metabolic differences (King et al., 2009; King et al., 2010). At the start of the exercise, the isoprene levels increase, followed by a decrease to a steady state mixing ratio. This is in line with the observations of King et al. and Senthilmohan et al. King et al. assume, that the increase of isoprene in breath at the onset of physical exercise might be due to a linkage of the breath isoprene level to cardiac output. Their model assumes that muscles represent reservoirs for isoprene that can be depleted through exercise.

4.3.2 6-MHO, 4-OPA, acetone

6-MHO and 4-OPA were previously reported to be generated through ozonolysis reaction with the surface of plant leaves (Fruekilde et al., 1998) and human skin oil. Additionally, from the reaction of ozone with human skin oil also acetone can be produced (Fooshee et al., 2015; Weschler et al., 2007; Wisthaler et al., 2005). For acetone, a huge difference between the two subjects could be observed in the measured mixing ratio: during the experiment without ozone (Figure 4.3a), subject 1 (ca. 15 ppb walking, 35 ppb running) emits roughly double the acetone than subject 2 (ca. 7 ppb walking, 17 ppb running). For the condition with 35 ppb of O_3 present, the difference between the two subjects is even bigger (see Figure 4.3b): While the acetone emission of subject 2 is only slightly higher (ca. 10 ppb walking, 20 ppb running) than for the condition without ozone, subject 1's acetone emission is more than doubled (ca. 35 ppb walking, 75 ppb running) compared to the experiment without ozone present.
Acetone is emitted via breath and skin as it is also an oxidation product from squalene (Blaikie et al., 2016; Morrison et al., 2020; Španěl et al., 2011; Wang et al., 2022). According to literature there is no influence of age and BMI on human acetone emission (King et al., 2009). In human breath, acetone is one of the most abundant compounds (King et al., 2009; Wang et al., 2022). In the

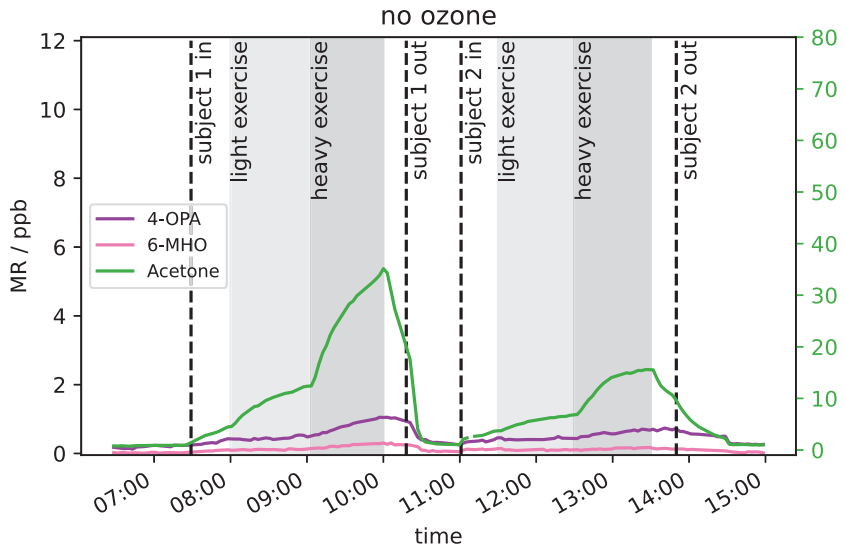

(A)

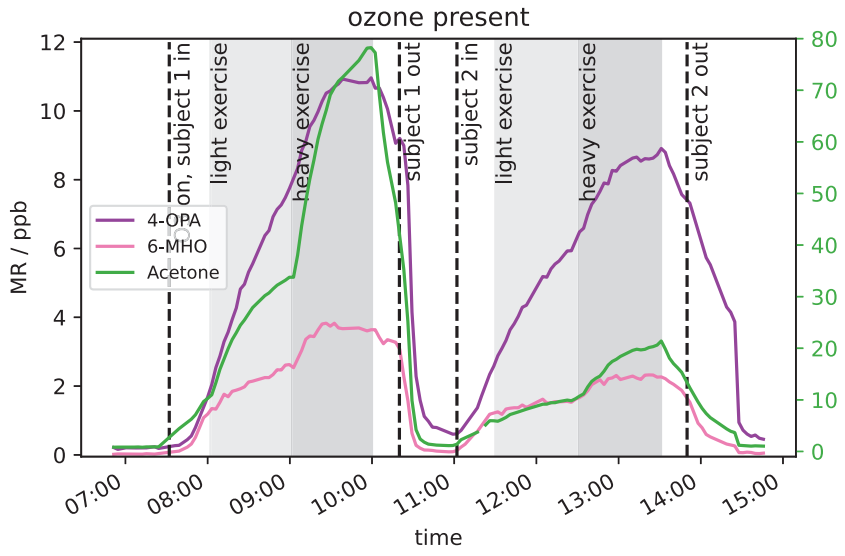

(B)

FIGURE 4.3: Mixing ratios of acetone, 6-MHO and 4-OPA for the two male subjects (A) without O_3 and (B) with O_3 present.

direct breath measurements performed during this study, a relative acetone increase from the first (without O_3) to the second day (O_3 present) of ca. 90% has been observed for subject 1.

$$ey = \frac{\Delta_{\mathrm{VOC}}}{\Delta O_3(empty - occupied)} * 100 \tag{4.1}$$

The effective yields (change in VOC mixing ratio per ozone consumption) of acetone and 6-MHO are shown in Table 4.1 and have been compared to investigate if most of acetone is emitted via breath or skin, as both are primary products from squalene ozonolysis and should therefore be in a similar range.

TABLE 4.1: Mixing ratio of breath acetone and effective yields (*ey*) of chamber acetone and 6-MHO for both subjects.

	Subject 1		**Subject 2**	
	Walking	**Running**	**Walking**	**Running**
$ey_{6\text{-MHO}}$	4%	5%	3%	3%
$ey_{acetone}$	35%	65%	5%	7%
Direct breath $MR_{acetone}$	1200 ppb	2250 ppb	750 ppb	800 ppb

The huge difference in acetone and 6-MHO yields for subject 1 show, that most of the acetone is from breath. This was confirmed by the direct breath measurement (sampled 10 min before starting and 10 min after stopping excercise).
Significant day to day variations in breath acetone have also been reported earlier (King et al., 2009; Španěl et al., 2011; Sun et al., 2017). The breath acetone level is known to be influenced by various factors including fasting, exercise and pulmonary factors (Anderson, 2015; Blaikie et al., 2016; King et al., 2009; Senthilmohan et al., 2000; Smith, Spanel, and Davies, 1999). King et al. found drastically increased acetone levels with exercise. This fits the results from the current study: at the onset of exercise, the acetone concentrations increase strongly for both subjects for low exercise (walking) and even stronger for high exercise (running). The difference between the two subjects might be due to fasting. Subject 1 did not have breakfast before the experiments, while subject 2 was doing the experiment in the afternoon and already had some food intake before. Breath acetone is closely related to fat metabolism (Anderson, 2015; Senthilmohan et al., 2000). Therefore, the acetone emission increases with fasting and exercise.
A slow increase of 4-OPA (max. at high exercise for subject 1 1 ppb , <1 ppb for subject 2) and an almost negligible increase of 6-MHO were observed in the present study. They are both products from the reaction of squalene with ozone. The increase in mixing ratios of those compounds with exertion during no ozone condition suggest a skin reservoir, which can be released during exertion. When 35 ppb of ozone were present, ca. 2.5 ppb and 1.7 ppb of 6-MHO were measured during low exercise (walking) for subjects 1 and 2, respectively. At the start of the high exercise (running), a sudden increase can be observed, which reaches a steady state mixing ratio (ca. 3.8 ppb

(subject 1) and 2.2 ppb (subject 2)) in roughly 15 min. 4-OPA mixing ratios in the chamber reach up to 8 ppb (subject 1) and 6 ppb (subject 2) during low exercise. Similar to 6-MHO, a sudden increase happens after the start of the high exercise, reaching a steady state mixing ratio of ca. 11 ppb (subject 1) and ca. 9 ppb (subject 2). The production of 6-MHO and 4-OPA from squalene ozonolysis have been reported in several studies including Coffaro and Weisel; Lakey et al. and Weschler and Nazaroff. The stronger increase of all three carbonyls (6-MHO, 4-OPA and acetone) during high exercise is most likely due to elevated body temperature at higher cardiac output and thereby increased water vapour on skin surface through sweating. Arata et al. reported an increase in gas-phase oxidation products from ozone-skin reactions with water vapour concentration.
Assuming a skin surface area of 1.7 m^2 (HarvardUniversity, n.d.), humans emit roughly 11.2 µg h^{-1} m^{-1} of 6-MHO and 5.2 µg h^{-1} m^{-1} 4-OPA (Wang et al., 2022), which is less then a tenth of the emission from plant surfaces (180-720 µg h^{-1} m^{-1}) (Fruekilde et al., 1998).

4.3.3 Minor products of OH/O_3 initiated chemistry

Several VOCs that can be produced through OH or ozone-initiated oxidation are shown in Figure 4.4. Without ozone present, methacrolein is the only compound which does not show a clear increase with the onset of high exercise (running) (see Figure 4.4a). For MVK, butanal, MEK and propanal increasing mixing ratios were measured after the start of high exercise, which might be due to more evaporation of volatiles due to higher body surface temperature. A strong increase after the onset of high exercise was also observed for acetone. However, the mixing ratios of those VOCs is one order of magnitude lower than the acetone mixing ratio. This was expected as they are only minor contributors to the total VOC emission of humans (Mochalski et al., 2014; Wang et al., 2022). In the direct breath measurement, we observed an increase in MEK from light to heavy exercise. However, this might be due to the fact that the subjects inhaled more MEK which was previously released from skin during the heavy exercise. Furthermore, MVK and MACR are common products of OH and ozone-initiated isoprene chemistry. They stem mainly from oxidation with OH of the breath isoprene. During the experiments performed in the presence of 35 ppb ozone, the mixing ratios increased for all compounds shown in Figure 4.4b. This fits the expectations: besides being products of isoprene oxidation, MVK and MACR are can possibly also come from ozonolysis in the condensed phase (Morrison et al., 2020). MEK can be produced by O_3/isoprene initiated chemistry, but the reaction rate is too slow compared to the air change rate, indicating it might be produced from the reaction of ozone with another compound present in human emission. However, the increase in MEK under O_3 presence is not as strong as for the other compounds. Acetone, propanal and butanal are common products of O_3 initiated chemistry (Mochalski et al., 2014; Morrison et al., 2020; Weschler and Nazaroff, 2023), which explains the increase in mixing

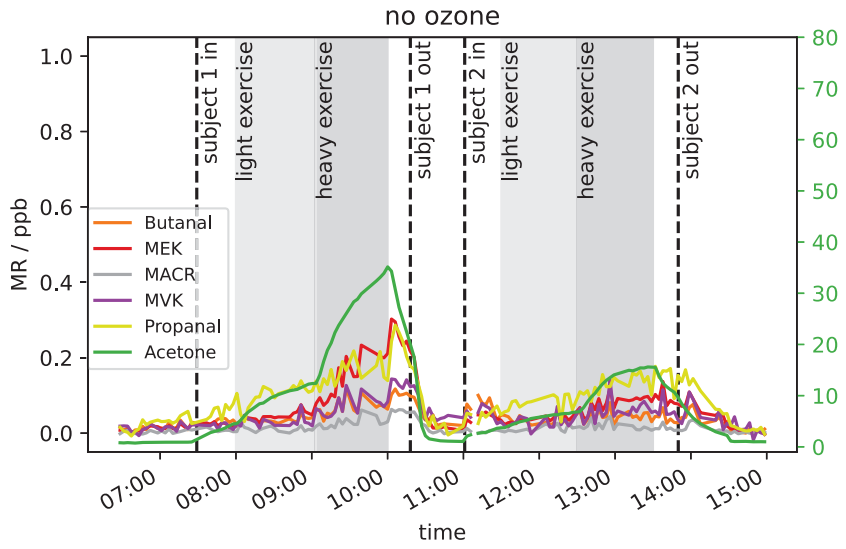

(A)

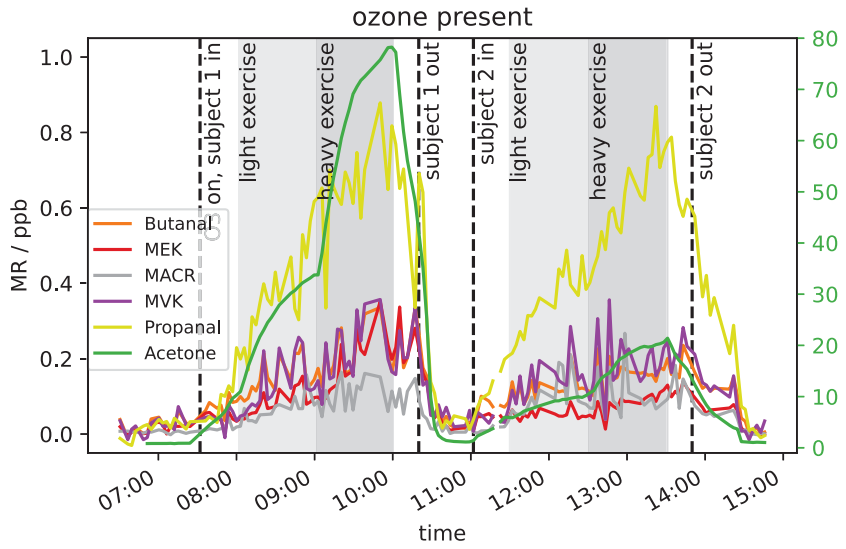

(B)

FIGURE 4.4: Mixing ratios of MVK, MACR, propanal, acetone, MEK and butanal for the two male subjects (A) without O_3 and (B) with O_3 present.

ratio for both subjects (cf. Figure 4.4a and 4.4b). Interestingly, the relative increase of propanal under ozone presence compared to the no ozone condition is roughly 400% ($\sim$0.1 ppb (low exercise) and $\sim$0.2 ppb (high exercise) without O_3 and $\sim$0.4 ppb (low exercise) and $\sim$0.8 ppb (high exercise) with O_3), while it only doubled roughly for the other compounds shown in Figure 4.4. This in in line with the study of Wang et al., who reported that propanal was one of the top 10 most emitted species (8th highest emission rate) for human whole-body emission under the presence of ozone. The same study did not rank propanal under top 10 species for the measurement of skin only emissions. A difference in the setups of those two experiments was the subject's clothing: for the human whole-body emission, long clothing was worn, while for the skin-only experiment the subjects wore short clothing. This might be an indication that the increase in propanal could come from the reaction of O_3 with a compound present in the clothing material. This assumption is supported by the fact, that on average we observed the same amount of propanal for subjects 1 and 2 during both ozone conditions (with and without O_3). Both subjects wore a new set of the same provided clothing (pre-washed with fragrant free detergent) for each of the experiments.

4.4 Conclusions

Significant differences in isoprene and acetone emission between two human volunteers during physical exercise could be observed. It is known that the isoprene emission differs widely within humans, depending strongly on the metabolic differences (King et al., 2009; King et al., 2010). Human acetone emissions depend on calorific intake, exercise and pulmonary factors (Anderson, 2015; Blaikie et al., 2016; King et al., 2009; Senthilmohan et al., 2000; Smith, Spanel, and Davies, 1999). The difference in acetone mixing ratio for the two subjects in this study is mainly due to breath acetone and can be explained by fasting of one subject. The acetone emissions were intensified by exercising. It is known that breath acetone is related to fat metabolism, therefore increasing with exercise and fasting. Generally, the workload intensity and the presence of ozone lead to elevated mixing ratios in the air. Aldehyde (propanal and butanal), MEK, MVK and MACR mixing ratios are 2-4 times higher in the exercise experiment than for sedentary people. Considering acetone, a larger cohort of subjects would be needed to investigate inter human differences. Compared to the annual global emission the emission from human body is still negligible (<0.2% for all compounds considered in this study). Acetone and isoprene were the two species which contributed most to their global annual emission (146 Tg/a and 464 Tg/a (Fischer et al., 2012; Pozzer et al., 2022)). Sedentary people contribute 0.05% to the global acetone budget while the contribution of isoprene to the global isoprene budget is only 0.004%. Assuming that ca. 70% of the world's population do 150 min of moderate exercise or 75 min of intense exercise per week (cf. WHO's estimate on exercise (*WHO Physical activity* n.d.)), the total annual acetone and isoprene emission from people exercising would be 1.14 Gg/a (acetone) and 0.19 Gg/a (isoprene) for moderate exercise and 1.58 Gg/a (acetone) and 0.22

Gg/a (isoprene) for intense exercise. This is <0.001% of the global annual emission of these species.

References

Anderson, Joseph C (2015).
"Measuring breath acetone for monitoring fat loss".
In: *Obesity* 23.12, pp. 2327–2334.

Arata, Caleb et al. (2019). "Heterogeneous ozonolysis of squalene: gas-phase products depend on water vapor concentration".
In: *Environmental science & technology* 53.24, pp. 14441–14448.

Bako-Biro, Zsolt et al. (2005). "Effects of indoor pollution sources and ventilation rate on ozone's surface removal rate and the occurrence of oxygenated VOCs in an office space". In: *Indoor Air*, pp. 2320–2324.

Bekö, Gabriel et al. (2020). "The Indoor Chemical Human Emissions and Reactivity (ICHEAR) project: Overview of experimental methodology and preliminary results". In: *Indoor Air* 30.6, pp. 1213–1228.

Blaikie, Thomas PJ et al. (2016).
"Portable device for measuring breath acetone based on sample preconcentration and cavity enhanced spectroscopy".
In: *Analytical chemistry* 88.22, pp. 11016–11021.

Bourtsoukidis, Efstratios et al. (2017).
"An aircraft gas chromatograph–mass spectrometer System for Organic Fast Identification Analysis (SOFIA): design, performance and a case study of Asian monsoon pollution outflow".
In: *Atmospheric Measurement Techniques* 10.12, pp. 5089–5105.

Coffaro, Breann and Clifford P Weisel (2022).
"Reactions and Products of Squalene and Ozone: A Review".
In: *Environmental Science & Technology* 56.12, pp. 7396–7411.

Fenske, Jill D and Suzanne E Paulson (1999).
"Human breath emissions of VOCs".
In: *Journal of the Air & Waste Management Association* 49.5, pp. 594–598.

Fischer, EV et al. (2012).
"The role of the ocean in the global atmospheric budget of acetone".
In: *Geophysical Research Letters* 39.1.

Fooshee, David R et al. (2015).
"Atmospheric oxidation of squalene: molecular study using COBRA modeling and high-resolution mass spectrometry".
In: *Environmental science & technology* 49.22, pp. 13304–13313.

Fruekilde, Palle et al. (1998).
"Ozonolysis at vegetation surfaces: a source of acetone, 4-oxopentanal, 6-methyl-5-hepten-2-one, and geranyl acetone in the troposphere".
In: *Atmospheric Environment* 32.11, pp. 1893–1902.

HarvardUniversity (n.d.).
B10numb3rs - The database of useful biological numbers.

Accessed: 2023-07-16.
URL: https://bionumbers.hms.harvard.edu/search.aspx.
Inc., Picarro (Jan. 2015).
PICARRO G2401 Analyzer for CO_2/C/CH_4/H_2 User's Guide.
King, Julian et al. (2009). "Isoprene and acetone concentration profiles during exercise on an ergometer".
In: *Journal of breath research* 3.2, p. 027006.
King, Julian et al. (2010). "Dynamic profiles of volatile organic compounds in exhaled breath as determined by a coupled PTR-MS/GC-MS study".
In: *Physiological measurement* 31.9, p. 1169.
Lakey, Pascale SJ et al. (2019). "The impact of clothing on ozone and squalene ozonolysis products in indoor environments".
In: *Communications Chemistry* 2.1, p. 56.
Mochalski, Paweł et al. (2014). "Emission rates of selected volatile organic compounds from skin of healthy volunteers".
In: *Journal of chromatography B* 959, pp. 62–70.
Morrison, Glenn C et al. (2020).
"Yields and variability of ozone reaction products from human skin".
In: *Environmental Science & Technology* 55.1, pp. 179–187.
Pozzer, Andrea et al. (2022). "Simulation of organics in the atmosphere: evaluation of EMACv2. 54 with the Mainz Organic Mechanism (MOM) coupled to the ORACLE (v1. 0) submodel".
In: *Geoscientific Model Development* 15.6, pp. 2673–2710.
Senthilmohan, Senti T et al. (2000). "Quantitative analysis of trace gases of breath during exercise using the new SIFT–MS technique".
In: *Redox Report* 5.2-3, pp. 151–153.
Smith, David, Patrik Spanel, and Simon Davies (1999).
"Trace gases in breath of healthy volunteers when fasting and after a protein-calorie meal: a preliminary study".
In: *Journal of applied physiology* 87.5, pp. 1584–1588.
Španěl, Patrik et al. (2011). "Breath acetone concentration; biological variability and the influence of diet".
In: *Physiological Measurement* 32.8, N23.
Stönner, C, A Edtbauer, and J Williams (2018).
"Real-world volatile organic compound emission rates from seated adults and children for use in indoor air studies".
In: *Indoor Air* 28.1, pp. 164–172.
Sukul, Pritam et al. (2021). "Deficiency and absence of endogenous isoprene in adults, disqualified its putative origin". In: *Heliyon* 7.1.
Sun, Meixiu et al. (2017). "Continuous monitoring of breath acetone, blood glucose and blood ketone in 20 type 1 diabetic outpatients over 30 days".
In: *J. Anal. Bioanal. Tech* 8, pp. 2155–9872.
Turner, Claire, Patrik Španěl, and David Smith (2005).
"A longitudinal study of breath isoprene in healthy volunteers using selected ion flow tube mass spectrometry (SIFT-MS)".
In: *Physiological measurement* 27.1, p. 13.

Wang, Nijing et al. (2020). "Total OH reactivity of emissions from humans: in situ measurement and budget analysis".
In: *Environmental Science & Technology* 55.1, pp. 149–159.
Wang, Nijing et al. (2022).
"Emission rates of volatile organic compounds from humans".
In: *Environmental Science & Technology* 56.8, pp. 4838–4848.
Weschler, Charles J and William W Nazaroff (2023).
"Human skin oil: a major ozone reactant indoors".
In: *Environmental Science: Atmospheres* 3.4, pp. 640–661.
Weschler, Charles J et al. (2007).
"Ozone-initiated chemistry in an occupied simulated aircraft cabin".
In: *Environmental Science & Technology* 41.17, pp. 6177–6184.
WHO Physical activity (n.d.). https://www.who.int/news-room/fact-sheets/detail/physical-activity. Accessed: 2023-07-05.
Wisthaler, Armin et al. (2005). "Products of ozone-initiated chemistry in a simulated aircraft environment".
In: *Environmental Science & Technology* 39.13, pp. 4823–4832.
Zannoni, Nora et al. (2022). "The human oxidation field".
In: *Science* 377.6610, pp. 1071–1077.

Appendix A

Python code for data analysis

A.1 Code file mergeV25Igor.py

```
# -*- coding: utf-8 -*-
"""
@author: lisa.ernle
"""

from pathlib import Path
import pandas as pd
import numpy as np

#####################################################################
##### TO BE ADJUSTED:
# general data path:
#GenPath = Path(r'C:\Campaigns\CAFE\CAFE_Africa\Data')
#GenPath = Path(r'C:\Campaigns\ICHEAR\ICHEAR_1\Data')
#GenPath = Path(r'C:\Campaigns\Fragmentation\data')
GenPath = Path(r'C:\Campaigns\O3exp\data')

# data from following date will be processed:
date = '20201005'
# explicit path:
path = GenPath / date

#####################################################################
### file with integration results
# IF you want to import direct Igor output, comment in and
 ↪  comment out (2)
# (1) adjust chrom list name
Chromlist = 'ChromList_tot_fin.txt'

# import Igor ChromList
Igor = pd.read_csv(path / Chromlist, sep='\t', header=0,
 ↪  parse_dates=['filetime', 'starttime', 'sampletime'],
 ↪  dayfirst=True)
# drop unnamed cols
```

```
Igor.drop(Igor.filter(regex='Unnamed'),axis=1, inplace=True)
'''
# IF you want to import integration results of all Igor-ChromLists comment in and comment out (1)
# (2)start: create file with integration data of all analytes
Chromlist = pd.DataFrame()
for f in path.glob('ChromList_???_?.txt'):
    # import each ChromList
    single_ChrLst = pd.read_csv(f, sep='\t', header=0, parse_dates=['filetime', 'starttime', 'sampletime'], dayfirst=True)
    # drop unnamed cols
    single_ChrLst.drop(single_ChrLst.filter(regex='Unnamed'), axis=1, inplace=True)
    # if ChromList df already contains data, drop filename, etc. for df which will be appended
    if 'filename' in Chromlist.columns:
        single_ChrLst.drop(single_ChrLst.iloc[:, :7], axis=1, inplace=True)
        Chromlist = pd.concat([Chromlist, single_ChrLst], axis=1, sort=True)
    # if ChromList df is still empty (1st iteration), use just imported file
    else:
        Chromlist = single_ChrLst
        Chromlist.drop(Chromlist.filter(regex='Unnamed'),axis=1, inplace=True)
# save chromlist with all analytes
# !!! filename CANNOT be "ChromList..." as existing total chromlist would be concatenated!!!
Chromlist.to_csv(path / 'ChrLst_tot.txt', sep='\t', index=False)
# as Igor variable is used below
Igor = Chromlist
'''
### (2)end
#####################################################################

# create path for v25merged file:
v25folder = date + '.v25'
v25path = path / v25folder
v25_tot = v25path / 'v25log.txt'

# check if v25logs are already merged & do so if necessary:
if not v25_tot.exists():
    v25log = pd.DataFrame()
    for f in v25path.glob('*.dat'):
```

```
68          v25 = pd.read_csv(f, sep='\t', header=0,
            ↪  parse_dates=['DateTime'], dayfirst=True)
69          v25log = v25log.append(v25,
            ↪  ignore_index=True).sort_values(by='DateTime',
            ↪  ascending=True)
70      # drop col #0 (=empty):
71      v25log = v25log.drop(v25log.columns[0], axis=1)
72      v25log.to_csv(v25path / 'v25log.txt', sep='\t', index=False)
73
74  v25merged = pd.read_csv(v25_tot, sep='\t', header=0,
    ↪  parse_dates=['DateTime'], dayfirst=True)
75
76  # Label different samples:
77  # shift(1) compares previous row with current row
78  v25merged['shiftedSmplState'] = v25merged['SmplState'].shift(1)
79  # & has higher precedence than == :() before and after &-operator
80  # cumsum sums up values
81  v25merged['Label'] = np.where((v25merged['SmplState'] ==
    ↪  'CoolTraps') & (v25merged['shiftedSmplState'] == 'MSStart'),
    ↪  1, 0).cumsum()
82
83  # eliminate useless cols:
84  del v25merged['shiftedSmplState']
85  if {'V_0', 'V_1', 'V_2', 'V_3'}.issubset(v25merged.columns):
86      v25merged.drop(['V_0', 'V_1', 'V_2', 'V_3'], axis=1,
        ↪  inplace=True)
87
88  # introduce Igor MSStart as key to groupby during merging:
89  Igor['SmplState'] = 'MSStart'
90
91  # merge v25data & Igor:
92  v25Igor = pd.merge_asof(v25merged, Igor, left_on='DateTime',
    ↪  right_on='starttime', by='SmplState', direction='nearest')
93
94  # link smplnames to smpls & mark smpls without MS-data with "No":
95  v25Igor['filename'] = np.where((v25Igor['SmplState'] ==
    ↪  'MSStart') & ((v25Igor['DateTime'] < v25Igor['starttime'] -
    ↪  pd.Timedelta('60 seconds')) | (v25Igor['DateTime'] >
    ↪  v25Igor['starttime'] + pd.Timedelta('60 seconds'))), 'No',
    ↪  v25Igor['filename'])
96  # groupby Label & filename
97  # have to apply some function (.fill) to get it as df not as
    ↪  groupbyObject:
98  v25Igor = v25Igor.groupby('Label').bfill()
99  # fill nan with last valid value:
100 v25smpls = v25Igor#.bfill()
101
```

```
# use smplvolume @MSStart:
v25smpls['V_Smpl'] = v25smpls['V_Smpl'].loc[v25smpls['SmplState']
    ↪  == 'MSStart']
v25smpls.loc[:, 'V_Smpl'] = v25smpls.loc[:, 'V_Smpl'].bfill()

# only keep v25data when there is MS data:
v25smpls = v25smpls[(v25smpls.filename != 'No')]
v25smpls = v25smpls[pd.notnull(v25smpls['filename'])]

# create smpls df:
smpls =  v25smpls.groupby('filename').mean()

# not logged:
del smpls['P_Inlet']

# average only during smpling:
Smpling = v25smpls.loc[(v25smpls['SmplState'] ==
    ↪  'Sample')][['filename', 'F_Cal',
    ↪  'F_Inlet']].groupby('filename').mean()
# replace cols where av during smpling is needed:
for col in smpls[['F_Cal', 'F_Inlet']]:
    smpls[col] = Smpling[col]

# replace cols where av during nextSmpl is needed:
smpls['F_Inj'] = smpls['F_Inj'].shift(-1)

#####################################################################

smpls = Igor.loc[:, ['filename', 'filetime', 'starttime',
    ↪  'sampletime', 'sampletyp']].merge(smpls, left_on='filename',
    ↪  right_index=True)

# remove samples from remove_smpls_date.txt (no peaks, etc.)
NoDataFile = 'remove_smpls_' + date + '.txt'
# open the .txt & read the content
NDfile = open(path / NoDataFile, 'r')
# read() gives back the whole content as one string
content = NDfile.read()
# separate the string at whitespace
NoData = content.split()
# CAFE Africa
#NoData = [date + '_'+i+'.D' for i in NoData]
# all other data
NoData = ['smpl_'+i+'.D' for i in NoData]
# close remove*.txt
NDfile.close()
# use only rows where index is not in NoData
```

```
smpls = smpls[~smpls.filename.isin(NoData)]

# save smpls as txt file:
smpls.to_csv(path / 'smpls.txt', sep='\t', index=False)

```

A.2 Code file CalOutlier.py

```
# -*- coding: utf-8 -*-
"""
@author: lisa.ernle
"""

from pathlib import Path
import pandas as pd
import numpy as np
import matplotlib.pyplot as plt
import matplotlib.dates as mdates
import math
from patsy import ModelDesc, Term, LookupFactor
import statsmodels.formula.api as smf
import scipy.stats as stats

######################################################################
# Calgas path:
Calgas_path = Path(r'C:\Instruments\MGC\Calgas')

######################################################################
### TO BE ADJUSTED:
#Calgas = pd.read_table(Calgas_path / 'MGC_Calgas2011.txt')
Calgas = pd.read_table(Calgas_path / 'MGC_Calgas2020_40L.txt')
#Calgas = pd.read_table(Calgas_path / 'PTR_Calgas2020.txt')

# general data path:
#GenPath = Path(r'C:\Campaigns\CAFE\CAFE_Africa\Data')
#GenPath = Path(r'C:\Campaigns\ICHEAR\ICHEAR_1\Data')
GenPath = Path(r'C:\Campaigns\ICHEAR\ICHEAR_2\Data')
#GenPath = Path(r'C:\Campaigns\O3exp\data')
# data from following date will be processed:
date = '20210426'
######################################################################

# explicit path:
path = GenPath / date

# samples dataframe:
```

```
samples = pd.read_table(path / 'smpls.txt',
    ↪ parse_dates=['sampletime'], dayfirst=True)

# for data before 09/2018, comment in
#samples.insert(loc=26, column='pw_GCtr', value=99.9)

# normalize areas by sample volume
for col in samples:
    if col.endswith(tuple(['_a', '_e'])):
        samples[col] = samples[col]/(1000*samples['samplevol'])

######################################################################
##### define functions for outlier labeling & identification in
    ↪ global scale
### outlier labeling: modified Z-scores
### can be replaced with np.median(data)
def calc_median(data):
    result = 0.0
    # len() starts counting from 1
    length = len(data)
    print(length)

    # modulus - returns remainder of division
    if length % 2 == 0:
        index01 = int((length/2) - 1)
        index02 = index01 + 1
        result = (data[index01] + data[index02])/2.0
    else:
        # floor division - rounds down to closest int cause
            ↪ indexing starts at 0
        result = data[length//2]
    return result

def calc_mad(data, median):
    medians = []
    for x in data:
        medians.append(abs(x - median))

    medians.sort()
    mad =  calc_median(medians)

    if mad == 0:
        mad = 2.2250738585072014e-308 # sys.float_info.min

    return mad

def iglewicz_hoaglin(data):
```

```
83
84      data.sort()
85      median = calc_median(data)
86      mad = calc_mad(data, median)
87      result = []
88
89      for x in data:
90          score = abs(0.6745 * (x - median) / mad)
91
92          if(score > threshold):
93              result.append(x)
94      print(median, result)
95      return result
96
97      median = np.nanmedian(data)
98      MAD = np.nanmedian([np.abs(x - median) for x in data])
99      # MAD becomes zero if more than 50\% of input values are the
        ↪  same, in this case, replace MAD with extremely low
        ↪  positive number, as later will be devision by MAD
100     if MAD == 0:
101         MAD = 2.2250738585072014e-308 # sys.float_info.min
102     # modified z-scores
103     MZS = [abs(0.6745*(x - median) / MAD) for x in data]
104     result = []
105     for i, val in enumerate(MZS):
106         if val >= threshold:
107             result.append(data[i])
108     #print(str(MZS))
109     return result
110
111 # threshold for modified Z-scores
112 ## Iglewicz/Hoaglin recommend 3.5. This means 2/3 or the abs
    ↪  deviation has to be 3.5 times higher than MAD. For Smpls with
    ↪  almost equal no. of points close to median and far away, this
    ↪  is much too high.
113 threshold = 1.5
114
115 # gESD is applicable for smpl size > 20
116 ### outlier identification: generalized ESD
117 def grubbs_stat(data):
118     std_dev = np.nanstd(data)
119     avg_data = np.nanmean(data)
120     abs_val_minus_avg = abs(data - avg_data)
121     max_of_deviations = np.nanmax(abs_val_minus_avg)
122     max_ind = np.nanargmax(abs_val_minus_avg)
123     Gcal = max_of_deviations/ std_dev
124     return Gcal, max_ind
```

```
125 def calculate_critical_value(size, alpha):
126     t_dist = stats.t.ppf(1 - alpha / (2 * size), size - 2)
127     numerator = (size - 1) * np.sqrt(np.square(t_dist))
128     denominator = np.sqrt(size) * np.sqrt(size - 2 +
        ↪  np.square(t_dist))
129     critical_value = numerator / denominator
130     return critical_value
131 def check_G_values(Gs, Gc, inp, max_index):
132     if Gs > Gc:
133         # replace values in original df for which Gs > Gc with
            ↪  NaN
134         cal.loc[(cal.Label == g) & (cal[col] == inp[max_index]),
            ↪  col] = np.nan
135         #print(col, "{} is an outlier. G > G-critical: {:.4f} >
            ↪  {:.4f} \n".format(inp[max_index], Gs, Gc))
136     #else:
137     #    print(col, "{} is NOT an outlier. G > G-critical: {:.4f}
        ↪  > {:.4f} \n".format(inp[max_index], Gs, Gc))
138
139 ##################################################################
140 ### ZEROs
141 # df containing only bgd smpls
142 zero = samples[samples['sampletyp'] ==
    ↪  'bgd'].reset_index(drop=True)
143 # remove useless cols
144 zero.drop(['starttime', 'filetime', 'reffile'], axis=1,
    ↪  inplace=True)
145 zero = zero.loc[:, ~zero.columns.str.endswith('_rt')]
146 zero.drop(zero.columns[3:20], axis=1, inplace=True) #3:25 for
    ↪  ICHEAR1
147
148 # add FlowCF col as in cal
149 zero['FlowCF'], zero['Label'] = [0, 0]
150
151 # columnwise outlier detection
152 for col in zero:
153     if col.endswith('_a'):
154
155         def check_G_values(Gs, Gc, inp, max_index):
156             if Gs > Gc:
157                 # replace values in original df for which Gs > Gc
                    ↪  with NaN
158                 zero.loc[zero[col] == inp[max_index], col] =
                    ↪  np.nan
159                 #print(col, "{} is an outlier. G > G-critical:
                    ↪  {:.4f} > {:.4f} \n".format(inp[max_index],
                    ↪  Gs, Gc))
```

```
160             #else:
161             #    print(col, "{} is NOT an outlier. G > G-critical: {:.4f} > {:.4f} \n".format(inp[max_index], Gs, Gc))
162 
163         data = zero[col].tolist()
164         modified_z_scores = iglewicz_hoaglin(data)
165         for i, val in enumerate(modified_z_scores):
166             zero.loc[zero[col] == modified_z_scores[i], col] = np.nan
167 
168         # ESD_Test fct
169         # significance level = alpha
170         def ESD_Test(input_series, alpha, max_outliers):
171             for iterations in range(max_outliers):
172                 # (I)
173                 Gcritical = calculate_critical_value(len(input_series), alpha)
174                 Gstat, max_index = grubbs_stat(input_series)
175                 # (II)
176                 check_G_values(Gstat, Gcritical, input_series, max_index)
177                 # replace values in input_series for which Gs > Gc with NaN
178                 input_series[max_index] = np.nan
179         # perform generalized ESD on col for r=len(modZscore + 1)
180         ESD_Test(data, 0.05, len(modified_z_scores)+1)
181         # where area was set to NaN, set integration error to NaN
182         zero[col[:-1]+'e'] = np.where(pd.isna(zero[col]), np.nan, zero[col[:-1]+'e'])
183         zero[col[:-2] + ' MR'] = 0
184 
185 ### bg df with 2 rows (mean, error)
186 bg = pd.DataFrame(index=['mean', 'sigma'])
187 for col in zero.columns[4:]:
188     if col.endswith('_a'):
189         bg[col] =  np.nanmean(zero[col]), np.nanstd(zero[col])
190     if col.endswith('_e'):
191         bg[col] = np.nanmean(zero[col]), np.nanstd(zero[col])
192 # subtract zero mean from zeros
193 for col in zero.columns[4:]:
194     if col.endswith('_a'):
195         zero[col] = zero[col] - bg.at[bg.index[0], col]
196 # Check if path exists, if not create:
197 Path(path / 'Cal').mkdir(parents=True, exist_ok=True)
198 # save files
```

```
199 bg.to_csv(path / 'Cal/bg.txt', sep='\t')
200 ##################################################################
201 ### CALs
202 # df containing exclusively cal smpls
203
204 cal = samples[samples['sampletyp'] ==
    ↪ 'Cal'].reset_index(drop=True)
205 # create flow factor col
206 cal.insert(loc=5, column='FlowCF',
    ↪ value=cal['F_Cal']/cal['F_Inlet'])
207 # remove useless cols
208 cal.drop(['starttime', 'filetime', 'reffile'], axis=1,
    ↪ inplace=True)
209 cal = cal.loc[:, ~cal.columns.str.endswith('_rt')]
210 cal.drop(cal.columns[6:22], axis=1, inplace=True) #6:26 for
    ↪ ICHEAR1
211
212 # subtract zero mean from cals
213 for col in cal.columns:
214     if col.endswith('_a'):
215         cal[col] = cal[col] - bg.at[bg.index[0], col]
216
217 # create empty list to fill in compound names later
218 cmpnds = []
219 # calculate MR of cal smpls
220 for col in cal.columns[7:]:
221     # get analyte's MR in Calgas from table
222     SpecDatName = col[:-2]
223     MRana = (Calgas['MR / ppb'][Calgas['SpecDat'] ==
        ↪ SpecDatName].values[0])
224     # If IndexError: index 0 is out of bounds for axis 0 with
        ↪ size 0 -> analyte names in dfCalgas do not match col
        ↪ names in df
225     # create compound dependent calibration factors
226     cal[col[:-2] + ' MR'] = cal['FlowCF'] * MRana
227     if col.endswith('_a'):
228         #create list with analyte names
229         cmpnds.append(SpecDatName)
230
231 # sort by FlowCF:
232 cal = cal.sort_values(by='FlowCF')
233 # if FlowCF in previous line is smaller than (present value -
    ↪ 0.0005), Label = 1:
234 cal['Label'] = np.where(cal.FlowCF.shift(1) < (cal.FlowCF -
    ↪ 0.0005), 1, 0)
235 # cumulative sum + 1 as later Label=0 will be added for bgd
    ↪ smpls:
```

```
236 cal['Label'] = cal['Label'].cumsum() + 1
237 cal = cal.reset_index(drop=True).sort_values(by=['Label',
    ↪ 'filename'])
238
239 # groupby label
240 gbo = cal.groupby('Label')
241 # for iteration groupby object is useless, df needed
242 for g, g_df in gbo:
243     for col in g_df:
244         #g_df.sort_values(by=col, inplace=True)
245         if col.endswith('a'):
246             data = g_df[col].tolist()
247             modified_z_scores = iglewicz_hoaglin(data)
248             for i, val in enumerate(modified_z_scores):
249                 cal.loc[(cal.Label == g) & (cal[col] ==
                    ↪ modified_z_scores[i]), col] = np.nan
250             def check_G_values(Gs, Gc, inp, max_index):
251                 if Gs > Gc:
252                     # replace values in original df for which Gs
                        ↪ > Gc with NaN
253                     cal.loc[(cal.Label == g) & (cal[col] ==
                        ↪ inp[max_index]), col] = np.nan
254                     print(col, "{} is an outlier. G > G-critical:
                        ↪ {:.4f} > {:.4f}
                        ↪ \n".format(inp[max_index], Gs, Gc))
255                 else:
256                     print(col, "{} is NOT an outlier. G >
                        ↪ G-critical: {:.4f} > {:.4f}
                        ↪ \n".format(inp[max_index], Gs, Gc))
257                 # significance level = alpha
258                 def ESD_Test(input_series, alpha, max_outliers):
259                     for iterations in range(max_outliers):
260                         Gcritical =
                            ↪ calculate_critical_value(len(input_series),
                            ↪ alpha)
261                         Gstat, max_index =
                            ↪ grubbs_stat(input_series)
262                         check_G_values(Gstat, Gcritical,
                            ↪ input_series, max_index)
263                         # replace outlier in input_series -> next
                            ↪ potential outlier will be checked
                            ↪ during next iteration
264                         input_series[max_index] = np.nan
265                 #perform generalized ESD on col for
                    ↪ r=len(modZscore + 1)
266                 ESD_Test(data, 0.05, len(modified_z_scores)+3)
```

```
267             # where area was set to NaN, set integration error to
                ↪ NaN
268             cal[col[:-1]+'e'] = np.where(pd.isna(cal[col]),
                ↪ np.nan, cal[col[:-1]+'e'])
269
270
271 ######################################################################
272 ### uncertainty calculation
273 ######################################################################
274 ## calibration curve
275 # Harris D.C., Quantitative Chemical Analysis, 8th Edition;
    ↪ Calibration curve guide pdf, table p.30
276 ## propagation of uncertainty
277 # Rasul et al. - Quantifying Uncertainty in Analytical
    ↪ Measurements
278
279 # add zeros to cal dataframe
280 cal = pd.concat([cal, zero],
    ↪ ignore_index=True).sort_values(by=['Label', 'filename'])
281
282 # dfLR df contains variables which are necessary for uncertainty
    ↪ calculation
283 dfLR = pd.DataFrame(data=np.nan, index=['area_mean', 'MR_mean',
    ↪ 'slope', 'intercept', 'r^2', 's_y', 'n_cals',
    ↪ 'f_cal_mean','f_inlet_mean', 'LOD / ppb', 'samplevol_mean',
    ↪ 'samplevol_std', 'bgMR_mean', 'bgMR_std'], columns=cmpnds)
284 df_calSmpls = pd.DataFrame()
285 df_calSmpls[['filename', 'sampletime', 'samplevol']] =
    ↪ cal[['filename', 'sampletime', 'samplevol']]
286
287 for col in cal.columns[3:]:
288     if col.endswith('_a'):
289         # add average flows to dfLR
290         dfLR.loc[['f_cal_mean'], [col[:-2]]] =
            ↪ np.round((cal['F_Cal']).mean(), 3)
291         dfLR.loc[['f_inlet_mean'], [col[:-2]]] =
            ↪ np.round((cal['F_Inlet']).mean(), 1)
292         # x values & x col name
293         x_i = cal[col[:-2]+' MR']
294         x = str(col[:-2]+' MR')
295         # MR, area; means added to dfLR
296         dfLR.loc[['MR_mean'], [col[:-2]]] =
            ↪ np.round((cal[col[:-2] + ' MR']).mean(), 3)
297         # y values & y col name
298         y_i = cal[col]
299         y = col
```

```
300             dfLR.loc[['area_mean'], [col[:-2]]] =
                ↪  np.round((cal[col]).mean(), 3)
301             # remove (x, y)pairs where y is NaN:
302             # if ValueError: Inputs must not be empty -> check if
                ↪  area for zeros = nan
303             finiteYmask = np.isfinite(y_i)
304             y_i = y_i[finiteYmask]
305             x_i = x_i[finiteYmask]
306             # in order to use colnames with empty space, -, ... one
                ↪  can use ModelDesc as ModelDesc.from_formula is
                ↪  patsy's parser & patsy is used to evaluate code in
                ↪  formulas
307             response_term = [Term([LookupFactor(y)])]
308             model_terms = [Term([])]
309             model_terms += [Term([LookupFactor(x)])]
310             fml = ModelDesc(response_term, model_terms)
311             lm = smf.ols(formula=fml, data=cal).fit()
312             # create variables for fit coefficients
313             slope = lm.params[x]
314             intercept = lm.params['Intercept']
315             # fill useful values in LR dataframe
316             dfLR.loc[['slope'], [col[:-2]]] = np.round(slope, 2)
317             dfLR.loc[['intercept'], [col[:-2]]] = np.round(intercept,
                ↪  2)
318             dfLR.loc[['r^2'], [col[:-2]]] = np.round(lm.rsquared, 4)
319             dfLR.loc[['n_cals'], [col[:-2]]] = len(x_i)
320             dfLR.loc[['LOD / ppb'], [col[:-2]]] =
                ↪  np.round((3*bg.loc['sigma', col]) / slope, 4)
321             # df_calSmpls with x_i(MR), y_i(=area), y_p(predicted
                ↪  area from cal curve)
322             df_calSmpls[col[:-2] + ' MR'] = np.round(x_i, 5)
323             df_calSmpls[col] = np.round(y_i, 3)
324             samples.loc[samples['sampletyp'] == 'amb'].sampletime
325             # for mean, std use only samples where area is not NaN
326             dfLR.loc[['samplevol_mean'], [col[:-2]]] =
                ↪  np.round(df_calSmpls.samplevol[df_calSmpls[col].notna()
                                ].mean(), 2)
327
328             dfLR.loc[['samplevol_std'], [col[:-2]]] =
                ↪  np.round(df_calSmpls.samplevol[df_calSmpls[col].notna()
                                ].std(), 3)
329
330             # add also bg MR to dfLR
331             dfLR.loc[['bgMR_mean'], [col[:-2]]] =
                ↪  np.round((bg.loc['mean', col] - dfLR.loc['intercept',
                ↪  col[:-2]]) / dfLR.loc['slope', col[:-2]], 4)
```

```
332         dfLR.loc[['bgMR_std'], [col[:-2]]] =
             ↪ np.round((bg.loc['sigma', col] -
             ↪ dfLR.loc['intercept', col[:-2]]) / dfLR.loc['slope',
             ↪ col[:-2]], 4)
333         # function to calculate s_y with calsmpl_MR x_i &
             ↪ calsmpl_area y_i
334         def calc_s_y(x_i, y_i):
335             # predicted y_p for x_i
336             y_p = slope * x_i + intercept
337             # add y_p to df_calSmpls
338             df_calSmpls[col[:-2]+' y_p'] = np.round(y_p, 3)
339             # calculate s_y
340             enumerator = sum((y_i - y_p)**2)
341             # #of calsmpls n
342             n = len(cal)
343             denominator = n - 2
344             s_y = math.sqrt(enumerator/denominator)
345             return s_y
346         dfLR.loc[['s_y'], [col[:-2]]] = calc_s_y(x_i, y_i)
347         ### PLOT
348         fig, ax = plt.subplots()
349         # choose point style
350         ax.plot(x_i, y_i, 'o')
351         # plot linear fit
352         ax.plot(x_i, slope*x_i + intercept, 'lightgrey',
             ↪ label='fit')
353         # plot error bars
354         ###calculate s_y somewhere above, change plt.plot with
355         #yErr = dfLR.loc[[s_y], [col[:-2]]]
356         # remove error bars where y was nan
357         #yErr = yErr[finiteYmask]
358         #plt.errorbar(x_i, y_i, yErr, linestyle='None', color =
             ↪ 'b', capsize=2)
359         # plot zeros (NOT included in linreg!)
360         plt.title(col[:-2])
361         plt.xlabel('MR / ppb')
362         plt.ylabel('area / cts')
363         # for some reason (()) is needed to print legend properly
364         ax.legend((col[:-2], 'y = {}x + {},
             ↪ r^2={}'.format(np.round(slope, 2),
             ↪ np.round(intercept, 2), np.round(lm.rsquared, 4))))
365         # check if path exists, if not create
366         Path(path / 'graphs/Calibration').mkdir(parents=True,
             ↪ exist_ok=True)
367         #save figure
```

```
368         fig.savefig(path /
            ↪ 'graphs/Calibration/{}.png'.format(col[:-2]),
            ↪ bbox_inches='tight', dpi=150)
369
370 df_calSmpls = np.round(df_calSmpls, 4)
371 # Check if path exists, if not create
372 Path(path / 'Cal').mkdir(parents=True, exist_ok=True)
373 # save files
374 #dfLR.to_csv(path / 'Cal/dfLR.txt', sep='\t')
375 #df_calSmpls.to_csv(path / 'Cal/CalSmpls.txt', sep='\t')
376
```

A.3 Code file timeline.py

```
1  # -*- coding: utf-8 -*-
2  """
3  @author: lisa.ernle
4  """
5
6  from pathlib import Path
7  import pandas as pd
8  import numpy as np
9  import statsmodels.formula.api as smf
10 #import glob
11 import matplotlib.pyplot as plt
12 import matplotlib.dates as mdates
13 import dateutil.parser
14 #import math
15
16 ### try
17 from pandas.plotting import register_matplotlib_converters
18 register_matplotlib_converters()
19
20 ######################################################################
21 ### TO BE ADJUSTED
22 # general data path
23 #GenPath = Path(r'C:\Campaigns\CAFE\CAFE_Africa\Data')
24 #GenPath = Path(r'C:\Campaigns\ICHEAR\ICHEAR_1\Data')
25 GenPath = Path(r'C:\Campaigns\ICHEAR\ICHEAR_2\Data')
26 #GenPath = Path(r'C:\Campaigns\O3exp\data')
27 # data from following date will be processed
28 date = '20210413'
29 analyte = 'C5H8'
30
31 ######################################################################
32 ### USE as it is if you like
```

```
# explicit path
path = GenPath / date

# import lin reg factors from calibration:
LR = pd.read_csv(path / 'Cal/dfLR.txt', index_col=0, sep='\t', header=0)
# if no calseries performed on that day, use the one in global data folder
#LR = pd.read_csv(GenPath / 'dfLR_2020xxxx.txt', index_col=0, sep='\t', header=0)
# create df containing CalSmpls
CalSmpls = pd.read_csv(path / 'Cal/CalSmpls.txt', index_col=0, sep='\t', header=0)
# samples dataframe
samples = pd.read_csv(path / 'smpls.txt', sep='\t', header=0, parse_dates=['sampletime'], dayfirst=True,
usecols=['filename', 'sampletime','sampletyp', 'samplevol', analyte+'_a', analyte+'_e'])

# import bgd smpls (already normalized to 1000*samplevol)
bg = pd.read_csv(path / 'Cal/bg.txt', index_col=0, sep='\t', header=0)

samples.replace('', np.NaN)
# normalize areas by sample volume, 1000 as same done in cal curve
for col in samples:
    if col.endswith(tuple(['_a', '_e'])):
        samples[col] = samples[col]/(1000*samples['samplevol'])

## create column with sample mixing ratio
# if bg mean is neg., add absolute bg mean to smpls as otherwise it will cause false neg MR just above LOD
if LR.loc['bgMR_mean', analyte] >= 0:
    samples[analyte + ' MR / ppb'] = (samples[analyte + '_a'] - LR.loc['intercept', analyte])/LR.loc['slope', analyte] - abs(LR.loc['bgMR_mean', analyte])
else:
    samples[analyte + ' MR / ppb'] = ((samples[analyte + '_a'] - LR.loc['intercept', analyte])/LR.loc['slope', analyte]) + abs(LR.loc['bgMR_mean', analyte])

#################################################################
##### UNCERTAINTY
### all uncertainties in ppb ###
## U_i relative - uncertainty from integration
```

```
65  samples[analyte + ' U_i'] = samples[analyte + '_e'] /
    ↪  samples[analyte + '_a']
66
67  ### uncertainty in x from in MR from linear regression, relative,
    ↪  MC method
68  # create new df with predictor, response values
69  lr_df = CalSmpls.loc[:, [analyte + ' MR', analyte + '_a']].copy()
70  lr_df.rename({analyte + ' MR' : 'x', analyte + '_a' : 'y'},
    ↪  axis=1, inplace=True)
71  ## linear model: fit input data from calibration
72  lm = smf.ols(formula='y ~ x', data=lr_df).fit()
73  # lm.params returnes 'Intercept', 'x' (=slope for fitting x)
74  # lm.conf_int() returnes array with confidence intervals for
75  # 'Intercept'[0], 'x'(=slope)[1]
76  # lm.bse returns std errors of model coefficients
77  # ('Intercept', 'x'), has to be <0.05 for 95\%
78  # confidence interval to reject null hypothesis
79  # lm.pvalues returnts the p-values for the model coefficients
80  # df with simulated values
81  #print(samples.loc[samples[analyte + '_a'].isna()].filename)
82  pred = pd.DataFrame(columns=['slope', 'intercept', 'area', 'MR'])
83  samples[analyte + ' U_lr'] = np.nan
84  for i, row in samples.iterrows():
85      # replace std err by std deviation for slope, intercept
86      pred['slope'] = np.random.normal(lm.params['x'], lm.bse['x'],
        ↪  50000)
87      pred['intercept'] = np.random.normal(lm.params['Intercept'],
        ↪  lm.bse['Intercept'], 50000)
88      pred['area'] = np.random.normal(samples.iloc[i,
        ↪  :].loc[analyte + '_a'], 0, 50000)
89      pred['MR'] = (pred['area'] - pred['intercept']) /
        ↪  pred['slope']
90      # relative uncertainty -> divide by MR
91      samples.at[i, analyte + ' U_lr'] =
        ↪  pred['MR'].std()/row[analyte+' MR / ppb']
92      #if pred['MR'].notna().values.any():
93      #    ax.hist(pred['MR'], 100)
94
95  # U_v relative
96  samples[analyte + ' U_v'] = 0.005
97
98  # U_MRcal uncertainty in mixing ratio of cal points (MFCs,
    ↪  Calgas)
99  def calc_U_MRcal(MR):
100     ### MFC properties (mean, full scale(=size) [sccm])
101     f_cal_mean = LR.loc['f_cal_mean', analyte]
102     FS_cal = 5
```

```
103     f_inlet_mean = LR.loc['f_inlet_mean', analyte]
104     FS_inlet = 500
105     ## flow uncertainty = combined MFC-uncertainty (attitude,
        ↪  accuracy, Temp.drift(max. estimated=5°C))
106     d_f_MFCcal = np.sqrt((FS_cal*0.002)**2 + (FS_cal*0.02)**2 +
        ↪  (5*0.0005*f_cal_mean)**2)
107     # realtive uncertainty cal flow
108     U_f_cal = d_f_MFCcal / f_cal_mean
109     # relative uncertainty Inlet flow
110     d_f_MFCinlet = np.sqrt((FS_inlet*0.002)**2 +
        ↪  (FS_inlet*0.02)**2 + (5*0.0005*f_inlet_mean)**2)
111     U_f_inlet = d_f_MFCinlet / f_inlet_mean
112     ### Calgas properties
113     # relative Uncertainty of Apel-Riemer Calgas MR = 5\%
114     U_MR_CG = 0.05
115     # relative uncertainty Calgas
116     ### uncertainty in calgas mixing ratio
117     U_MRcal = np.sqrt(U_f_cal**2 + U_f_inlet**2 + U_MR_CG**2)
118     return U_MRcal
119 samples[analyte+' U_MRcal'] = calc_U_MRcal(samples[analyte + ' MR
    ↪  / ppb'])
120
121 ######################################################################
122 ##### calculate total uncertainty [ppb]
123 samples[analyte + ' U_tot / ppb'] = abs(np.sqrt((samples[analyte
    ↪  + ' U_i']**2) + (samples[analyte + ' U_lr']**2) +
    ↪  (samples[analyte + ' U_v']**2) + (samples[analyte + '
    ↪  U_MRcal']**2))*samples[analyte + ' MR / ppb'])
124
125 ######################################################################
126 # output file, plots
127 # create file with MR for all compounds:
128 MRamb = pd.DataFrame()
129
130 # use only amb smpls:
131 MRamb['filename'] = samples.loc[samples['sampletyp'] ==
    ↪  'amb'].filename
132 MRamb['DateTime'] = samples.loc[samples['sampletyp'] ==
    ↪  'amb'].sampletime
133 MRamb[analyte+' /
    ↪  ppb']=round((samples.loc[samples['sampletyp']=='amb'][analyte+'
    ↪  MR / ppb']),4)
134 MRamb[analyte+'_u / ppb'] =
    ↪  round((samples.loc[samples['sampletyp'] =='amb'][analyte+'
    ↪  U_tot / ppb']), 4)
135 MRamb.reset_index(drop=True, inplace=True)
136
```

```
137 ### PLOT
138 ######################
139 # PLOT raw: default figsize 8x6 inch^2
140 fig, ax1 = plt.subplots() # inBrackets: figsize=(width,height)
141 ax2 = ax1.twinx()
142 ax3 = ax1.twinx()
143 # 3rd y-axis moved right of 2nd y-axis:
144 ax3.spines['right'].set_position(('outward', 40))
145
146 # amb:
147 amb, = ax1.plot(samples.loc[samples['sampletyp'] ==
    ↪ 'amb'].sampletime, samples.loc[samples['sampletyp'] ==
    ↪ 'amb'][analyte + ' MR / ppb'], 'o', label='amb')
148
149 # cal:
150 cal, = ax2.plot(samples.loc[samples['sampletyp'] ==
    ↪ 'Cal'].sampletime, samples.loc[samples['sampletyp'] ==
    ↪ 'Cal'][analyte +' MR / ppb'],'o', label='cal', color='r')
151
152 # zero:
153 zero, = ax3.plot(samples.loc[samples['sampletyp'] ==
    ↪ 'bgd'].sampletime, samples.loc[samples['sampletyp'] ==
    ↪ 'bgd'][analyte + ' MR / ppb'], 'o', label='zero', color='y')
154
155 # create plot data list to access parameters in the plots:
156 data = [amb, cal, zero]
157 # add legend for ax1 & ax2 object
158 ax1.legend(data, [smpltyp.get_label() for smpltyp in data])
159 ax1.xaxis.set_major_locator(mdates.HourLocator(interval=2))
160 ax1.xaxis.set_major_formatter(mdates.DateFormatter('\%H:\%M'))
161 fig.autofmt_xdate()
162
163 a = str(samples.sampletime[0])
164 day = dateutil.parser.parse(a).date()
165
166 plt.title(day)
167 ax1.set_xlabel('time')
168 ax1.set_ylabel(analyte+'\nMR / ppb')
169
170 # set y-limit
171 #ax1.set_ylim(-0.05, 5.0)
172
173 ax1.tick_params(axis='y', colors=amb.get_color())
174 ax2.tick_params(axis='y', colors=cal.get_color())
175 ax3.tick_params(axis='y', colors=zero.get_color(), )
176
177 # Check if path exists, if not create:
```

```
178 Path(path / 'graphs/all').mkdir(parents=True, exist_ok=True)
179 # save plot
180 #fig.savefig(path / 'graphs/all/{}_MR.png'.format(analyte),
    ↪ bbox_inches='tight', dpi=200)
181 fig.savefig(path / 'graphs/all/{}_MR.pdf'.format(analyte),
    ↪ bbox_inches='tight', dpi=300)
182 ##########################
183 # plot amb with errorbars:
184 fig, ax4 = plt.subplots() # inBrackets: figsize=(width,height)
185 # amb:
186 ax4.errorbar(MRamb.DateTime, MRamb[analyte+' / ppb'],
    ↪ yerr=MRamb[analyte+'_u / ppb'].to_numpy(), fmt='.',
    ↪ color=('#00008B'), ecolor='#2969D0')
187
188 ax4.xaxis.set_major_locator(mdates.HourLocator(interval=2))
189 ax4.xaxis.set_major_formatter(mdates.DateFormatter('\%H:\%M'))
190 fig.autofmt_xdate()
191
192 b = str(MRamb.DateTime[0])
193 day = dateutil.parser.parse(b).date()
194
195 plt.title(day)
196 ax4.set_xlabel('time')
197 ax4.set_ylabel(analyte+'\nMR / ppb')
198
199 # set y-limit
200 #ax4.set_ylim(-0.05, 7)
201 # Check if path exists, if not create:
202 Path(path / 'graphs/amb').mkdir(parents=True, exist_ok=True)
203 # save amb_errorbar plot
204 #fig.savefig(path / 'graphs/amb/{}_MRamb.png'.format(analyte),
    ↪ bbox_inches='tight', dpi=200)
205 fig.savefig(path / 'graphs/amb/{}_MRamb.pdf'.format(analyte),
    ↪ bbox_inches='tight', dpi=300)
206 ###
207 # Check if path exists, if not create:
208 Path(path / 'amb').mkdir(parents=True, exist_ok=True)
209 # create filepath for MRfile:
210 ambFile = path / 'amb/MGC_{}.txt'.format(date)
211
212 # check if file exists & create if necessary:
213 if not ambFile.exists ():
214     #MRamb.to_csv(ambFile, sep='\t', index=False)
215 else:
216     # Open MRfile.txt:
217     MRfile = pd.read_csv(ambFile, sep='\t', header=0,
        ↪ parse_dates=['DateTime'], dayfirst=True)
```

```
218     # add/overwrite col for current analyte:
219     MRfile[analyte + ' / ppb'] = MRamb[analyte + ' / ppb']
220     MRfile[analyte+'_u / ppb'] = MRamb[analyte+'_u / ppb']
221     # sort cols alphabetically:
222     MRfile.sort_index(axis=1, inplace=True)
223     # bring cols 'filename' & 'DateTime' to colIndex=0,1
224     # create list with col headers:
225     headers = list(MRfile)
226     # df.pop returns item & drops it from data frame, insert at
        ↪ loc=0 and index move col to head of list
227     headers.insert(0, headers.pop(headers.index('DateTime')))
228     headers.insert(0, headers.pop(headers.index('filename')))
229     # df.loc[rows, cols] orders cols by col names in list
        ↪ 'headers'
230     MRfile = MRfile.loc[:, headers]
231     #save MRfile:
232     #MRfile.to_csv(ambFile, sep='\t', index=False,
        ↪ float_format='\%.4f')
233
```

Publication list Lisa Ernle

Bekö, Gabriel et al. (2020). "The Indoor Chemical Human Emissions and Reactivity (ICHEAR) project: Overview of experimental methodology and preliminary results". In: *Indoor Air* 30.6, pp. 1213–1228.

Bourtsoukidis, Efstratios et al. (2019). "Non-methane hydrocarbon (C 2–C 8) sources and sinks around the Arabian Peninsula". In: *Atmospheric Chemistry and Physics* 19.10, pp. 7209–7232.

Bourtsoukidis, Efstratios et al. (2020). "The Red Sea Deep Water is a potent source of atmospheric ethane and propane". In: *Nature Communications* 11.1, p. 447.

Dienhart, Dirk et al. (2021). "Measurement report: Observation-based formaldehyde production rates and their relation to OH reactivity around the Arabian Peninsula". In: *Atmospheric Chemistry and Physics* 21.23, pp. 17373–17388.

Eger, Philipp et al. (2019). "Influence of anthropogenic emissions from shipping and industry on Cl-radical generation around the Arabian Peninsula during AQABA." In: *Geophysical Research Abstracts*. Vol. 21.

Ernle, Lisa, Monika Akima Ringsdorf, and Jonathan Williams (2023). "Influence of ozone and humidity on PTR-MS and GC-MS VOC measurements with and without a Na 2 S 2 O 3 ozone scrubber". In: *Atmospheric Measurement Techniques* 16.5, pp. 1179–1194. DOI: https://doi.org/10.5194/amt-16-1179-2023.

Ernle, Lisa et al. (2023). "Assessment of aldehyde contributions to PTR-MS *m/z* 69.07 in indoor air measurements". In: *Environmental Science: Atmospheres*. Accepted.

Karu, Einar et al. (2021). "Atomic emission detector with gas chromatographic separation and cryogenic pre-concentration (CryoTrap–GC–AED) for atmospheric trace gas measurements". In: *Atmospheric Measurement Techniques* 14.3, pp. 1817–1831.

Li, Mengze et al. (2022). "Human metabolic emissions of carbon dioxide and methane and their implications for carbon emissions". In: *Science of the Total Environment* 833, p. 155241.

Nussbaumer, Clara M et al. (2021). "Measurement report: In situ observations of deep convection without lightning during the tropical cyclone Florence 2018". In: *Atmospheric Chemistry and Physics* 21.10, pp. 7933–7945.

Paris, Jean-Daniel et al. (2021). "Shipborne measurements of methane and carbon dioxide in the Middle East and Mediterranean areas and the contribution from oil and gas emissions". In: *Atmospheric Chemistry and Physics* 21.16, pp. 12443–12462.

Pfannerstill, Eva Y et al. (2019). "Shipborne measurements of total OH reactivity around the Arabian Peninsula and its role in ozone chemistry". In: *Atmospheric Chemistry and Physics* 19.17, pp. 11501–11523.

Shenolikar, Justin et al. (2019). "Lifetimes and Loss mechanisms of NO _{3} and N _{2} O _{5} during the AQABA ship campaign." In: *Geophysical Research Abstracts*. Vol. 21.

Tadic, Ivan et al. (2019). "Photochemical net ozone production rates as a function of NO x, O 3 and HO x abundances in the marine boundary layer around the Arabian Peninsula: Results from the ship-based 2017 AQABA campaign". In: *AGU Fall Meeting Abstracts*. Vol. 2019, A11K–2697.

Tauer, Sebastian et al. (2019). "HOx during AQABA campaign." In: *Geophysical Research Abstracts*. Vol. 21.

Voigt, Christiane et al. (2022). "Cleaner skies during the COVID-19 lockdown". In: *Bulletin of the American Meteorological Society* 103.8, E1796–E1827.

Wang, Nijing et al. (2020a). "Measurements of carbonyl compounds around the Arabian Peninsula: overview and model comparison". In: *Atmospheric Chemistry and Physics* 20.18, pp. 10807–10829.

Wang, Nijing et al. (2020b). "Total OH reactivity of emissions from humans: in situ measurement and budget analysis". In: *Environmental Science & Technology* 55.1, pp. 149–159.

Wang, Nijing et al. (2022). "Emission rates of volatile organic compounds from humans". In: *Environmental Science & Technology* 56.8, pp. 4838–4848.

Zannoni, Nora et al. (2021). "Effect of ozone, clothing, temperature, and humidity on the total OH reactivity emitted from humans". In: *Environmental Science & Technology* 55.20, pp. 13614–13624.

Zannoni, Nora et al. (2022). "The human oxidation field". In: *Science* 377.6610, pp. 1071–1077.